Implications of stochastic ion channel gating and dendritic spine plasticity for neural information processing and storage

Cian O'Donnell

Doctor of Philosophy

Institute for Adaptive and Neural Computation
School of Informatics
University of Edinburgh

2011

Abstract

On short timescales, the brain represents, transmits, and processes information through the electrical activity of its neurons. On long timescales, the brain stores information in the strength of the synaptic connections between its neurons. This thesis examines the surprising implications of two separate, well documented microscopic processes — the stochastic gating of ion channels and the plasticity of dendritic spines — for neural information processing and storage.

Electrical activity in neurons is mediated by many small membrane proteins called ion channels. Although single ion channels are known to open and close stochastically, the macroscopic behaviour of populations of ion channels are often approximated as deterministic. This is based on the assumption that the intrinsic noise introduced by stochastic ion channel gating is so weak as to be negligible. In this study we take advantage of newly developed efficient computer simulation methods to examine cases where this assumption breaks down. We find that ion channel noise can mediate spontaneous action potential firing in small nerve fibres, and explore its possible implications for neuropathic pain disorders of peripheral nerves. We then characterise the magnitude of ion channel noise for single neurons in the central nervous system, and demonstrate through simulation that channel noise is sufficient to corrupt synaptic integration, spike timing and spike reliability in dendritic neurons.

The second topic concerns neural information storage. Learning and memory in the brain has long been believed to be mediated by changes in the strengths of synaptic connections between neurons — a phenomenon termed synaptic plasticity. Most excitatory synapses in the brain are hosted on small membrane structures called dendritic spines, and plasticity of these synapses is dependent on calcium concentration changes within the dendritic spine. In the last decade, it has become clear that spines are highly dynamic structures that appear and disappear, and can shrink and enlarge on rapid timescales. It is also clear that this spine structural plasticity is intimately linked to synaptic plasticity. Small spines host weak synapses, and large spines host strong synapses. Because spine size is one factor which determines synaptic calcium concentration, it is likely that spine structural plasticity influences the rules of synaptic plasticity. We theoretically study the consequences of this observation, and find that different spine-size to synaptic-strength relationships can lead to qualitative differences in long-term synaptic strength dynamics and information storage. This novel theory unifies much existing disparate data, including the unimodal distribution of synaptic strength, the saturation of synaptic plasticity, and the stability of strong synapses.

Acknowledgements

Many people need thanking. First, my supervisors Matt Nolan and Mark van Rossum. Both have been absolutely fantastic. I have learned a lot from by watching them, chatting to them, and working with them over the years. Matt is a man of boundless ambition, but with the modesty to back it up with hard work and 'real science'. He taught me that a thing is not worth doing unless it brings something new to the world. Mark is the man who's door is always open. Many, many hours were spent pacing around his office squiggling on the whiteboard while he explained to me what was what. He taught me that theory can have power in neuroscience, but only in the right places. Matt, Mark, for all your time and tutoring I thank you both.

The Neuroinformatics DTC was a great place to be. The broad training we got, the exposure to machine learning, the range of projects taken on by the students, and the general enthusiasm of everyone — faculty, students, and admin staff — made it a great environment to learn in. For that I'd like to thank the faculty: Jim, David and Peggy; ANC fellows David and Matthias; Pat, administrator extraordinaire; and all the students. I'd also like to thank the Nolan group, who always had time to answer my naive questions on experimental biology: Arianna, Derek, Helen, Hugh, Mel, Paul and Ruth.

On the personal side, I have to thank my friends and family. My friends included many DTC students, my flatmates, and general pals. There was always time to enjoy Edinburgh and realise the world outside work. My brother, Fionntán, and sisters, Eimear and Meabh, have also made the journey easier. It was great to see them so often. The other person who deserves a special mention is my girlfriend, Clare. I feel lucky to have found someone who makes me so happy.

Finally, and most importantly, I need to thank my parents John and Máire. They always valued education. Although it might just have come from them both being teachers, I think it goes back further. I think my grandparents gave them both a deep respect for learning, which they passed on to us. I was never told what to do: to go to college, to focus on science, nothing. Nothing but encouragement every step of the way. We were brought up to be ambitious but humble at the same time. Seamus Heaney summed up something like it when he said:
"We should keep our feet on the ground to signify that nothing is beneath us, but we also should also lift up our eyes to say nothing is beyond us".

Mum, Dad, thanks.

Declaration

I declare that this thesis was composed by myself, that the work contained herein is my own except where explicitly stated otherwise in the text, and that this work has not been submitted for any other degree or professional qualification except as specified.

(*Cian O'Donnell*)

Contents

Chapter 1

Introduction

The brain represents information as changes in the electrical potential across the membranes of its neurons. Processing of this information can be grouped into two categories: events that happen within single neurons, and events that involve multiple neurons. Single-neuron computation is mediated by a spatially extended dendritic tree and the currents passing through membrane ion channels. Multi-cellular neuronal computation, in contrast, relies on the synaptic connections between neurons. The strength of these connections shape the patterns of activity on the neuronal network. Importantly, these connections can change their strength in an activity-dependent manner on both fast and slow timescales [Bliss and Lomo, 1973]. This property of plasticity allows information about the past to be stored within the circuitry of the present, and is generally believed to underlie memory storage in the brain [Hebb, 1949, Bliss and Collingridge, 1993a, Milner et al., 1998, Morris et al., 2003].

This thesis begins from two established biological findings — that ion channels open and close stochastically and that dendritic spines are plastic — and examines their implications for single cell information processing and synaptic information storage, respectively.

1.1 Overview

Channel noise

In Chapters 2 and 3, we examine ion channel noise. Although data from indirect measurements had long predicted that individual ion channels open and close stochastically Verveen and Derksen [1968], Hille [1970], Katz and Miledi [1970, 1971, 1972], it

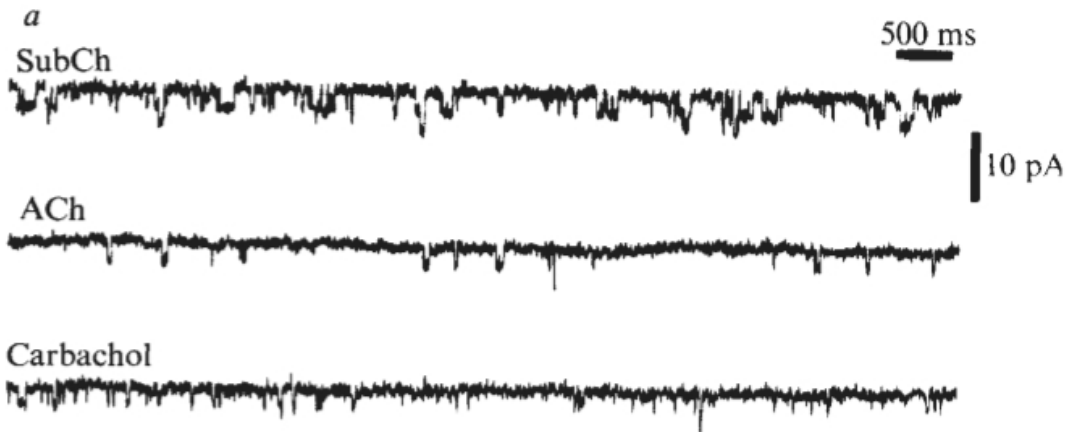

Figure 1.1: Single-channel currents from frog muscle fibres show individual ion channels opening and closing stochastically [taken from Neher and Sakmann, 1976]. Three different curves represent current of same channel type in the presence of various agonists which modulate the channel open probability.

was not until the advent of the patch-clamp electrophysiological technique and single channel recordings in the 1970s that it could be directly measured [Neher and Sakmann, 1976] (Figure 1.1). Because of this inherent stochasticity, any signals generated or processed using ionic currents must possess an intrinsic variability. In principle, this noise could limit the precision of the neural code. However, single ion channels exhibit relatively small conductances (1-100 pS) and are usually expressed in large numbers (tens or hundreds of thousands per cell) [Hille, 2001]. From the law of large numbers we might then expect that the momentary variance of the total macroscopic conductance through a population of ion channels will be negligible — leaving the mean conductance as a good representation of the population behaviour.

The mean approximation for macroscopic ion channel dynamics has been used extensively in computational models and is sufficient to account for many biophysical phenomena. The classic example is the Hodgkin-Huxley model of the squid giant axon action potential [Hodgkin and Huxley, 1952].

Even given the success of this approximation, it is important to note that the vast majority of the data that these models aim to reproduce originate from electrical recordings at the cell body (soma), which, because of its relatively large size, is typically the most experimentally accessible region of the neuron. Electrical activity in other parts of the cell, such as thin axons and dendrites, remains largely difficult to record from directly and so is less well understood. For two reasons, these are also the subcellular locations where the stochastic effects of ion channel gating likely have the largest

impact. First, the local input resistance is larger the thinner an axon or dendrite is. The greater the input resistance, the greater the membrane potential fluctuations from stochastic ionic currents. Second, if we assume a homogeneous density of ion channels per unit area cell membrane throughout the cell, then the total number of ion channels per subcellular electrical compartment is likely to be less for smaller compartments, due to their smaller surface areas.

These considerations suggest that previous estimates of the impact of channel noise based on somatic recordings may underestimate its influence at more distal locations in the cell. Although several analytical and computational studies have characterised the effects of stochastic channel gating in single compartment models, its importance in more realistic neuronal morphologies is comparatively unknown [van Rossum et al., 2003, Diba et al., 2004, 2006, Jacobson et al., 2005, Kole et al., 2006].

In Chapter 2 we examine the role of channel noise in triggering spontaneous action potentials in small neuron models. We use stochastic numerical simulations (with the PSICS simulator; Cannon et al., 2010) and theoretical calculations to explore the contributions of sodium and potassium channel populations to membrane noise and spike generation in the Hodgkin-Huxley squid axon model. We find that, surprisingly, K^+ channels can contribute more to membrane noise than Na^+ channels, and that spontaneous firing propensity depends on anatomical factors such as cable length and diameter. We argue that these processes suggest a novel model for spontaneous firing of peripheral nerves in certain neuropathic pain conditions.

In Chapter 3 we explore the effects of channel noise on the process of synaptic integration in dendritic neurons. We find that the magnitude of membrane noise from stochastic channel gating depends on neuronal morphology, and that channel noise is sufficient to introduce substantial unreliability and jitter into axonal spike trains from distributed synaptic input. We show that the majority of this variability arises from the dendrites and not the soma or axon, and so may have been underestimated in earlier *in vitro* slice experiments which relied on somatic recordings [Mainen and Sejnowski, 1995, Nowak et al., 1997].

Dendritic spines and synaptic plasticity

In Chapter 4, we study synaptic plasticity. Most excitatory synapses in the brain do not terminate directly on the dendrites of their target neuron, but instead tend to form on small membrane protrusions called dendritic spines. These spines are diverse in

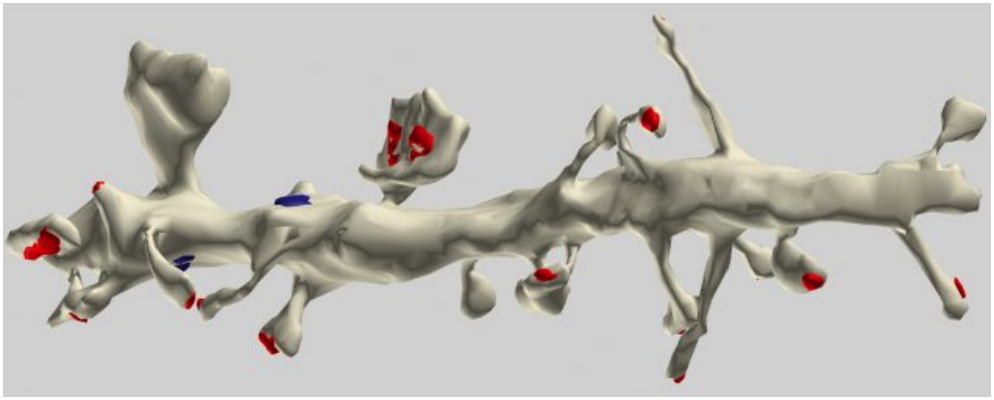

Figure 1.2: Segment of rat hippocampal neuron dendrite reconstructed from serial-section electron microscopy. Protrusions from main shaft are dendritic spines. Red patches signify excitatory post-synaptic densities, blue patches signify inhibitory post-synaptic densities (Image from Kristen Harris lab, online at "Synapse Web").

both shape and size (Figure 1.2), and their function is not entirely clear. Because of their tiny size ($<1\mu m^3$), they have proven difficult to access experimentally. Computational models and fluorescence imaging experiments, however, have suggested that spines perform little electrical function — the synaptic current at the dendrite is similar with or without the spine — but may instead serve to compartmentalise biochemical signals. Indeed, modern calcium (Ca^{2+}) imaging experiments support the idea that spines can isolate Ca^{2+} concentration changes from the dendrite [Yuste and Denk, 1995]. Because Ca^{2+} signalling is a crucial step in the molecular synaptic plasticity cascade, spines might therefore enable synapse-specific plasticity rules. Importantly, the size and shape of the spine, among other factors, can strongly influences both the amplitude and time course of these Ca^{2+} signals, and hence implicating spines in the process of memory storage.

This argument has gained prominence with the recent discovery that the dendritic spines are highly dynamic structures *in vivo* [reviewed by Holtmaat and Svoboda, 2009]. Some spines appear and disappear on a timescale of minutes, but other spines persist throughout an animal's entire lifetime. Interestingly, spine size is found to be tightly correlated with the strength of the synapse it hosts [Matsuzaki et al., 2001], even while the synaptic strength changes during a plasticity event [Matsuzaki et al., 2004]. The function of this relationship is not known, and, more surprisingly, the implications for spine Ca^{2+} signaling have not been well studied. Because spine Ca^{2+} signals play such an important role in synaptic plasticity, spine structural plasticity could possibly introduce a strength dependence in the synaptic learning rules. This could constitute a

previously unknown mechanism for enhancing memory storage.

In Chapter 4 we theoretically examine the implications of this spine-size to synaptic strength relationship for Ca^{2+}-dependent synaptic plasticity. We show that imperfect coupling between spine size and Ca^{2+} influx fundamentally alters synaptic stability. If Ca^{2+} influx is not adequately compensatd for changes in spine size, then strong synapses are stabilized and synaptic strength distributions are unimodal. In contrast, over-compensation of Ca^{2+} influx leads to binary, persistent synaptic strengths with bimodal distributions. We use detailed biophysical spine models to demonstrate that CA1 pyramidal neuron spines fall into the undercompensating, stable class. This finding unifies several previously disparate experimental data.

Chapter 2

Channel noise triggering spontaneous activity in thin axons

2.1 Background

2.1.1 Neural variability

Many components of the nervous system are inherently stochastic, making neural computation an unavoidably noisy process (Table 2.1). Importantly, it is not clear whether this variability is a "bug or a feature". In other words, is the stochasticity an undesirable source of noise which sets constraints on neural computation? Or is it exploited by biology to play a beneficial role in neural information processing? Ultimately, addressing this question will require examination of each of the sources of variability in the nervous system [Faisal et al., 2008, Ribrault et al., 2011].

We begin with an example. A series of electrophysiological recordings from a salamander retinal ganglion cell are depicted in Figure 2.1 [Gollisch and Meister, 2008]. Despite the circuit proximity of these cells to the sensory periphery, spike trains are variable from trial-to-trial even when presented with an identical stimulus. Both spike count and individual spike times are stochastic. The degree of variability (measured as either standard deviation of spike count or individual spike time jitter) is dependent on the stimulus. Some stimuli elicit relatively reliable responses (e.g. grating 6), while other stimuli prompt more variable responses (e.g. grating 2). Although the identities of the possible sources of this spike train variability are well known, their relative contributions are unclear. We list the candidate sources of trial-to-trial variability in Table 2.1. It is important to note that some of these sources of variability may simply

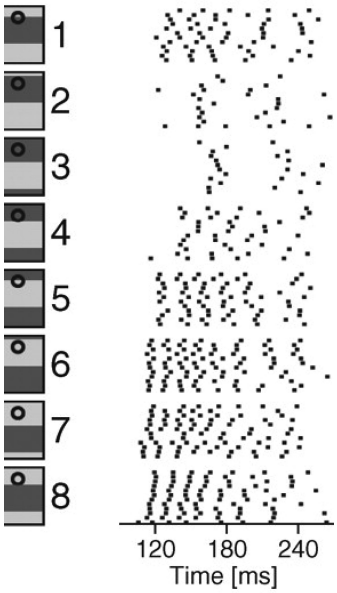

Figure 2.1: Raster plots of spike train responses of a single salamander retinal ganglion cell over several trials (right) for eight different stimulation gratings presented for 150ms (left). Circle denotes cell's visual receptive field. Adapted from Gollisch and Meister [2008].

reflect deterministic processes that are not visible to the experimenter (marked with an asterisk), while others are true sources of randomness.

From the sources of variability extrinsic to the single neuron, neuromodulation and network state can be thought of as approximately deterministic factors that are simply hidden to the experimentalist. Because they are difficult to control for in most experiments, they are often simply acknowledged as a possible source of measurement variability despite their likely computational functions.

In contrast, the first three factors in the left-hand column of Table 2.1 are usually thought of as true sources of stochasticity. The first element is synaptic unreliability. Single presynaptic vesicles at most synapses are released probabilistically in an all-or-nothing manner. The probability of release can vary between 0 and 1, and is activity dependent on both short (10s of ms) and long (hours) timescales. This unreliability introduces inherent stochasticity into synaptic transmission, and is generally believed to add substantial variability into neural activity and loss of transmitted information [Zador, 1998, Manwani and Koch, 2001].

The second factor is the location of vesicle release. Detailed biophysical modeling suggests that heterogeneity in the location of vesicle release (whether vesicles are

Extrinsic to neuron	*Intrinsic to neuron*
Synaptic unreliability	Adaptation*
Location of vesicle release	Stochastic ion channel gating
Neurotransmitter vesicle size heterogeneity	Ion channel diffusion/trafficking/recycling
Neuromodulation*	Thermal (Johnson) noise
Varying network state*	Ion channel shot noise
	Intra-cellular ionic concentrations*

Table 2.1: The sources of electrical variability in the nervous system. The two columns list factors extrinsic (left) and intrinsic (right) to the single neuron. Asterisks denote items that may be approximately deterministic and functional but are often considered sources of variability from the experimentalist's point-of-view.

released at the centre or the periphery of the synapse) can have a surprisingly large contribution ($\sim$36%) to synaptic current variability [Franks et al., 2003].

The third factor is heterogeneity in vesicle size. Presynaptic neurotransmitter vesicle outer diameter has been measured to range from 30-70nm, with a mean of ~42nm and standard deviation of ~9nm [Takamori et al., 2006]. If we assume spherical vesicles with a membrane thickness of 4nm [Takamori et al., 2006], and that inner vesicle volume is proportional its number of neurotransmitter molecules, then the coefficient of variation of vesicle molecule number is ~0.7. This vesicle size heterogeneity plays no known functional role and is thought to contribute substantial variability to postsynaptic response amplitudes [Franks et al., 2003].

The right-hand side of Table 2.1 lists sources of trial-to-trial variability intrinsic to the single neuron. The first element, adaptation, refers to the history-dependent activation or inactivation levels of membrane ion channels, some of which can have 'memory' timescales in the 100s of ms [Storm, 1988, Marder et al., 1996]. Adaptation may be considered an approximately deterministic source of trial-to-trial variability.

The remaining five factors in Table 2.1 arise from the biophysics of membrane ion channel currents:

1. Stochastic ion channel gating, the focus of this thesis, is the thermally-induced switching of ion channels between different conformational states. Although the probabilities of transitions between states can be dependent on external variables, such as local membrane potential or neurotransmitter concentration, switching itself appears to be an entirely stochastic process [Hille, 2001]. Hence, any

membrane currents through ion channel populations are inherently noisy.

2. Ion channels are not static fixtures in the cell membrane, but instead are continually diffusing laterally within the membrane, being trafficked to specific compartments within the cell, and being recycled by removal or insertion from the membrane to and from and the cytosol [Triller and Choquet, 2005]. Because these processes operate on slower timescales (tens to hundreds of milliseconds) than those of most other sources of electrical noise (tens to hundreds of microseconds), they are unlikely to contribute to fast variability in neural activity. However, their presence implies the continual fluctuation of ion channel number and type in a given neuronal compartment, and so perhaps contribute to the trial-to-trial variability observed in neural activity patterns experimentally. Although not considered in this thesis, they could be incorporated into future studies by allowing the present model parameters, such as ion channel number, to fluctuate over time according to stochastic rules which are derived from biophysics and constrained by modern experimental data. It is not known how large or small an effect this mechanism would have on voltage-gated ion channel noise.

3. Johnson noise is the thermal fluctuations in membrane potential across a conductor (e.g. the cell membrane), present in all physical electrical circuits. Johnson noise is calculated to be negligible for neural membranes [Lecar and Nossal, 1971b, Manwani and Koch, 1999a].

4. Ion channel shot noise arises from the moment-to-moment fluctuations in the rate of ions passing through an membrane ion channel, either in or out of the cell. Shot noise is also likely negligible. As an example, consider a HH Na^+ channel open at resting potential (-65mV) with a single-channel conductance of 10pS [Hille, 2001]. Na^+ ions flow into the cell at a mean rate of 7.1×10^6/s, but the actual number of ions flowing likely fluctuates over time. If the flow obeyed a Poisson process (where each ion's passage was random with a fixed probability of occurence and independent of other ions' passage), then the standard deviation of the count of ions over some interval would simply equal the square root of the mean. For our example HH Na^+ channel over 1ms, these fluctuations would therefore be approximately 1.2% of the mean, and hence negligible.

5. The flow of ionic currents across the cell membrane necessarily alters the concentrations of these ions both inside and outside the cell. In the long-term, the

resting concentration of each ion channel species is maintained by active membrane pumps and ion exchangers which continually move ions in or out of the cell. However, in the short term, and particularly in small compartments of the dendritic or axonal arbour, elevated neural activity can transiently drive the intracellular concentrations away from their steady-state levels. In the case of Ca^{2+} ions, these deviations may serve important biochemical and computational functions. There is also evidence for Na^{+} gating of K^{+} channels [Yuan et al., 2003]. In contrast, K^{+} concentration changes are not known to serve any functional role. Regardless, variations in intra-cellular concentration of ion channels could contribute a source of trial-to-trial variability to membrane currents and neural activity. In modeling studies the extracellular matrix is often considered so great in volume that its fractional change in ionic concentration from membrane current flow is negligible, although even this assumption is unlikely to be completely true [Egelman and Montague, 1999].

Of the six factors intrinsic to the single cell, the contributions of adaptation, channel diffusion/trafficking and ionic concentration fluctuations are mostly unknown but probably context dependent, Johnson and shot noise are negligible, and the effects of stochastic ion channel gating remain unclear, despite substantial theoretical and experimental attention (reviewed below).

2.1.2 Stochastic ion channel gating

Ion channels open and close stochastically

Ion channels are pore-forming macromolecular proteins that, when inserted into a cell membrane, allow the selective passage of ionic currents in and/or out of the cell [Hille, 2001]. Each ion channel can, at any given moment, occupy only one of multiple discrete conformational states; at least one of which is an open/conducting state, and at least one of which is a closed/non-conducting state. Transitions between states are both exceedingly rapid ($<1\mu$s) and, like all molecular reactions, stochastic in nature — they are driven by thermal agitation. Crucially, however, state transitions are not truly random but instead follow certain statistical rules. Many ion channels contain sensor regions which cause the transition probabilities to depend on external factors such as the cell membrane potential, or the presence of a ligand. Switches between conformational states are almost always assumed to be Markovian — transition probabilities depend only on the present state and not on previous states. Here, we focus only on the

stochastic gating of voltage-gated ion channels, not on ligand-gated channels, which theoretical models have predicted to have minimal contribution to neuronal noise [van Rossum et al., 2003, Franks et al., 2003].

Ion channels underlie the excitability of all neurons, and facilitate much electrical and chemical computation within the nervous system. For example, the opening of a voltage-gated Na^+ channel passes an inward current which depolarises the cell, increasing the probability that other nearby Na^+ channels also open. If enough channels open together, this positive feedback can continue to rapidly depolarise the cell autonomously. Hodgkin and Huxley successfully identified this mechanism as the process underlying the onset of the action potential [Hodgkin and Huxley, 1952].

Importantly, the methods employed by Hodgkin and Huxley were not sensitive enough to allow them to detect the presence of single ion channels, and their mathematical model of the squid giant axon conductances was instead restricted to a macroscopic and empirical description without knowledge of the molecular mechanisms underneath. Subsequent theoretical work has shown the direct mathematical relationship between the stochastic gating of single channels and the macroscopic currents recorded from channel populations. However, even though the molecular processes underlying stochastic channel gating are now well understood [Hille, 2001], the vast majority of studies persist in using the macroscopic (and deterministic) HH-style models to describe ion channel populations in neural simulations. There are several reasons: 1) the conceptual success of the original HH model; 2) the ease of adaptability of the HH formalism to other conductances; 3) the technical difficulty of accurately measuring single channel properties; 4) the gap in computational demands necessary to numerically simulate a HH-style model over a stochastic-channel model and 5) a scarcity of both experimental and theoretical studies demonstrating a physiologically-relevant implication or function of the membrane potential noise generated by stochastic ion channel gating. Below we review the main findings from these studies.

Experimental studies of ion channel noise

Although the experimental observation of neuronal noise and variability originally dates to Pecher [1939], the direct study of membrane noise began with Katz and colleagues in the early 1950s who described spontaneous miniature events in the neuromuscular junction [Fatt and Katz, 1950, 1952]. Detailed study of membrane noise in nerve cells continued with Verveen and colleagues in the 1960s [Verveen, 1960, Derksen and Verveen, 1966, Verveen et al., 1967, Verveen and Derksen, 1968], and

numerous others in the 1970s [reviewed by Hille, 1970, Katz and Miledi, 1970, 1971, 1972, DeFelice, 1981].

The experimental studies that specifically examined membrane noise from ion channel fluctuations can be split into two categories:

1. Those where channel noise is combined with fluctuation analysis as an indirect method to measure the gating properties of single ion channels [e.g. Sigworth, 1980].

2. Those which attempt to characterise the features of channel noise to estimate its functional importance.

Here we focus on the latter type (see Alvarez et al., 2002 for a tutorial and further references on fluctuation analysis).

Several experimental studies have focused on the functional implications of ion channel noise. Sigworth [1980] used fluctuation analysis to estimate the number of Na^+ channels at a single frog node of Ranvier as ~ 30000, and subsequently used formulae calculated by Lecar and Nossal [1971a,b] to estimate fluctuations in the current threshold of action potential generation due to channel noise as a $\sim 1\%$ spread, relative to threshold. Johansson and Arhem [1994] found that the stochastic opening of a small number of channels in cultured hippocampal neurons were sufficient to trigger spontaneous action potentials. White et al. [1998] recorded subthreshold membrane potential oscillations in stellate cells of layer II entorhinal cortex (EC) and found that they could only reproduce the co-existence of both oscillations and spiking in a computational model if they included stochastic gating of Na^+ channels, suggesting a form of periodic stochastic resonance. Subsequently, Dorval and White [2005] used the dynamic clamp technique to inject a 'virtual' Na^+ conductance which was either deterministic or stochastic to EC stellate cells in vitro. Only the stochastic conductance could reproduce the observed membrane potential oscillations. Similarly, Dudman and Nolan [2009] used computational models of the same cell type to demonstrate that stochastic channel gating can also account for the clustered firing patterns displayed by these cells when stimulated by steady current pulses in vitro.

Diba et al. [2004] characterised somatic subthreshold voltage noise in cultured hippocampal neurons due to stochastic ion channel gating. In general, voltage fluctuations were small, with a standard deviation <0.3 mV. Noise levels increased upon depolarisation and, based on experiments using pharmacological blockers, appeared to arise

primarily from K^+ channels. Jacobson et al. [2005] reported similar results from neocortical pyramidal cells from layer IV/V of rat somatosensory cortex brain slices, with similar amplitude (submillivolt) voltage fluctuations. However, Jacobson et al. [2005] also suggested that, although ion channel fluctuations were likely the dominant source of low frequency noise in their preparation, synaptic input appeared to be the dominant contributor to membrane noise at frequencies >100 Hz. It is also possible that these results would be different in the in vivo situation where synaptic input is likely to be more prominent than compared to the in vitro slice preparation. Yaron-Jakoubovitch et al. [2008] made simultaneous somatic and dendritic patch-pipette recordings in the same neocortical pyramidal cell type as Jacobson et al. [2005], and found that voltage noise spectra in the dendrite and soma were surprisingly similar, despite the measured differences in local input impedance between the two sites. They argue that this effect can be explained if the noise sources within the neuron are distributed homogeneously. Such an arrangement would ensure approximate isopotentiality throughout the cell, so reducing the heterogeneity in local membrane impedance. We compare this finding to our own simulation results in Chapter 3.

Finally, Kole et al. [2006] used fluctuation analysis to measure the properties and distribution of hyperpolarisation-activated cation (Ih) channels in LV neocortical pyramidal cells in vitro. They found that although the Ih single-channel conductance was exceedingly small (<1 pS), Ih channels likely contribute substantially to voltage noise in the distal dendrites of these cells, for four reasons: 1) Ih channels' relatively slow activation kinetics makes them less susceptible to filtering by the membrane capacitance (see Results); 2) Ih channels were present in large number, increasing the amplitude of their current fluctuations (see Results); 3) Ih channels were mostly present in distal dendrites of the cell where the dendrites' narrow diameters result in a high local membrane impedance, so amplifying voltage fluctuations; 4) because Ih is an inward current which depolarises the cell, it is likely to amplify the current noise from other sources, such as voltage-gated Na^+ channels (see Results).

Theoretical studies of ion channel noise A great deal of theoretical studies have been directed at membrane noise from stochastic ion channels, beginning with Lecar and Nossal, who used stochastic differential equations and a reduced dynamical system model of the action potential to attempt to quantify the magnitude of membrane noise on action potential threshold fluctuations [Lecar and Nossal, 1971a,b]. They compared the contributions from three different intrinsic noise sources: Na^+ channel noise, John-

son noise and excess noise, and, after comparing to experimental data, concluded that measured threshold fluctuations most likely arise from stochastic Na^+ channel gating [Lecar and Nossal, 1971b]. Skaugen and Walløe [1979] were the first to examine the consequences of stochastic gating of ion channels through numerical simulation. They found that in the stochastic version of HH squid giant axon model the current threshold was lowered compared to deterministic models, the membrane could spike spontaneously, and that the frequency-current curve was smeared around the threshold. Subsequent simulation work by DeFelice and colleagues [Clay and DeFelice, 1983, Strassberg and DeFelice, 1993] further elaborated on the direct link between the microscopic (stochastic) and macroscopic (deterministic) versions of the HH model. Rubinstein [1995] simulated a model of the frog node of Ranvier and reproduced the spread in action potential firing threshold due to stochastic channel gating predicted by Lecar and Nossal, in agreement with earlier experiments [Verveen, 1960]. Chow and White [1996] examined the dependence of spontaneous firing rate in the stochastic HH model on membrane patch area and found it to decrease exponentially with area. Interspike intervals were distributed roughly exponentially after a $\sim$ 18 ms gap corresponding to the refractory period, similar to a Poisson process with a dead time. This observation prompted them to analytically approximate the system as a boundary escape problem, with stochastic gating of the activation subunit of the Na^+ channel as the noise source. They calculated the mean escape time as a function of area and found it to agree well with numerical simulation results (we will comment on this finding in the Results).

Schneidman et al. [1998] used numerical simulation to study the reliability and precision of spike timing stochastic HH model. They found that ion channel stochasticity lead to dropping of spikes that appeared in the deterministic simulations, 'spontaneous' spikes that did not appear in the deterministic simulations, and jitter in spike timing ($\sim$ 1 ms). They also demonstrated that spike reliability and precision are increased for fluctuating stimuli of larger amplitude and faster temporal structure. DC stimuli, in contrast, lead to poor spike time precision and reliability, in general agreement with experimental findings [Mainen and Sejnowski, 1995, Nowak et al., 1997] and theoretical arguments [Cecchi et al., 2000].

Manwani and Koch [1999a] used a perturbative approach to estimate the contributions of thermal noise, channel noise and synaptic noise (from Poissonian inputs) to total membrane noise in a single compartment. They found that synaptic noise is likely dominant, but it should be noted that this result will depend on parameter

choices. Steinmetz et al. [2000] used similar methods to demonstrate the voltage and channel type dependence of ion channel noise spectra for both the HH model and a commonly used neocortical pyramidal cell model [Mainen et al., 1995].

The above theoretical studies focused on single-compartment neuron models. The impact of stochastic ion channel gating in spatially extended models of single neurons has received much less attention. The first simple step in this direction is to model an extended but homogeneous cable axon. Such studies of HH cable axons have demonstrated several phenomena: 1) very thin axons can spike spontaneously [Horikawa, 1991, Faisal et al., 2002, 2005]. Faisal et al. [2005] proposed that the emergence of this spontaneous behaviour imposes a practical lower limit of 0.1μm on axon diameters in nature. This prediction corresponded well with anatomical measurements of the thinnest axon diameters in many species (also mentioned by Horikawa, 1991); 2) channel noise introduces variations in spike propagation speed, and hence jitter in timing at the presynapse [Horikawa, 1991, Faisal et al., 2002, Faisal and Laughlin, 2007]; 3) 'splitting' of spike times into multimodal distributions [Faisal and Laughlin, 2007] and 4) occasionally, channel noise may introduce spike failure (<1%; Faisal and Laughlin, 2007).

Manwani and Koch [1999b] used information theory to build a framework for quantifying the effects of ion channel noise, along with other noise sources, on signal propagation from the synapse to the soma via a single passive dendrite.

Few studies have examined the effects of channel noise in multi-compartmental models with realistic dendritic morphologies and active membrane conductances. These factors may enhance the impact of ion channel noise for at least three reasons: 1) dendrites typically have a higher local impedance than at the soma; 2) complex dendritic morphologies introduce additional dimensions for potential non-linear amplification of noise sources and 3) dendrites typically contain ion channels in relatively few numbers. Although this is a poorly understood issue, we here review the existing studies. van Rossum et al. [2003] studied a detailed multicompartmental model of a retinal ganglion cell and found that 1) channel noise had a substantial impact on spike timing, particularly for tonic stimuli; 2) the model with detailed dendritic morphology displayed greater channel noise effects than a spherical model of equivalent total surface area and 3) the simple presence of dendrites increased timing variability from synaptic stimulation, due to nonlinear dendritic events. Diba et al. [2006] modeled action potential backpropagation into the dendritic tree of a reconstructed neocortical pyramidal neuron, and found channel noise to have little impact on its reliability or timing. They

did, however, note that channel noise introduced substantial variability into dendritic spike generation. Kole et al. [2006] used a multicompartmental model of a neocortical LV pyramidal neuron to demonstrate that stochastic ion channel gating introduced jitter and unreliability into spike timing from a synaptic stimulation in the apical dendrite. Despite these studies, the exact impact of dendritic morphology on channel noise effects remain unclear (to be studied in Chapter 3).

Finally, there has been much controversy in the literature regarding the use of approximate mathematical models of stochastic ion channel gating using stochastic differential equations (SDEs). SDE methods may be useful because they would be much computationally cheaper to implement than the alternative full 'exact' numerical simulations when large numbers of ion channels must be taken into account. Additionally, the SDE description carries the potential benefit of facilitating further analytical study [e.g. Lecar and Nossal, 1971a,b, Chow and White, 1996], although their complexity has limited this use thus far. The disagreements have arisen on the accuracy of the SDE methods in reproducing the behaviour of full Markov numerical simulations [Mino et al., 2002]. It is likely that there are three main reasons for the discrepancy: 1) the Langevin approximation as formulated by Fox and Lu [1994], Fox [1997] systematically underestimates ion channel variability [Bruce, 2009, Sengupta et al., 2010] [although see Goldwyn et al., 2010, Linaro et al., 2011, for improved methods]; 2) the approximate models typically assume Gaussian conductance fluctuation distributions which may not exactly match the actual binomial statistics, particularly at subthreshold voltages where the open probability for many channel types is close to zero [Hille, 2001] and 3) most SDE models assume that the channel fluctuation amplitude varies instantaneously with the membrane potential, whereas in the full scheme the fluctuations of slow-gating current are most likely to lag membrane potential dynamics. Because of the recent development of an efficient Monte Carlo simulator (PSICS) which dramatically reduces the need for the speedups afforded by the SDE models, we restrict our work to full numerical simulation of complete ion channel models with Markovian kinetics. Although in principle these simulations can be arbitrarily accurate, their quantitative predictions on the behaviour of real ion channel populations are mostly limited by the experimental difficulty of accurately measuring channel transition rates to constrain the models in the first instance.

2.1.3 Spontaneous activity in peripheral neurons involved in neuropathic pain

We apply our stochastic channel findings to a clinically relevant problem: the spontaneous firing of peripheral nerves in neuropathic pain conditions. Here we review peripheral nerve physiology — first in health, then in disease.

Healthy peripheral nerve organisation and sensory signal transduction. Peripheral signal transduction from environment to brain proceeds as follows [Julius and McCleskey, 2006]. Stimuli are first detected by receptors at the nerve terminals, embedded in the skin, for example. The activated receptors pass an ionic current into the nerve terminal contributing to a 'generator potential'. When this potential is sufficiently depolarised to recruit enough Na^+ channels, an action potential is triggered. The AP propagates down the nerve, via the dorsal root ganglion (DRG) where the cell body is located, to eventually activate synapses at nerves in the dorsal horn of the spinal cord which subsequently relays information to the brain.

Peripheral afferent nerves can provide different modes of information to the brain: temperature, mechanical stimulation and the presence of noxious chemicals [reviewed by Meyer et al., 2006]. A subpopulation of these fibres are responsive to gentle cutaneous stimuli such as cooling, warmth and touch (texture, shape). The remainder respond to stimuli of a higher intensity that might produce injury and pain. These fibres are hence termed nociceptors (receptors for noxious stimuli). Unlike most sensory nerves, nociceptors typically respond to multiple types of stimuli: thermal, mechanical and chemical. Nociceptors are generally divided into two broad classes (there are also further subclasses): the thicker, myelinated A-fibres with fast conduction velocity (>2m/s), and thinner (<2μm diameter), unmyelinated C-fibres with slow conduction velocity (<2m/s). A-fibres are responsible for fast, sharp pain sensation to acute stimuli. They are capable of sustained regular firing at moderate rates (>10 Hz). C-fibres, in contrast, mediate slower 'burning' pain sensations. They often fire at low rates (1–5 Hz) with more irregularity. We will focus exclusively on C-fibres, because the dysregulation of their anatomical properties and ion channel composition during neuropathic pain states make them likely candidates to be affected by membrane noise from stochastic ion channel gating.

Spontaneous activity in peripheral nerves linked to pain. Neuropathic pain refers to pain that originates from pathologies of the nervous system [Campbell and Meyer, 2006]. There are many different trauma and disorders that lead to neuropathic pain conditions in humans [Scadding and Koltzeburg, 2006]. The range of potential sites of abnormality underlying various pain conditions are also numerous [adapted from Campbell and Meyer, 2006]:

1. Spontaneous activity can emerge from the site of injury [Blumberg and Jänig, 1984, Meyer et al., 1985] due to both nociceptor sensitisation and ion channel dysregulation.

2. The nerve cell body in the DRG can change its expression of different ion channels, mediating hyperexcitability [Cummins and Waxman, 1997].

3. Denervation of the injured fibres leads to release of growth factors and cytokines, which interact with surviving nerves.

4. Uninjured nerves often reinnervate the skin area left by the injured nerve and have been found to develop spontaneous activity [Wu et al., 2001], and sensitisation of the nociceptors.

5. Pre- and post-synaptic sensitisation can develop in the dorsal horn due to abnormal input from the site of injury.

6. Descending modulatory mechanisms from the cortex and thalamus can regulate the excitability of dorsal horns neurons.

7. Both peripheral and central immune responses to injury can directly act on pain pathways.

We focus here on the first two mechanisms from this list because they are most closely related to ion channel gating.

Spontaneous firing is found to originate from site of injury [Blumberg and Jänig, 1984], both from A-fibres and C-fibres. Although A-fibres fire rhythmically at brisk rates, firing rates of C-fibres are extremely low (<1 Hz), and individual spike timing irregular [Blumberg and Jänig, 1984, Xiao and Bennett, 2007]. Both of these C-fibre features are consistent with a noise driven process. Spontaneous activity in thin peripheral fibres has been linked, in animal models, to ongoing spontaneous pain [Djouhri

et al., 2006]. *We propose that the spontaneous events in C-fibres are driven by membrane noise from stochastic ion channel gating.*

We now review mechanisms which might be important for membrane noise from stochastic ion channel gating: 1) ion channel regulation and 2) anatomical factors influencing electrical properties.

Na^+ channels are perhaps the most obvious candidates for inducing changes in excitability because of their regenerative depolarising effects on membrane potential. Peripheral nerves can express at least six of the nine Na^+ channel alpha subunits found in neural tissue ($Na_V1.1$, $Na_V1.3$, $Na_V1.6$–1.9; Dib-Hajj et al., 2010). Individual cells can even express five different Na^+ subunits simultaneously — more than any other known cell type in the nervous system. We here briefly mention the function of four prominent types: $Na_V1.3$, $Na_V1.7$, $Na_V1.8$ and $Na_V1.9$ [reviewed by Dib-Hajj et al., 2010].

Na_V1.3 is a TTX-sensitive channel subunit which is widely expressed in the peripheral nervous system during embryogenesis, but then disappears in adulthood in DRG neurons. However, injury to neurons causes an upregulation of $Na_V1.3$, even in adulthood, and is found at the distal tips of painful neuromas [Black et al., 2008]. The channel rapidly inactivates, and is thought to amplify small depolarising inputs.

Na_V1.7 is a TTX-sensitive channel subunit which is preferentially expressed in DRG and sympathetic ganglion neurons. It produces a fast activating and inactivating current which is believed to amplify generator potentials and gate action potential generation. The subunit is strongly implicated in pain in humans because mutations to its gene, *SCN9A*, have been discovered in certain families with hereditary pain disorders. Dominant gain-of-function mutations have been linked to severe pain disorders, while a recessive loss-of-function mutation has been linked to congenital insensitivity to pain (along with muted olfaction) [Dib-Hajj et al., 2007].

Na_V1.8 is a TTX-resistant channel subunit that is expressed exclusively in DRG neurons, and primarily in nociceptive neurons. This makes it an attractive potential target for therapeutic drug intervention. The current provides the main driving force for the upswing of the action potential in DRG neurons, particularly during repetitive firing. Its regulation during pain states is, however, unclear.

$Na_V1.9$ is a TTX-resistant channel subunit that is selectively expressed in small-diameter DRG neurons, most of which are nociceptors. Because it has relatively hyperpolarised activation levels, and only very slowly inactivates, it is believed to underlie a persistent Na^+ current that sets the resting membrane properties of these neurons. Although its regulation has been implicated in inflammatory pain, its role in neuropathic pain conditions is less clear.

Much less is known about the roles of other channel types in peripheral nerves during neuropathic pain, but it is likely that at least K^+ channels are important [Cregg et al., 2010].

It is possible that neuroanatomical factors could also influence excitability of peripheral nerves. Basic cable theory dictates that the input resistance at a fibre terminal depends primarily on four factors: cable diameter, cable length, membrane conductances, and the axoplasmic resistivity. For a very long passive cable (much longer than the electrotonic length) the steady state input resistance R_{in} (Ω) at the terminal is given by [Rall, 1959, Koch, 1999]

$$R_{in} = \frac{2\sqrt{R_m r_a}}{\pi d^{3/2}}$$

where R_m is the specific membrane resistance (Ωcm^2), r_a is the axoplasmic resistivity (Ωcm), and d is the cable diameter (μm). Note that input resistance is inversely related to cable diameter. The diameters of regenerated nerve terminals are found to be narrower than comparable fibres from control animals [Dyck and Hopkins, 1972]. Hence, regenerated nerves likely have an elevated membrane impedance leading to amplification of voltage changes from ion channel currents. Consistent with this, compression of the dorsal root ganglion induces spontaneous activity [Howe et al., 1977, Sugawara et al., 1996]. Hence, changes in nerve anatomy could enhance the propensity for spontaneous activity in thin peripheral nerves.

The aims of this study are to:

- Clarify which properties of ion channel gating are most crucial for determining the magnitude of current noise from voltage-gated ion channels.
- Study the factors underlying spontaneous action potential generation in single-compartment and cable axon models.
- Examine whether this is a plausible candidate mechanism which might underlie

the spontaneous activity observed in thin peripheral nerves during several neuropathic pain states.

2.2 Methods

All simulations implemented using the Parallel Stochastic Ion Channel Simulator (PSICS) because it is specifically designed for efficient simulations of stochastic ion channel gating in single neuron models. See Cannon et al. [2010] and http://psics.org/ for algorithmic details. Analysis done using Matlab (The Mathworks) and Igor Pro (Wavemetrics).

Hodgkin-Huxley models

All simulations of the Hodgkin-Huxley model used standard versions of the voltage-dependent equations for Na^+ and K^+ subunit gating schemes, at 6.3°C [Hodgkin and Huxley, 1952].

The classic continuous formalism for an ion channel population models conductances as

$$g_i(V,t) = \bar{g}_i m^j h^k$$

where $g_i(V,t)$ is the ith voltage and time-dependent conductance, $\bar{g}_i$ is maximal conductance through this ion channel population, m and h are activation and inactivation gating variables respectively, and j and k are the number of activation and inactivation gates, respectively. m and h are continuous and deterministic variables which evolve according to the first-order ODEs

$$\frac{dm}{dt} = \frac{m_\infty(V) - m}{\tau_m(V)}$$

$$\frac{dh}{dt} = \frac{h_\infty(V) - h}{\tau_h(V)}$$

where $m_\infty(V)$ and $h_\infty(V)$ are the steady-state values for the activation and inactivation variables, respectively, and τ_m and τ_h are time constants of activation an inactivation respectively. These in turn are dependent on the voltage-dependent transition rates by

$$m_\infty(V) = \frac{\alpha_m}{\alpha_m + \beta_m}$$

$$h_\infty(V) = \frac{\alpha_h}{\alpha_h + \beta_h}$$

and

$$\tau_m = \frac{1}{\alpha_m + \beta_m}$$

$$\tau_h = \frac{1}{\alpha_h + \beta_h}$$

In the HH squid axon model, the Na^+ conductance has three activation subunits, m, and one inactivating subunit, h. The K^+ conductance has four activation subunits, n. The voltage-dependencies of the transition rates for the HH m, h and n gating variables, $\alpha_{m,h,n}$ and $\beta_{m,h,n}$ are given by

$$\alpha_m(V) = \frac{0.1(V+40)}{1-e^{-(V+40)/10}} \qquad \beta_m(V) = 4e^{-(V+65)/18}$$

$$\alpha_h(V) = 0.07e^{-(V+65)/20} \qquad \beta_h(V) = \frac{1}{1+e^{-(V+35)/10}}$$

$$\alpha_n(V) = \frac{0.01(V+55)}{1-e^{-(V+55)/10}} \qquad \beta_n(V) = 0.125e^{-(V+65)/80}$$

where V is membrane voltage in mV and the transition rates have units $1/\text{ms}$.

We convert these deterministic models to a discrete stochastic channel gating model in two steps. First, the HH gating variables (e.g. m, h and n in the squid giant axon model) are changed from representing the fractional macroscopic conductances through a population of ion channels to the microscopic probability of a single ion channel being in a particular state (e.g. either open or closed). Now, a single ion channel can be thought of as containing four independently gating two-state subunits. The channel is open only if all four subunits are simultaneously open. Each subunit may transition probabilistically between states with transition rates specified by the macroscopic voltage-dependent kinetic schemes. For example, a single HH K^+ channel model might look like:

$$\begin{array}{cccc} O & O & O & O \\ \updownarrow & \updownarrow & \updownarrow & \updownarrow \\ C & C & C & C \end{array}$$

where C and O represent the subunit's open and closed states, respectively. The probability that a subunit switches from closed to open during a short time interval Δt is $p(C \to O, \Delta t) = \alpha_n(V)\Delta t$. Similarly, the probability that an open subunit switches to closed during Δt is $p(O \to C, \Delta t) = \beta_n(V)\Delta t$.

The second step involves reformulating the single channel state-diagram from one containing multiple independent complexes to an equivalent single-complex scheme.

C_m	Membrane capacitance	1 μF/cm^2
r_a	Axial resistivity	35 Ωcm
γ_{Na}	Na^+ single-channel conductance	20 pS
ρ_{Na}	Na^+ channel density	60 /μm^2
E_{Na}	Na^+ reversal potential	+50 mV
γ_K	K^+ single-channel conductance	20 pS
ρ_K	K^+ channel density	18 /μm^2
E_K	K^+ reversal potential	-77 mV
ρ_{Leak}	Leak conductance density	3 pS/μm^2
E_{Leak}	Leak reversal potential	-55 mV
V_m	Resting membrane potential	-65 mV

Table 2.2: Parameters for Hodgkin-Huxley model simulations.

If we assume that each K^+ channel subunit is identical then we can rewrite the state diagram as

$$n_0 \underset{\beta}{\overset{4\alpha}{\rightleftharpoons}} n_1 \underset{2\beta}{\overset{3\alpha}{\rightleftharpoons}} n_2 \underset{3\beta}{\overset{2\alpha}{\rightleftharpoons}} n_3 \underset{4\beta}{\overset{\alpha}{\rightleftharpoons}} n_4$$

where the subscript on each state indicates the number of open subunits. Note that the transition rates are also scaled to reflect the relative numbers of subunits in each state. In this scheme, only the n_4 state is 'open' (and hence conducting), while all others are 'closed'. Although not strictly necessary, this step ensures more efficient simulations because it reduces the number of random numbers necessary for each time step. In addition, the single-complex formalism allows for more complicated channel gating schemes where subunits are not independent.

In all presented simulations the single channel conductance for both Na^+ and K^+ was 20 pS. Although this value is close to that reported experimentally for the squid giant axon K^+ conductance [Llano et al., 1988], it is slightly larger than estimates for the Na^+ conductance [Bezanilla, 1987]. These values were chosen for simplicity (it removes one confounding factor when comparing channel type noise contributions) and to enable comparison with the literature [Strassberg and DeFelice, 1993, Chow and White, 1996, Schneidman et al., 1998]. Leak channels were modelled deterministically equivalent to Hodgkin and Huxley [1952]. Full parameters are given in Table 2.2.

Dorsal root ganglion cell models

Our DRG model was adapted from a previously published small DRG neuron model [Sheets et al., 2007]. The model included two Na^+ current types ($Na_V1.7$ and $Na_V1.8$), a delayed rectifier K^+ current (underlying the downswing of the action potential), a transient A-type K^+current and a leak conductance. Although small DRG neurons do express other Na^+ (and possibly K^+) channel types [Black et al., 2008], these populations account for the majority of membrane current flow. Single channel conductances in all models were set to 20 pS for simplicity. It is likely that in reality these ion channels have single-channel conductances from a range of parameters [Hille, 2001], but at present the single-channel properties for these Na^+ channels remain unknown [Catterall et al., 2005]. In particular, channels that have not been well quantified, such a weakly voltage-gated leak channels, may have large single-channel conductances and might so contribute substantially to membrane voltage noise [Hille, 2001].

2.3 Results

2.3.1 Stochastic potassium channel gating can trigger spontaneous action potentials

Previously, it has been demonstrated that a Hodgkin-Huxley (HH) type neural model with discrete Markovian stochastic ion channels instead of the classic continuous deterministic rate equations can fire spontaneous action potentials if the membrane patch is small [Skaugen and Walløe, 1979, Clay and DeFelice, 1983, Strassberg and DeFelice, 1993, Chow and White, 1996, Schneidman et al., 1998]. However, the relative contributions of the Na^+ and K^+ channel populations to spontaneous activity are less well understood. To investigate, we simulate the HH squid axon model using the PSICS simulator [Cannon et al., 2010] with stochastic Markovian ion channels while varying the membrane patch area under three different conditions: first, both sodium (Na^+) and potassium (K^+) channels stochastic ('all stochastic'), second, Na^+ stochastic but K^+ deterministic, and third, Na^+ deterministic but K^+ stochastic. Leak channels were deterministic in all conditions. Comparing the spontaneous firing rate between the three conditions allows us to find whether Na^+ or K^+ channels contribute most to spontaneous activity.

As observed previously [Chow and White, 1996], if a fixed density of ion channels is assumed, then firing rate depends on the membrane surface area. Firing rate decreases approximately exponentially with increasing membrane patch area (Figure 2.2) such that membrane areas greater than $\sim$400 μm^2 produced almost no spontaneous action potentials, similar to the deterministic model. This exponential dependence of spontaneous rate with membrane area is consistent with a stochastic barrier-escape problem [Chow and White, 1996].

When either Na^+ or K^+ channels are switched to deterministic mode, spontaneous firing rate is reduced compared to the all stochastic mode. Surprisingly, however, stochastic K^+-channel gating alone triggers greater spontaneous firing rates than stochastic Na^+-channel gating alone (Figure 2.2b). At first impression, this result might be counter-intuitive because the opening of Na^+ channels is necessary for the initiation phase of an action potential, while K^+channels are conventionally considered responsible for the repolarising phase. A simple conceptual model for spontaneous spike generation might therefore be that the chance opening of a few Na^+ channels depolarises the membrane and activates the runaway Na^+channel opening underlying

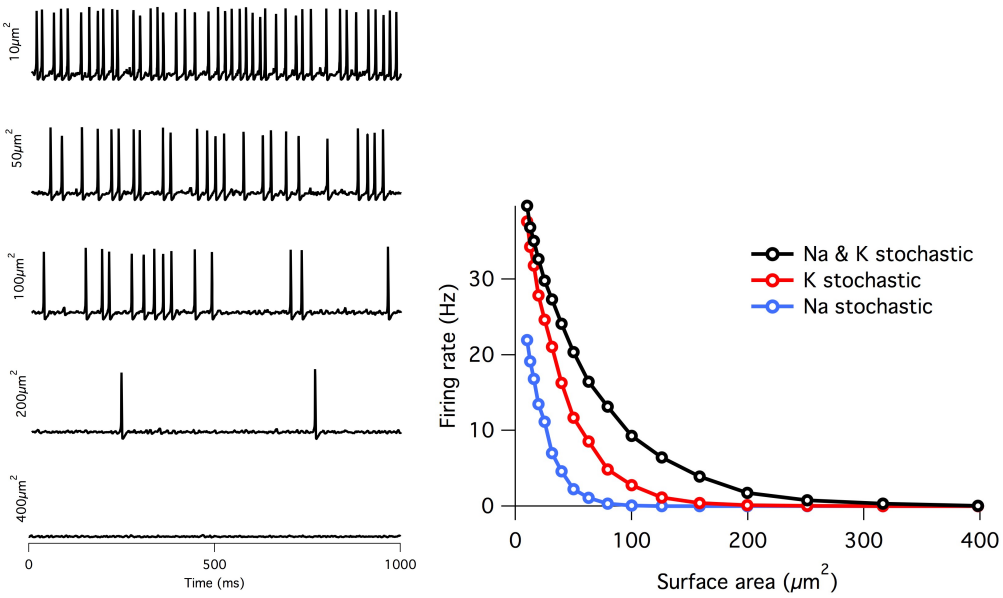

Figure 2.2: Spontaneous action potentials in an isopotential HH model. **a**: Example membrane potential traces from the single compartment stochastic HH model of varying membrane surface areas. **b**: Spontaneous firing rate decreases approximately exponentially with increasing surface area. Firing rates at all areas were greater for the 'all stochastic' model (black) than the K^+ stochastic model (red), which was in turn greater than the Na^+ stochastic model (blue).

the action potential. However, stochastic *closure* of K^+ channels would also depolarise the membrane, similarly activating Na^+ channels to trigger an action potential. We test this possibility by examining in more detail the dynamics of Na^+ and K^+ currents. We adapt a measure from the neural coding literature called the 'spike-triggered average' (STA) [Dayan and Abbott, 2001]. Our STA, $I_x^{STA}(\tau)$, is the average total current of the ion channel population x at time interval τ prior to a spontaneous action potential at time t_i over n such events,

$$I_x^{STA}(\tau) = \frac{1}{n}\left[\sum I_x(t_i - \tau)\right]$$

We find that the STA potassium current, I_K^{STA}, drops when $1 < \tau < 5$ ms, while there is a parallel increase in the STA sodium current I_{Na}^{STA}. The drop in I_K^{STA} precedes the increase in I_{Na}^{STA} (Figure 2.3a), indicating that spontaneous action potential firing in this model is primarily driven by K^+ channel fluctuations, not Na^+ noise, as assumed previously [Chow and White, 1996].

We test this explanation by simulating K^+ channel conductance in deterministic mode and repeating the STA measurement (dashed curves, Figure 2.3a). As predicted, in this case we find that spontaneous spikes are not preceded by a drop in K^+ conductance, but instead driven by an elevated Na^+ conductance fluctuation.

Following the initial phase of spike generation, both Na^+ and K^+ currents grow rapidly as the action potential forms: I_{Na}^{STA} increases because many Na^+ channels are opening due to depolarisation, and I_K^{STA} increases both because of K^+ channels (slowly) opening due to depolarisation and because the driving force for K^+ channels is increasing as the membrane potential moves away from the K^+ reversal potential.

Further examination of the trial-to-trial Na^+ and K^+ currents shows that the conclusions drawn from the STA measurement are also representative of single trials. In Figure 2.3b we plot the change in I_{Na} and I_K between 7.5 and 2.5ms prior to each recorded action potential for the 'all stochastic' model. We see that the majority of points fall in the lower-left quadrant, corresponding to a drop in I_K and increase in I_{Na}. If we draw the identity line $I_{Na} = I_K$ over the same graph, we can group the data into two categories: points north-west of the line correspond to action potentials that were primarily driven by a drop in I_K, while points south-east of the line correspond to action potentials driven by increases in I_{Na}. Most (64.5%) action potentials are K^+-driven.

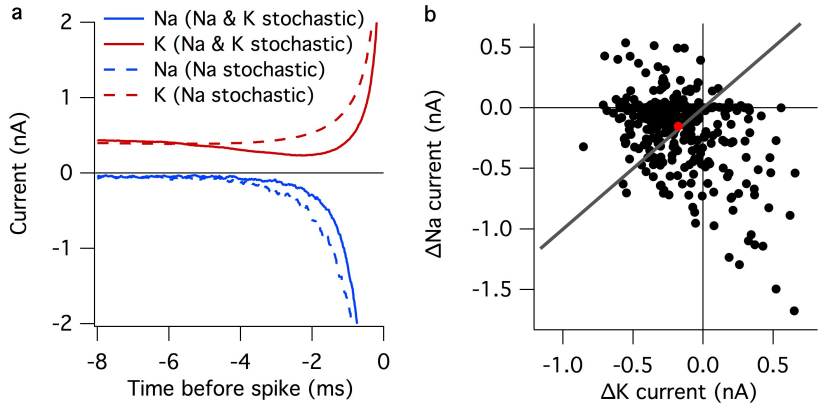

Figure 2.3: Spike-triggered averaged Na^+ and K^+ currents preceding a spontaneous action potential. **a**: STA currents (see text) from Na^+ and K^+ channels in a 10 μm^2 surface area compartment. All stochastic curves in solid and the Na^+-only stochastic in dashed. **b**: Change in Na^+ current (vertical axis) vs change in K^+ current (horizontal axis) for many individual spikes between 7.5 ms and 2.5 ms before a spontaneous action potential. Red dot indicates mean. Grey line denotes identity where $\Delta I_{Na} = \Delta I_K$.

2.3.2 The factors determining a conductance's contribution to membrane noise

What properties of the HH K^+ conductance cause it to trigger more spontaneous action potentials than the Na^+ conductance? There are at least six possible factors that can determine a channel populations' contribution to membrane noise, which we examine in turn.

1. Open probability

First, Na^+ and K^+ have different steady-state open probabilities (p_o) at resting membrane potential. The steady-state probability of a single ion channel being open is identical to the steady-state permeability fraction of the corresponding macroscopic conductance in the classic HH formalism. In the case of the HH Na^+ conductance this is obtained from the product of the steady-state values of the m_∞ and h_∞ gating variables:

$$g_{Na\infty} = \bar{g}_{Na}(m_\infty)^3 h_\infty$$

where $\bar{g}_{Na}$ is the maximal conductance through the Na^+ channel population. Hence the open probability $p_o = (m_\infty)^3 h_\infty$. The gating variables m_∞ and h_∞ can in turn be

expressed in terms of the forward and backward gating rates $\alpha_{m/h}$ and $\beta_{m/h}$ as

$$m_\infty(V) = \frac{\alpha_m(V)}{\alpha_m(V) + \beta_m(V)}$$

$$h_\infty(V) = \frac{\alpha_h(V)}{\alpha_h(V) + \beta_h(V)}$$

The steady-state K^+ permeability is similarly given by $g_{K\infty} = \bar{g}_K(n_\infty)^4$ so that $p_o = (n_\infty)^4$. At the resting potential of -65 mV in the HH squid axon model, the steady-state open probabilities are $\sim$0.0001 and $\sim$0.01 for the Na^+ and K^+ channels, respectively. A simple binomial model of an ion channel predicts that the variance in the single channel current $\sigma_i^2 = i^2 p_o(1-p_o)$, where i is the single-channel current. The variance is parabolic in p_o: zero when $p_o = 0$ or 1, and maximal when $p_o = 0.5$ (Figure 2.4). Below spike threshold, most ion channels have open probabilities < 0.5. In this range, the variance increases with increasing p_o. Therefore, ion channel populations with greater p_o at resting membrane potential tend to have larger current fluctuations than populations with lesser p_o. This factor predicts greater K^+ channel noise than Na^+ channel noise,

$$\frac{\sigma_{iK}^2}{\sigma_{iNa}^2} \approx \frac{i_K^2}{i_{Na}^2}\frac{0.01}{0.0001} = \frac{i_K^2}{i_{Na}^2} \times 100$$

2. Number of channels

Second, because in the binomial model the number of channels in the population, N, is proportional to the variance, σ_o^2, channel populations with greater N have greater fluctuations in their absolute number of open channels (Figure 2.4). The standard deviation of the number of open channels, σ_o — a more common measure of the width of a distribution — grows proportional to $\sqrt{N}$. If we assume identical single-channel conductance, the Na^+ population has 3.33$\times$ more channels in the standard HH model than the K^+ population (Table 2.2), favouring greater fluctuations in Na^+ channel open numbers.

3. Driving force

The third factor is the differences in driving force for each conductance. As we assume that these ion channel current-conductance relationships are Ohmic (linear), then the current through an open channel is proportional to the difference between the membrane potential and the channel's driving force,

$$i_x = \gamma_x(V_m - E_x)$$

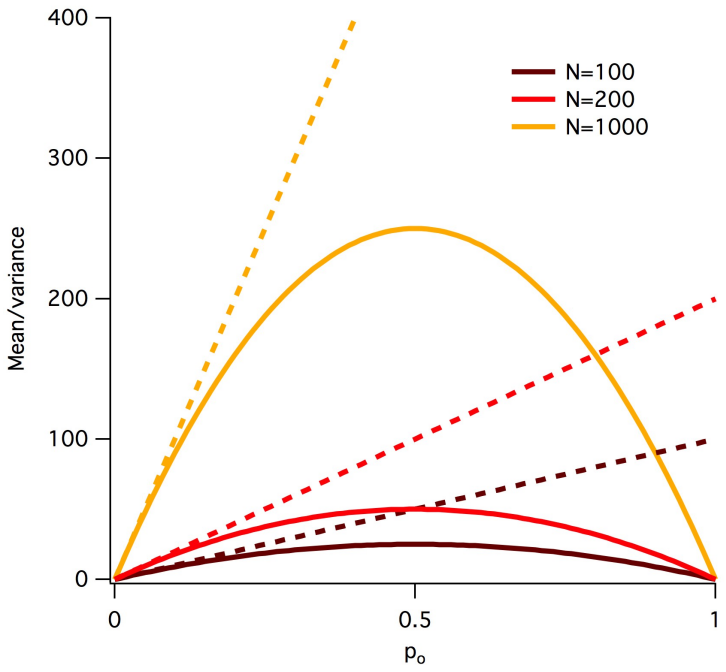

Figure 2.4: Binomial distributions predict greater fluctuations for ion channels with p closer to 0.5. Mean (dashed line) and variance (solid curve) in the number of open channels as function of open probability p_o for N=100, 200 and 1000.

where i_x is the single-channel current, γ_x is the single-channel conductance, V_m is the membrane potential and E_x is the conductance's reversal potential, given by the Nernst equation. In the HH model, $E_{Na} = +50$ mV, $E_K = -77$ mV, and $V_{rest} = -65$ mV, giving Na^+ a driving force of +115 mV and K^+ a driving force of -12 mV. This means that the single-channel Na^+ current is about $10\times$ greater than the K^+ current at V_{rest}, assuming identical γ_x.

4. Single-channel conductance

Fourth, the single-channel conductance γ_x is another important factor determining a channel's contribution to membrane noise. For the same channel population current per unit squared cell membrane, a larger γ_x implies smaller N, and a larger i_x. Both of these factors increase current fluctuations relative to an equivalent deterministic model. In our implementation of the HH model, however, we assume the same single-channel conductance for both Na^+ and K^+ (20 pS).

These four factors can be put together to construct a binomial model of the amplitude of channel noise at steady state. This model does not have any notion of dynamics or channel kinetics. We calculate the steady-state open probabilities directly from the

Hodgkin-Huxley equations, and use them to test the binomial model's ability to reproduce simulated voltage-clamp data and probe its predictions on the relative magnitudes of Na^+ and K^+ channel noise (Figure 2.5).

We find that, as expected, the binomial model exactly predicts the conductance and current fluctuations from voltage-clamp simulation data at resting potential of -65 mV (Figure 2.5c,f). We use the binomial model to estimate the steady-state variance in open channel numbers and total current from the Na^+ and K^+ populations at a range of membrane potentials (Figure 2.5a–b,d–e). Although the variance (and hence noise) in the number of open channels is greater for the K^+ population than the Na^+ population, the Na^+ current variance is greater than the K^+ current. This is due to the great difference in their driving potentials (115 mV for Na^+ vs 12 mV for K^+). Hence, the binomial model predicts that the amplitude of current noise from the Na^+ channel population is greater than that from the K^+ channel population. This prediction is at odds with our simulation results that K^+ channel noise contributes more to spontaneous action potential generation than Na^+ noise. We resolve this discrepancy in the next section.

5. Channel gating kinetics

The fifth factor (not included in the above binomial model) is that the Na^+ and K^+ conductances have different gating kinetics. These differences are important because the current fluctuations from the ion channel populations are differentially filtered through the membrane impedance, hence potentially altering each channel's contributions to membrane voltage noise. One measure of the characteristic timescale(s) of a conductance is given by $\tau_i = \frac{1}{\alpha_i+\beta_i}$, where α_i and β_i are the conductance gate's forward and backward transitions rates, respectively. At -65 mV $\tau_m \sim 0.24$ ms (sodium activation), $\tau_h \sim 8.5$ ms (sodium inactivation), and $\tau_n \sim 5.5$ ms (potassium activation). A linearisation of the HH membrane equation at resting potential (-65 mV) gives a membrane time constant $\tau_V \sim 1.4$ ms [Chow and White, 1996]. Because $\tau_V > \tau_m$, we might expect Na^+ channel fluctuations to be substantially filtered by the membrane impedance. A detailed exploration of this issue, however, requires examination of each channel population's current noise power spectrum and the membrane impedance.

The voltage noise power spectrum $S_V(\omega)$ is given by a generalisation of Ohm's law:

$$S_V(\omega) = S_I(\omega)|Z(\omega)|^2$$

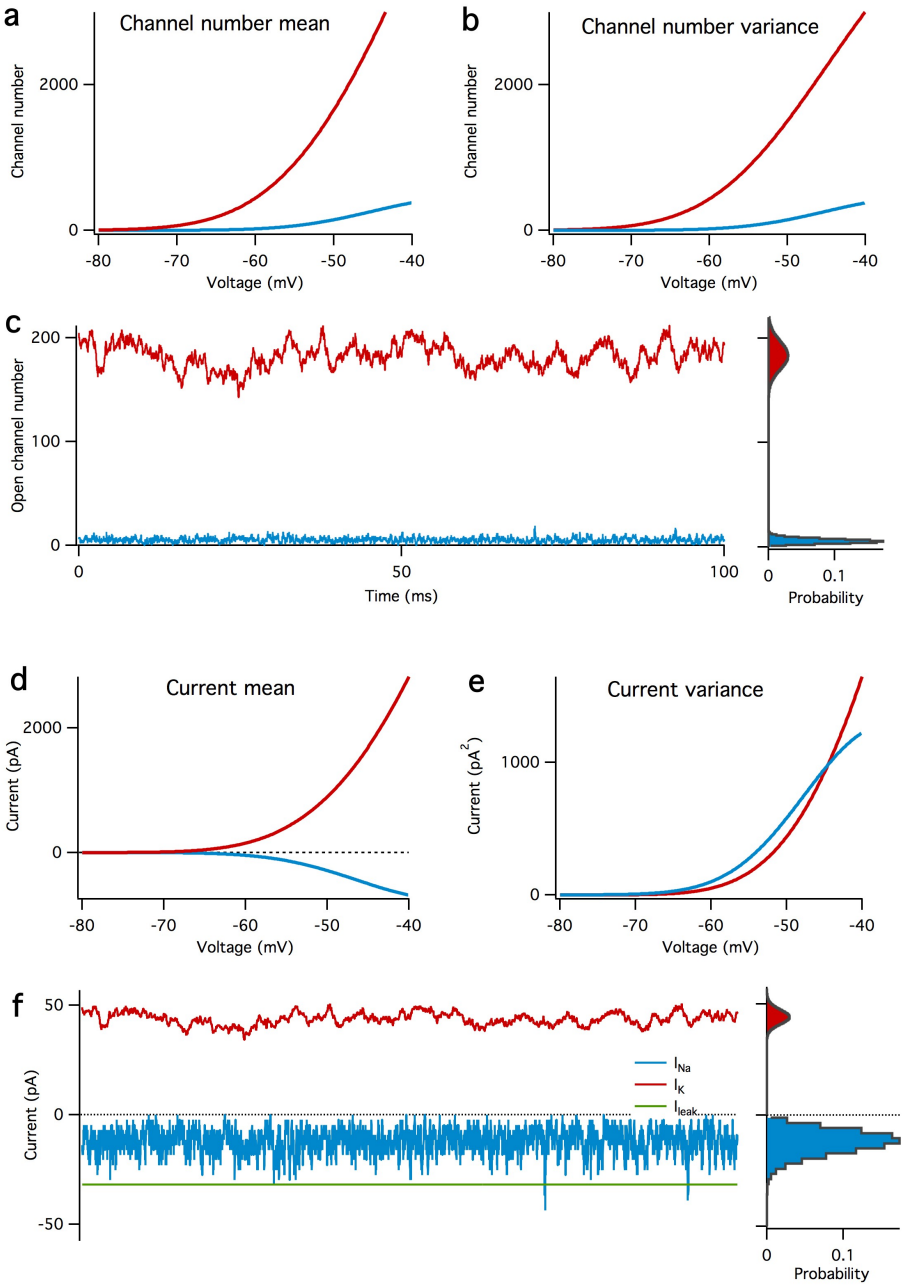

Figure 2.5: A binomial model reproduces the steady-state features of simulated voltage clamp data at -65 mV. **a**: mean number of open channels as function of voltage for Na^+ (blue) and K^+ (red) HH conductances. **b**: Variance in number of open channels for conductances in *a*. **c**: Example time series of Na^+ and K^+ open channels numbers from voltage-clamp simulation at resting potential (left) with histogram of open channel numbers (right). Grey curves on histograms are binomial prediction. **d-f**: Similar figures as *a-c* but for total channel population currents instead of open numbers.

where $S_I(\omega)$ is the power spectrum of a current noise source, $Z(\omega)$ is the membrane impedance and $\omega = 2\pi f$, where f is the frequency in Hz. The membrane impedance's frequency dependence is shaped both by the membrane capacitance and the properties of the total set of membrane ion channels [Katz and Miledi, 1972, DeFelice, 1981, Koch, 1999]. As an example, we will calculate the membrane impedance of the simplest case, the passive (linear) membrane. Here, the current-balance membrane equation is given by

$$\tau \frac{dV}{dt} = -V(t) + RI_{in}(t)$$

where $\tau = RC$ is the membrane time constant, $V(t)$ is the voltage relative to resting membrane potential, R is the input resistance and $I_{in}(t)$ is an injected current. For instance, we can imagine the injected current as a sinusoidal function of time at some frequency f_c, so $I_{in}(t) = \sin(2\pi f_c t)$. The voltage response in the frequency domain, $\tilde{V}(f)$, is obtained by taking the Fourier transform of the current-balance equation:

$$\begin{aligned}
\tau \int_{-\infty}^{\infty} \frac{dV}{dt} e^{-i2\pi ft} dt &= -\tilde{V}(f) + R\tilde{I}(f) \\
i2\pi f\tau \tilde{V}(f) &= -\tilde{V}(f) + R\tilde{I}(f) \\
\tilde{V}(f)\,(1 + i2\pi f\tau) &= R\tilde{I}(f) \\
\tilde{V}(f) &= \frac{R\tilde{I}(f)}{1 + i2\pi f\tau}
\end{aligned}$$

Then the complex input impedance is given by the ratio of voltage response to input current

$$Z(f) = \frac{\tilde{V}(f)}{\tilde{I}(f)} = \frac{R}{1 + i2\pi f\tau}$$

Since we are interested here only in the magnitude of the response as a function of frequency (not the phase shift), we take the absolute value of $Z(f)$

$$|Z(f)| = \frac{R}{\sqrt{1 + (2\pi f\tau)^2}}$$

Note that if $f = 0$, as for a DC signal, then $|Z(f)| = R$. We also see that if f is large, then $|Z(f)| \propto 1/f$. Hence, the capacitance acts as a low-pass filter with a $1/f$ dropoff at high frequencies. It attenuates high-frequency current fluctuations [Katz and Miledi, 1972, DeFelice, 1981].

Although this analysis ignores the contribution of voltage-dependent conductances to the impedance, it is straightforward to calculate their additional contribution numerically. We use a built-in function in the NEURON simulator [Carnevale and Hines, 2006]. In the HH model at V_{rest}, the presence of Na^+ and K^+ conductances introduce

a resonance into the impedance at ~ 100 Hz, but the $1/f$ behaviour still dominates at higher frequencies (Figure 2.6c). The resonant peak in the impedance is the electrical signature of an inductor. Although such an inductor has no physical counterpart in the biological cell membrane, small signals from active ion channels that oppose changes in membrane potential can sometimes behave as phenomenological inductances [Mauro et al., 1970, Koch, 1984, 1999]. In the HH model, this role is played by the delayed-rectifier K^+ channels.

We can calculate the current noise power spectrum from a population of ion channels directly from the channel kinetic scheme by first calculating the population's autocovariance function. The conditional probability that a two-state channel is open at time t given that it was open at time 0, $p_{o|o}(t)$ is [DeFelice, 1981]

$$p_{o|o}(t) = p_\infty + (1 - p_\infty)e^{-t/\tau}$$

where p_∞ is the steady-state open probability $p_\infty = \frac{\alpha}{\alpha+\beta}$. The autocorrelation $R_o = p_\infty p_{o|o}$. The autocovariance of the channel $C_o(t)$ can then be written as

$$\begin{aligned} C_o(t) &= \langle [p_o(t_0) - p_\infty]\,[p_o(t) - p_\infty] \rangle \\ &= \langle p_o(t_0) p_o(t) \rangle - p_\infty^2 \\ &= R_o - p_\infty^2 \\ &= p_\infty p_{o|o} - p_\infty^2 \\ &= p_\infty \left(p_\infty + (1 - p_\infty)e^{-t/\tau} \right) - p_\infty^2 \\ &= p_\infty (1 - p_\infty) e^{-t/\tau} \end{aligned}$$

The autocovariance $C_N(t)$ of the current noise through a population of N such channels, $C_I(t)$, is simply given by

$$\begin{aligned} C_I(t) &= N i^2 C_o(t) \\ &= N i^2 p_\infty (1 - p_\infty) e^{-t/\tau} \end{aligned}$$

where i is the single-channel current. Note that the autocovariance function at $t = 0$ is equal to the variance, $C_I(0) = N i^2 p_\infty (1 - p_\infty) = \sigma^2$, and decays exponentially with time constant τ, so that when $t \gg \tau$, $C_I(t) \to 0$. This implies that the current noise 'forgets' its history beyond a certain time in the past.

The Wiener-Khinchin theorem [van Kampen, 1992] states that the power spectrum is then equal to the real part of the Fourier transform of the autocovariance function

(we drop the subscript from p_∞ for convenience)

$$\begin{aligned} S_I(\omega) &= 4\int_0^\infty C_I(t)e^{-i\omega t}dt \\ &= 4Ni^2p(1-p)\int_0^\infty e^{-t/\tau}e^{-i\omega t}dt \\ &= 4Ni^2p(1-p)\tau\frac{1}{1+\omega^2\tau^2} \\ &= S_I(0)\frac{1}{1+\omega^2\tau^2} \end{aligned}$$

where $\omega = 2\pi f$ and $S_I(0) = 4Ni^2p(1-p)\tau$. The prefactor $4\times$ arises from our spectral density definition[1]. Hence for the two-state channel population, the power spectrum is a single Lorenztian function with a corner frequency $f_c = 1/(2\pi\tau)$. Above this corner frequency, the power of the signal falls off $\propto 1/f^2$.

In an analogous way we can calculate the power spectra of the HH Na^+ and K^+ channel populations. For example, for a HH K^+ channel composed of four identical and independent subunits, the conditional probability that the channel is open at time t given that it was open at time 0 is

$$p_{K,o|o} = (n_\infty + (1-n_\infty)e^{-t/\tau_n})^4$$

Hence, the autocovariance of the current noise from the HH K^+ channel population is

$$\begin{aligned} C_{IK}(t) &= N_K i_K^2\left(n_\infty^4 p_{K,o|o} - (n_\infty^4)^2\right) \\ &= N_K i_K^2 n_\infty^4\Big[(1-n_\infty)^4e^{-4t/\tau_n} + 4n_\infty(1-n_\infty)^3e^{-3t/\tau_n} \\ &\quad +6n_\infty^2(1-n_\infty)^2e^{-2t/\tau_n} + 4n_\infty(1-n_\infty)e^{-t/\tau_n}\Big] \end{aligned}$$

and the power spectrum of the current noise is

$$\begin{aligned} S_{IK}(\omega) &= 4N_k n_\infty^4 i_K^2\tau_n\Bigg[(1-n_\infty)^4\frac{4}{16+\omega^2\tau_n^2} + n_\infty(1-n_\infty)^3\frac{12}{9+\omega^2\tau_n^2} \\ &\quad +n_\infty^2(1-n_\infty)^2\frac{12}{4+\omega^2\tau_n^2} + n_\infty^3(1-n_\infty)\frac{4}{1+\omega^2\tau_n^2}\Bigg] \end{aligned}$$

This is the sum of four Lorenztians with corner frequencies equal to $4/(2\pi\tau_n)$, $3/(2\pi\tau_n)$, $2/(2\pi\tau_n)$ and $1/(2\pi\tau_n)$.

[1]There are two sources behind the $4\times$ prefactor. First, $2\times$ comes from the fact that we integrate $C_I(t)$ only from $0 \to \infty$, not from $-\infty \to \infty$ (because $C_I(t)$ is symmetrical, $\int_{-\infty}^{\infty} C_I(t)dt = 2\int_0^\infty C_I(t)dt$). Second, we are calculating here only the single-sided spectral density, for $f \geq 0$. This introduces another $2\times$ because $\int_{-\infty}^{\infty} S_I(\omega)d\omega = 2\int_0^\infty S_I(\omega)d\omega$. These choices are simply a matter of convention, and vary between fields.

We can similarly calculate the Na^+ current noise power spectrum. Here,

$$p_{Na,o|o} = \left(m_\infty + (1-m_\infty)e^{-t/\tau_m}\right)^3 \left(h_\infty + (1-h_\infty)e^{-t/\tau_h}\right)$$

and the Na^+ current noise autocovariance is

$$\begin{aligned} C_{INa}(t) &= N_{Na} i_{Na}^2 \left(m_\infty^3 h_\infty p_{Na,o|o} - (m_\infty^3 h_\infty)^2\right) \\ &= N_{Na} i_{Na}^2 m_\infty^3 h_\infty \Big[m_\infty^3 (1-h_\infty) e^{-t/\tau_h} \\ &\quad + 3m_\infty^2 h_\infty (1-m_\infty) e^{-t/\tau_m} \\ &\quad + 3m_\infty h_\infty (1-m_\infty)^2 e^{-2t/\tau_m} \\ &\quad + h_\infty (1-m_\infty) e^{3-3t/\tau_m} \\ &\quad + 3m_\infty^2 (1-m_\infty)(1-h_\infty) e^{-t(1/\tau_m+1/\tau_h)} \\ &\quad + 3m_\infty (1-m_\infty)^2 (1-h_\infty) e^{-t(2/\tau_m+1/\tau_h)} \\ &\quad + (1-m_\infty)^3 (1-h_\infty) e^{-t(3/\tau_m+1/\tau_h)} \Big] \end{aligned}$$

Then, the power spectrum of the Na^+ current noise is

$$\begin{aligned} S_{INa}(\omega) &= 4N_{Na} i_{Na}^2 (m_\infty^3 h_\infty)^2 \Bigg[\frac{1-h_\infty}{h_\infty} \frac{\tau_h}{1+\omega^2\tau_h^2} \\ &\quad + \left(\frac{1-m_\infty}{m_\infty}\right) \frac{3\tau_m}{1+\omega^2\tau_m^2} \\ &\quad + \left(\frac{1-m_\infty}{m_\infty}\right)^2 \frac{6\tau_m}{4+\omega^2\tau_m^2} \\ &\quad + \left(\frac{1-m_\infty}{m_\infty}\right)^3 \frac{3\tau_m}{9+\omega^2\tau_m^2} \\ &\quad + 3\left(\frac{1-h_\infty}{h_\infty}\right)\left(\frac{1-m_\infty}{m_\infty}\right)\left(\frac{\tau_m\tau_h}{\tau_m+\tau_h}\right) \frac{1}{1+\left(\omega\tau_m\tau_h/(\tau_m+\tau_h)\right)^2} \\ &\quad + 3\left(\frac{1-h_\infty}{h_\infty}\right)\left(\frac{1-m_\infty}{m_\infty}\right)^2\left(\frac{\tau_m\tau_h}{\tau_m+2\tau_h}\right) \frac{1}{1+\left(\omega\tau_m\tau_h/(\tau_m+2\tau_h)\right)^2} \\ &\quad + \left(\frac{1-h_\infty}{h_\infty}\right)\left(\frac{1-m_\infty}{m_\infty}\right)^3\left(\frac{\tau_m\tau_h}{\tau_m+3\tau_h}\right) \frac{1}{1+\left(\omega\tau_m\tau_h/(\tau_m+3\tau_h)\right)^2} \Bigg] \end{aligned}$$

This is the sum of seven Lorentzians with corner frequencies equal to $1/(2\pi\tau_h)$, $1/(2\pi\tau_m)$, $2/(2\pi\tau_m)$, $3/(2\pi\tau_m)$, $(\tau_m+\tau_h)/(2\pi\tau_m\tau_h)$, $(\tau_m+2\tau_h)/(2\pi\tau_m\tau_h)$ and $(\tau_m+3\tau_h)/(2\pi\tau_m\tau_h)$.

Now we combine the membrane impedance with the current noise spectra to calculate each channel population's contribution to voltage noise. In Figure 2.6d we plot the theoretical power spectra of the voltage noise from the HH Na^+ and K^+ channel populations, calculated at $V_m = V_{rest} = -65$ mV. The sum of the Na^+ and K^+ power spectra

give the total voltage noise power spectrum (grey line in Figure 2.6d). This predicts almost exactly the power spectrum measured from simulation (dashed line in Figure 2.6d). We can calculate the voltage noise variance from each channel population by integrating the power spectra:

$$\sigma_x^2 = \int_0^\infty S_x(\omega) d\omega$$

where subscript x indicates the relevant channel population. These are graphed in Figure 2.6e. It is clear the K^+ channel fluctuations contributes $\sim 4\times$ voltage noise than Na^+ current fluctuations, despite Na^+ current noise having greater amplitude than K^+ current noise.

One caveat to these calculations is that they assume that the voltage remains at a fixed potential. In reality, of course, the voltage will fluctuate due to the current noise through the channel populations, but the approximation holds if these fluctuations are small. Because here we simulate a large membrane area ($1000\mu m^2$) with low membrane resistance, voltage changes are small and there is only a small discrepancy between the voltage noise calculated analytically and the estimate from simulation (Figure 2.6e). However, because the greatest effects of stochastic channel gating are expected for small membrane areas with large voltage excursions, this analysis might be considered more a tool for estimating the contribution of each ion channel to membrane noise, rather than for providing an exact analytical description of the system.

6. Polarity of current flow

The sixth factor is the polarity of current flow — some channels (e.g. Na) have reversal potentials positive to the cell's typical voltage range and tend to pass inward currents, while other channels (e.g. K) do the opposite. This property influences how a channel population contributes to membrane noise through voltage excursions from the mean.

Because all ion channels in this single-compartment model share the same membrane potential, they must interact. Both Na^+ and K^+ channels are more likely to open upon membrane depolarisation. Importantly, open Na^+ channels further depolarise the cell, hence increasing the probability for their neighbours to open and acting as a positive feedback loop. Hence, stochastic Na^+ channels increase excitability of the cell through regenerative depolarising excursions in membrane potential [Dudman and Nolan, 2009]. Open K^+ channels, in contrast, hyperpolarise the cell and act as negative feedback to changes in membrane potential. This negative feedback coupled with their relatively slow kinetics can, in some cases, enable stochastic K^+channels

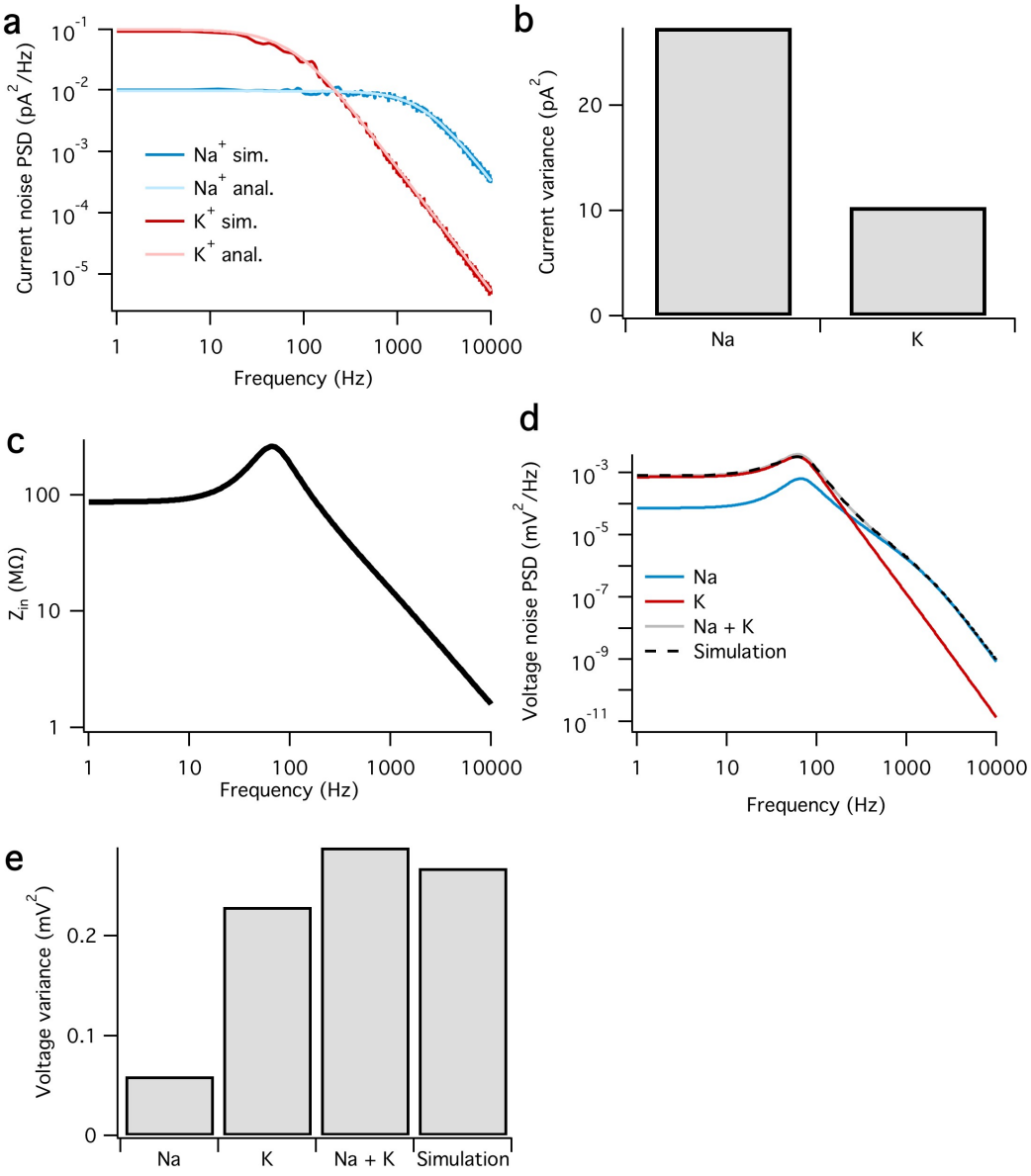

Figure 2.6: The membrane filters Na^+ noise more than K^+ noise. **a**: Spectral density of current noise from HH Na^+ and K^+ channels. Dark coloured curves are PSD estimates from simulation data, light coloured curves are theoretical, derived from channel kinetic schemes. **b**: Variance of Na^+ and K^+ current noise. Note Na^+ channel noise variance is greater than K^+ channel noise. **c**: Total HH membrane impedance as a function of signal frequency, numerically calculated using NEURON. **d**: Voltage noise of Na^+ and K^+ channels calculated from current noise spectra and membrane impedance. Grey curve is sum of Na^+ and K^+ noise, while the dashed curve is an estimate of the voltage noise spectrum measured from simulation data. **e**: Theoretical variance of voltage noise from Na^+ and K^+ channels compared with estimates from simulation. Note K^+ channels contribute more than Na^+ channels.

to drive sub-threshold oscillations [Schneidman et al., 1998] and membrane resonance [Hutcheon and Yarom, 2000].

Recapitulation

In summary, the relative importance of each channel type for membrane noise (and spontaneous spiking) from stochastic channel gating is determined by their number, single-channel conductance, voltage dependencies and gating kinetics. The sum properties of HH K^+ channels at subthreshold voltages make their contributions to membrane noise greater than that from HH Na^+ channels.

2.3.3 Cable length non-monotonically influences spontaneous firing rate in thin axons

Spontaneous firing also occurs in multi-compartmental cable models of thin axons with stochastic ion channels [Horikawa, 1991, Faisal et al., 2002, 2005]. Simulations suggest that axons with diameters less than $\sim 0.1\mu$m would generate too many spontaneous events to permit uncorrupted information transmission [Faisal et al., 2005]. This critical diameter corresponds well with the lower limit of axon diameter found in the animal kingdom [Faisal et al., 2005]. Although the importance of axon length is unknown, two considerations suggest that it is worth examination. First, cable length is one factor which determines its local electrophysiological properties such as voltage attenuation, input resistance and spike threshold [Rall, 1959, Jack et al., 1975, Koch, 1999]. Second, the spontaneous firing or hyperexcitability of peripheral nerves have been implicated in several pathological pain conditions [Campbell and Meyer, 2006]. Ranging up to 1m in length, these fibres are amongst the longest in the nervous system.

We simulate the HH axon model as a multi-compartmental cable, and vary both the diameter and length to examine spontaneous spike generation (Figure 2.7). Although the HH model may not quantitatively predict the behaviour of mammalian-fibres due to differences in ion channel properties, it may nevertheless be useful for gaining qualitative insights into the parameters important for spontaneous spiking in thin unmyelinated nerve fibres.

Decreasing cable diameter increases spontaneous firing rate for cables of all length [Horikawa, 1991, Faisal et al., 2002, 2005]. Surprisingly, however, there is a non-monotonic relationship between spontaneous firing rate and cable length. At short lengths ($< 100\,\mu$m), longer cables have lower firing rates. Beyond some critical length,

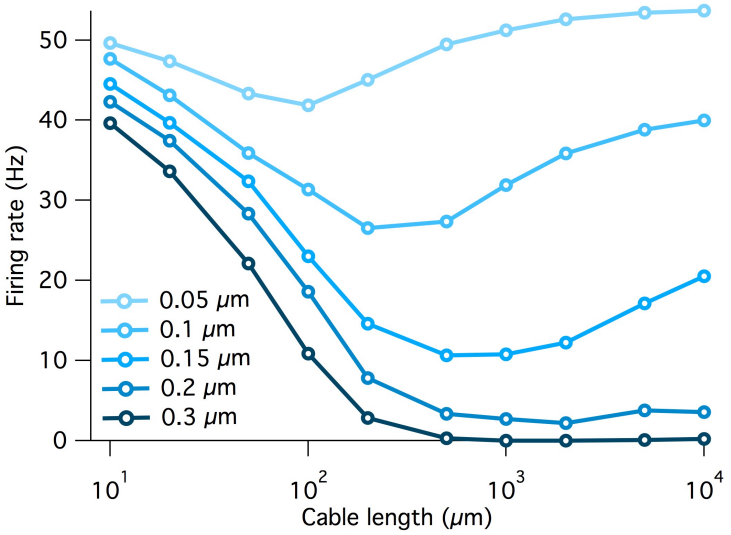

Figure 2.7: Spontaneous firing rate in a thin axon depends on both cable length and diameter in a stochastic HH model with fixed channel densities (Table 2.2).

however, firing rate begins to increase again with increasing cable length. The critical length ranges from ~ 100 μm in cables 0.05 μm in diameter to > 1000 μm for cables more than 0.2 μm in diameter.

We give a qualitative explanation for this non-monotonic relationship as follows. At short lengths, the cable is isopotential. Hence, increasing the cable length initially decreases the spontaneous firing rate by increasing the membrane surface area and decreasing the input resistance. This dampens voltage fluctuations and reduces the likelihood of spontaneous spiking. Then, above some critical value related to the electrotonic length, the cable loses its isopotentiality and has multiple compartments that are semi-independent from each other. These compartments can be considered independent spike generation zones which together elevate the total cable's firing rate. Further increasing cable length increases the number of these zones, so that firing rate continues to increase. Eventually firing rate saturates due to refractoriness and cancellation of multiple spikes.

2.3.4 Cable terminals are preferential zones for spontaneous spike generation

Classic cable theory predicts that local electrophysiological membrane properties depend on cable location, because the cable terminals impart special boundary conditions on the solutions to membrane potential equations [Rall, 1959]. Hence, not all locations

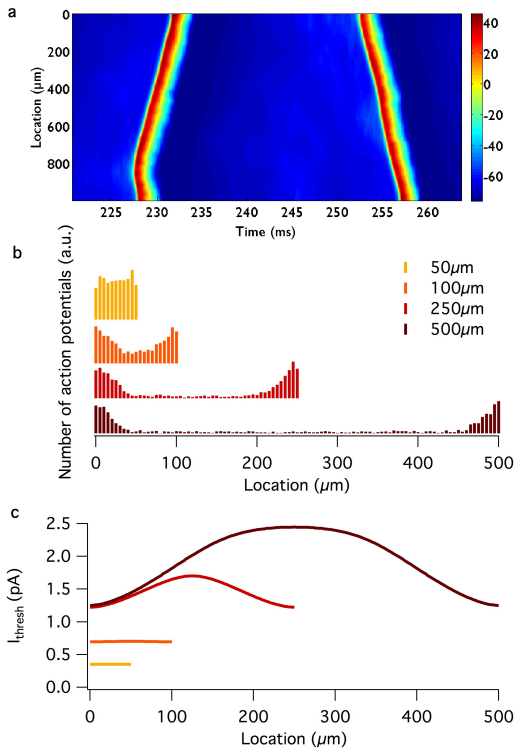

Figure 2.8: Cable terminals are preferential regions for spontaneous spike generation. **a**: Example membrane potential traces (colour) as a function of cable location (vertical axis) and time (horizontal axis). Two spontaneous action potentials are visible. **b**: Histograms of spike initiation locations for 0.1 μm diameter cables of varying length. Spike initiation is most probable at cable terminals. **c**: Steady-state current threshold as a function of cable location for deterministic versions of same cable axons in *b*.

in an axon are equal. We examine whether spontaneous action potential generation depends on cable location by tracking the origins of spontaneous spikes in a thin axon model and varying cable length.

Very short cables ($< 50\mu$m) are isopotential, so at these lengths it does not make sense to speak of independent origins of spontaneous spikes. For longer, non-isopotential cables, spikes are more likely to originate near the cable terminals than in the centre (Figure 2.8b). This is because cable endpoints have the highest input resistance and lowest current spike threshold in the cable (Figure 2.8c, see Rall, 1959, Jack et al., 1975, Koch, 1999). An intuitive explanation for this property is that current injection at the cable centre must locally charge the membrane but also flow axially in two directions away from the injection site, whereas current injection at the cable end need flow only in one axial direction, leaving more charge to depolarise the local membrane.

2.3.5 Stochastic dorsal root ganglion cell models are more excitable

One of the HH squid axon model's greatest strengths is that it has been well studied. However, we also wish to know if the above findings on spontaneous firing generalise to mammalian cells. To address this issue, we convert an existing macroscopic deterministic model of a rat peripheral dorsal root ganglion neuron [Sheets et al., 2007] to its equivalent microscopic stochastic version and compare the behaviour of deterministic and stochastic simulations.

With model parameters taken verbatim from Sheets et al. [2007], membrane noise from stochastic ion channel gating is not large enough to trigger spontaneous action potentials, even for axons as thin as 0.1μm in diameter (in contradiction with the proposal of Faisal et al., 2005). However, when a tonic current stimulus above a certain threshold is given to the cable terminal, action potentials are evoked. We vary the magnitude of the current stimulus and count the number of spikes elicited in 1s (Figure 2.9). The stochastic version of the model has a lower spike threshold and fires more action potentials on average than the deterministic version. Hence, stochastic ion channel gating increases the excitability of these neurons. The magnitude of the increase in excitability decreases with increasing axon diameter, but still persists for axons even of 1μm thickness. In addition, thinner axons have a lower spike threshold than thicker axons, in common with deterministic models (Figure 2.9c).

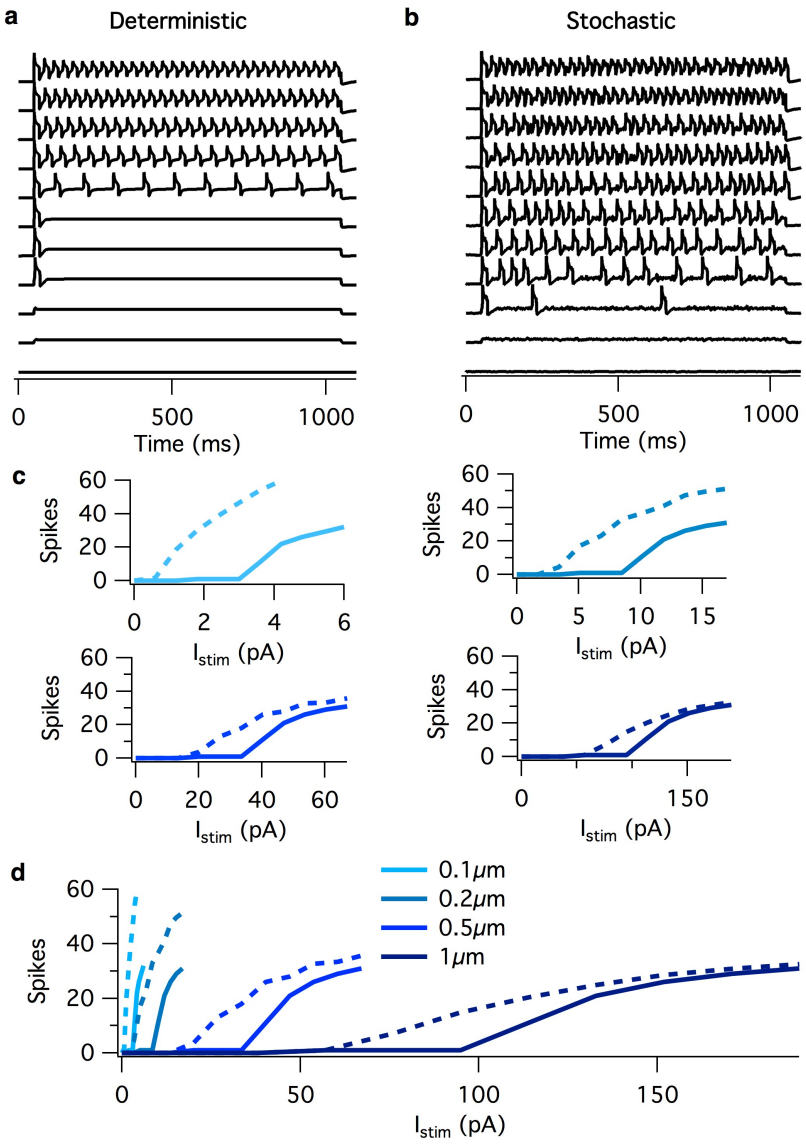

Figure 2.9: Stochastic channel gating makes dorsal root ganglion cell model hyperexcitable. **a-b**: Example voltage traces from deterministic (a) and stochastic (b) simulations of a 0.2 μm diameter cable. Stimulus intensity increases from bottom to top. **c**: Stimulus-response curves for deterministic (solid) and stochastic (dashed) cables of varying diameter. **d**: Replot of same data from *c*. Excitability of cable increases with decreasing cable diameter, for both deterministic and stochastic models.

2.4 Discussion

2.4.1 Potassium channels are the dominant noise source driving spontaneous spiking in the stochastic single-compartment Hodgkin-Huxley model

We have shown that the fluctuations from stochastic gating of potassium channels is the dominant source of noise in the stochastic HH model by three different measures. First, a HH model where only K^+ channels gate stochastically spontaneous fires at higher rates than a HH model where only Na^+ channels gate stochastically (Figure 2.2) [Skaugen and Walløe, 1979, Schneidman et al., 1998, van Rossum et al., 2003]. Second, examining the dynamics of Na^+ and K^+ currents in the milliseconds preceding a spontaneous action potential in the 'all stochastic' HH model shows that, on average, spikes are generated by a drop in K^+ current that precedes the increase in Na^+ current (Figure 2.3). Third, direct calculation of the voltage noise spectra from each channel population at resting potential shows that K^+ channel fluctuations contribute ~75% of the total membrane noise (Figure 2.6). This finding, although consistent with results reported by Schneidman et al. [1998], van Rossum et al. [2000], is in contrast with data reported by Chow and White [1996], Faisal et al. [2005]. We discuss these two studies separately.

Chow and White [1996] used approximate analytical methods to directly calculate the spontaneous firing rate in the stochastic HH model, and compared the predictions to numerical simulations to find good agreement. Our own simulations produce quantitatively similar results to their simulations (data not shown), so it is likely that these data are correct. However, their analytical calculations were based on the assumption that spontaneous spiking is driven *solely* by stochastic activation of Na^+ channels, which we show to be false (Figure 2.2). If anything, their analytical model should be a better approximation of our simulations where K^+ channels are modeled deterministically. However, their calculations do not match even this. The errors could have arisen in any of the multiple approximating steps necessary the calculation. For example, they assume a static absolute voltage threshold when in reality the HH model has 1) no hard threshold for any type of stimulus [Izhikevich, 2007] and 2) different apparent spike thresholds for stimuli of different temporal structure [Koch, 1999]. A full analytical solution would require inclusion of both the deterministic and stochastic components of the Na^+ and K^+ dynamics, which may prove intractable.

Faisal et al. [2005] find in cable axon HH models that Na^+ channels contribute more to spontaneous spiking than K^+ channels. We believe this to be a numerical simulation error, for two reasons. First, it is inconsistent not just with our simulations (when implemented with both PSICS and NEURON), but also those of Schneidman et al. [1998] and van Rossum et al. [2003]— implemented with another simulator, 'NeuronC'. Second, it does not follow from basic theoretical calculations (Figure 2.6). Without access to their simulator, it is difficult to tell where the error lies. Even so, it is possible that Na^+ channel noise does drive spontaneous spiking in models other than the HH squid giant axon.

We summarise again the factors important for determining a specific channel population's contribution to membrane noise:

1. Channel open probability, p_o. Fluctuations are greatest for a channel population when $p_o = 0.5$, and minimal when $p_o \sim 0$ or $p_o \sim 1$. Because membrane voltage is a primary factor in determining channel open probability, it can hence also influence membrane noise.

2. Number of channels, N. The s.d. of the fluctuations in open channel number is proportional to $\sqrt{N}$. Hence, increasing the size of the channel population will increase the amplitude of its current noise.

3. Reversal potential. Channels with a larger driving force ($V_m - E$, where V_m is the membrane potential and E is the channel's reversal potential) have a larger single-channel current and hence larger amplitude population current fluctuations.

4. Single channel conductance, γ. The s.d. of current fluctuations from a population of ion channels is proportional to γ. Hence, channels with large γ may constitute significant sources of membrane noise.

5. Channel kinetics. Because the membrane capacitance acts as a low-pass filter, in general the current noise from channels with slower gating kinetics are less attenuated than current noise from channels with faster gating kinetics. Additionally, because channel transition rates are generally positively dependent on temperature while the membrane capacitive filtering is independent of temperature, increasing temperature should generally decrease voltage noise from stochastic ion channel gating.

6. Polarity of current flow. Most (but not all) channels have increased open probabilities upon depolarisation. Hence, channels that mediate inward (depolarising) currents can generally amplify their current fluctuations through positive feedback via the membrane potential. Outward currents, in contrast, tend to oppose changes in membrane potential. In this case stochastic channel gating can drive membrane potential oscillations [Schneidman et al., 1998].

2.4.2 Both axon diameter and length influence spontaneous spiking

It has been previously demonstrated in computational models that small single compartments [Skaugen and Walløe, 1979, Strassberg and DeFelice, 1993, Chow and White, 1996, Schneidman et al., 1998] and thin cable axons [Horikawa, 1991, Faisal et al., 2005] can spike spontaneously due to channel noise. We show that the firing rate in thin HH axons also depends non-monotonically on cable length (Figure 2.7). Short cables (<50 μm) spike at high rates, consistent with single-compartment models. Firing rate then initially decreases with cable length until a minimum value which is dependent on cable diameter. Beyond this length, firing rate tends to increase again, until saturation for very long axons.

This result suggests that long, thin cable axons are likely loci to expect spontaneous spiking due to channel noise in the nervous system. This anatomy, along with irregular firing patterns, are reminiscent of the unmyelinated C-fibres of the peripheral nervous system. The spontaneous firing of C-fibres has been associated with neuropathic pain conditions [Djouhri et al., 2006].

2.4.3 Cable terminals are preferential zones for spontaneous spike generation

We also show that most spontaneous spikes in a stochastic HH cable axon originate near the end points (Figure 2.8). This result is predicted from basic biophysical cable theory, which says that the input resistance of a cable and the current threshold for spike generation are lowest at the cable ends [Rall, 1959, Jack et al., 1975, Koch, 1999].

Axonal action potentials in most cells in the nervous system are not generated at cable terminals, but at an axon initial segment adjoined to or near the soma. In this case, the ‘end effect’ is not present because the soma acts as a large current sink. However,

the one cell type where action potentials *are* normally generated at the distal end of the axon is the peripheral nerve, which must relay information from the skin (or relevant organ) back past the soma to the spinal cord. Hence, peripheral nerves may again be likely places to expect spontaneous spiking from stochastic ion channel gating.

One caveat to these conclusions is that we have assumed a homogeneous density of ion channels along the axon. Although unmyelinated axons do not show the extreme regionalization of myelinated axons, they may also exhibit inhomogeneity in ion channel expression. One particularly well-studied example is the nonuniform sodium channel distribution in the proximal axon of central neurons, which determines the exact site of action potential initiation [Lörincz and Nusser, 2008]. Our choice of a homogeneous density of channels throughout the membrane should be considered a simple case upon which future studies which include spatial dependencies can be based. It is likely that spatial inhomogeneity in ion channel expression will imply that the magnitude and impact of current fluctuations from stochastic channel gating will also depend on spatial location within the axon. The exact consequences will depend on the specific inhomogeneity involved. However, the broad effects of such an arrangement might be predicted from the six factors we discuss above. For example, if a particular type of Na^+ channel were more densely expressed in one region of the axon than another, then from factor 2 (above), we predict that membrane noise would also be greater in the region with greater channel number.

2.4.4 Stochastic ion channel gating might underlie some types of spontaneous firing in neuropathic pain

Although the HH squid giant axon model qualitatively captures the essential mechanisms underlying action potentials in all spiking neurons, its biophysical properties are quantitative very different to mammalian axons. In particular, we would like to know whether spontaneous action potential generation is possible in a plausible model of a peripheral nerve fibre to test whether it may underlie certain chronic neuropathic pain conditions. We adapt an existing model of a dorsal root ganglion cell [Sheets et al., 2007] containing two Na^+ channel types ($Na_V1.7$, $Na_V1.8$), two K^+ channel types (K_{dr} and K_a) and a leak conductance, and implement stochastic Markov models of each channel type. We find that, unlike the HH axon model, this DRG model does not spike spontaneously even for axons of 0.1 μm diameter — approximately the narrowest found physiologically [Dyck and Hopkins, 1972]. However, when we inject long

current steps of varying amplitude into the cable terminal, we find that the stochastic model has both a lower current threshold for spiking, and spikes more frequently than the deterministic model for all stimulus intensities (Figure 2.9). Hence, stochastic ion channel gating makes the DRG neuron model hyperexcitable. This finding is generic to all noise driven model neurons with a spike threshold, irrespective of where the variability arises from.

In addition, there is a strong relationship between the current threshold and cable diameter, such that narrower cables are more excitable than wider cables (Figure 2.9d). Hence, the narrow diameters of fibres found in regenerating axons sprouts [Dyck and Hopkins, 1972] might be one factor which contributes to their tendency to generate spontaneous activity.

We propose that stochastic ion channel gating underlies the spontaneous activity found in some thin peripheral nerves during neuropathic pain conditions. We summarise the reasons as:

- Increased numbers of peripheral nerves fire spontaneously during pain states [Blumberg and Jänig, 1984, Wu et al., 2001].
- Spontaneous activity is very low rate (<1Hz) and irregular, consistent with a noise driven process [Blumberg and Jänig, 1984, Xiao and Bennett, 2007].
- Regenerated peripheral nerves in pain states have narrower diameters than control nerves [Dyck and Hopkins, 1972], facilitating spontaneous spiking (Figures 2.7 and 2.9d) [Faisal et al., 2005].
- Peripheral nerves are among the longest in the nervous system, again facilitating spontaneous spiking (Figure 2.7).
- Cable theory predicts that nerve terminals are preferential zones for spontaneous spike initiation (Figure 2.8) [Rall, 1959, Jack et al., 1975, Koch, 1999] - spikes are naturally generated at these locations in peripheral nerves [Julius and McCleskey, 2006].

Most common ideas for remedying neuropathic pain states due to spontaneous activity in the peripheral nerves are based on the concept of reducing excitability of the nerves, which are often hyperexcitable. Pharmacological intervention is usually either targeted at reducing Na^+ currents or increasing K^+ currents. This novel mechanism for spontaneous activity based on stochastic ion channel gating is fully compatible with these

suggestions, but also prompts some new interventions that are partially noise-specific. We list several testable possibilities here:

1. Dilate thin fibres. This would increase fibre diameter, reduce membrane impedance, and hence reduce cell excitability (this is common to a deterministic model). This might possibly be achieved by modifying cell osmolarity (either by directly altering extracellular fluid composition or by manipulation of the endogenous machinery for cell osmoregulation), or by modifying the molecular mechanisms that maintain the actin cytoskeleton which supports neural process structure.

2. Reduce axoplasmic resistivity. Because membrane impedance is inversely related to axial resistivity, decreasing axoplasmic resistivity should reduce the excitability of the cell (this is also common to a deterministic model). Although it is not clear how this might be achieved, it is known that different cell types within and between species can exhibit a range of axoplasmic resistivities [Stuart and Spruston, 1998]. If well understood, it might be possible for future experimentalists to manipulate the machinery which regulates this property.

3. Introduce ion channels with small conductance or fast kinetics, or block/down-regulate ion channels with large-conductance or slow kinetics. Current noise from channels with faster kinetics is attenuated more greatly by membrane capacitance than current noise from slower channels. Current noise amplitude is smaller in channels with smaller single-channel conductance. If new fast/small-conductance channels replaced existing channels, noise would be reduced. If instead these new channels were simply added to the existing set of channels, they would act as current sinks to other noise sources without greatly contributing to noise themselves. Endogenous channels with large conductance/slow kinetics could either be blocked pharmacologically, or genetically down-regulated. Although genetic interventions are not feasible for human patients at present, in future this might be possible using gene therapy or viral delivery systems similar to those already used in rodents.

4. Increase temperature. Since ion channels tend to have a transition rate Q-value >1 [Hille, 2001], increasing temperature shifts channel current noise power to higher frequencies, which results in greater noise attenuation by the membrane capacitance. Potential caveats to this intervention include the fact that other ion channel properties important for channel noise, such as single-channel conduc-

tance, are also temperature dependent [Hille, 2001]. Therefore the consequences of temperature change on membrane noise require careful consideration. Although this may prove impossible to achieve in vivo in the central nervous system, the relative accessibility of the peripheral nervous system might allow temperature changes to be implemented in human patients here without invasion, perhaps through externally-applied heating or cooling packs.

Chapter 3

Channel noise and synaptic integration in central neurons

3.1 Background

The results presented in this chapter have been published previously [Cannon et al., 2010].

3.1.1 Moving from axonal to dendritic membranes

In the previous chapter we outlined six factors important for determining an ion channel population's contribution to membrane potential noise. We noted that one of these factors, the membrane impedance, was particularly critical in shaping membrane noise. We also found that even though voltage noise from stochastic channel gating tends to be small at subthreshold potentials (~1 mV s.d.), it can have strong effects in nonlinear membranes when they are near spike threshold. In the previous chapter, these phenomena were studied mainly in the HH squid axon model. Now we study related effects in model neurons where we include a dendritic arbour. This step is important for two reasons.

First, most central neurons have a much more complicated morphology than the single compartments or homogeneous cable axons we have studied so far [Fiala et al., 2008]. This distributed layout has the effect of electrically decoupling different locations. The cell's multiple synaptic inputs first cause local changes in membrane potential out in their respective dendrites, which are then integrated together at the soma [Magee, 2000]. It is not clear how channel noise would affect this process. For

example, because synaptic potentials must now travel some distance before reaching the spike initiation point, there may be increased opportunity for their waveforms to get corrupted by channel noise along the way.

Second, dendrites may possess different types and numbers of ion channels compared to the axon [Magee, 2008]. In addition, they may have different anatomy to axons (cable diameter, length, branching structure). Together, these features determine a dendrite's impedance and excitability properties, which are quantitatively (and perhaps qualitatively) quite different from the axon. Hence, conclusions on the impact of channel noise in axonal membrane models may not prove good predictors of the impact of channel noise in dendritic membrane models.

3.1.2 Dendrites express active membrane conductances

Dendrites are an almost ubiquitous property of central nervous system neurons. Although no two cells have identical dendritic arbours, neurons of the same type (as defined by their brain region, neurotransmitter, ion channel complement and axonal targets) often have qualitatively similar dendritic arbours. In some cell types, dendritic morphology has been linked explicitly to the cell's circuit function [Agmon-Snir et al., 1998]. Other theories propose that dendritic arborisation patterns are optimised to maximise synaptic connectivity options [Chklovskii, 2004]. However, a vast body of research has also demonstrated that dendrites can posses many voltage-gated ion channels [Magee, 2008]. This fact implies that the process of synaptic integration — the conversion of many synaptic input trains into a single output spike train — is nonlinear in dendritic neurons. We have already found in Chapter 2 that channel noise can have surprisingly large effects in axonal membranes, precisely because of their strong nonlinearity — the spike threshold. Near such points all excitable systems are highly sensitive to noise [Lindner et al., 2004]. We now briefly review the known active properties of dendrites.

Many types of voltage-gated ion channels are found in the dendrites of central neurons [Magee, 2008], with the exact complement dependent on cell type. Their number and sub-cellular distribution also depends on cell type. The presence of these channels leads to many interesting effects [reviewed by Spruston et al., 2008]. Inward currents such as those mediated by Na^+ and Ca^+ channels can amplify subthreshold excitatory post-synaptic potentials (EPSPs), whereas outward currents mediated by K^+ channels have the opposite affect of attenuating EPSPs. If many excitatory synaptic inputs are

activated on the same dendritic branch simultaneously, they can even evoke dendritic action potentials [Spruston et al., 2008]. Under certain conditions, dendritic spikes can actively propagate forward along the dendrite to the soma and trigger an axonal action potential. However, dendritic membrane is typically only weakly excitable compared with axonal membrane [Jarsky et al., 2005]. This, along with the unfavourable impedance gradient introduced by dendritic branching structure [Jack et al., 1975], makes dendritic spike initiation and propagation a much less reliable processes than axonal spike initiation and propagation. If a dendritic spike is generated, it is often subject to strong voltage attenuation en route to the soma, and hence may or may not trigger an axonal action potential [Golding and Spruston, 1998]. The source of this variability is not clear. Interestingly, instead of being seen as a problem, the unreliability could be computationally useful because it enables the potential gating of dendritic control over axonal output [Jarsky et al., 2005]. For example, a given synaptic stimulus may initiate a dendritic spike reliably, but whether it propagates to the soma and triggers an action potential might be conditional on the presence of other similar events from neighbouring branches, or excitatory synaptic input on its path to the soma [Häusser and Mel, 2003]. Conversely, dendritic spike propagation could be blocked or cancelled by properly timed inhibitory input. Consistent with this viewpoint, inhibitory synapses onto pyramidal cells in both hippocampus and neocortex are found to be targeted at proximal dendrites, soma, or even axon initial segment [Klausberger and Somogyi, 2008].

A second function of active dendritic membrane is the backpropagation of axosomatic action potentials into the dendrites [Stuart and Sakmann, 1994]. This backpropagation might serve, for example, as a Hebbian signal to the synapses to trigger synaptic plasticity via the NMDA receptor [Magee and Johnston, 1997, Letzkus et al., 2006, Sjöström and Häusser, 2006]. Without voltage-gated ion channels, backpropagated action potentials (BAPs) in pyramidal neurons tend to passively decay quite rapidly [Stuart and Sakmann, 1994].

Larkum et al. [1999] demonstrated that the dual excitability of soma and dendrites of LV neocortical pyramidal neurons provides these cells with a powerful mechanism for co-incidence detection of inputs arriving from different cortical layers. They found that when a simulated EPSP injected to the apical dendrite was coupled closely in time with a somatic action potential, the single BAP interacted nonlinearly with the dendritic EPSP to produce a large prolonged Ca^{+}-mediated dendritic spike, that subsequently drove a burst of three somatic action potentials. The activation of this burst

was sensitive to the relative timing of the dendritic EPSP and the somatic AP, over a window of ~20 ms.

Even more complicated behaviour can arise during extended synaptic input. The inactivation properties of Na^+ channels in CA1 pyramidal neurons make them incapable of supporting the backpropagation of fast trains of sequential action potentials [Colbert et al., 1997]. Interestingly, Remy et al. [2009] found that triggering a dendritic spike can reduce the ability of that dendritic branch to trigger subsequent dendritic spikes due to Na^+ channel inactivation. Furthermore, if the dendritic spike triggers an axonal action potential that back-propagates to the dendrites, there is a global inactivation of dendritic Na^+ channels, leading to reduced excitability of all dendritic branches. Recovery from inactivation took several hundred milliseconds. Hence, dendritic excitability (at least in CA1 pyramidal neurons) is strongly history-dependent.

In summary, the process of synaptic integration in spatially extended dendritic neurons is complex due to the nonlinear properties of active ion channels, highly cell-type specific, and still not fully understood. The potential effects of channel noise in such situations are particularly unclear.

3.2 Methods

All simulations implemented using the Parallel Stochastic Ion Channel Simulator (PSICS). See Cannon et al. [2010] and http://psics.org/ for algorithmic details. Analysis done using Matlab (The Mathworks), Igor Pro (Wavemetrics) and R (http://www.r-project.org/).

For simulations of resting noise dendritic neurons (Sections 3.3.1–3.3.3), neuronal morphologies were downloaded from the Neuromorpho database (www.neuromorpho.org). Neurons were identified in the database as follows. Layer V pyramidal cells: p18 and p22 from Dendritica; g0692P1, g0699P1 and gR002P1 from Svoboda lab. Dentate gyrus granule cells: n271, n272 and n518 from Turner lab; 428883, B106885 from Claibourne lab. Purkinje cells: alxP, e4cb3a1 and e1cb4a1 from Martone lab; p19 and p20 from Dendritica. CA1 pyramidal cells: n409 from Turner lab; NM1 from Ascoli lab; ri04 and ri06 from Spruston lab; pc4c from Gulyas lab. Substantia nigra dopaminergic neurons: Nigra2a955, Nigra11h941-1, Nigra24a953, Nigra12h945 from Dendritica. Parvalbumin interneurons: pv08e, pv22b, pv22e, pv22j and pv22m from Gulyas lab. In these simulations the densities of voltage-gated channels were based on a previously published study [Mainen and Sejnowski, 1996]. The leak conductance was modeled as voltage-independent Na^+ and K^+ channels with $p_o = 0.7$. The following channels were included: fast Na^+ channels ($1/\mu m^2$); non-inactivating K^+ channels ($0.05/\mu m^2$); high-voltage Ca^{2+} channels ($0.15/\mu m^2$); Na^+ and K^+ leak channels ($0.016/\mu m^2$). The resting membrane potential was set by modifying the ratio of Na^+ to K^+ leak channels. In all simulations reported here this was -60 mV. We chose single-channel conductances of 20 pS for all ion channels, as this is similar to values reported for single channel recordings made from neuronal dendrites [Magistretti et al., 1999, Chen and Johnston, 2004]. This value is intermediate for cloned mammalian ion channels, which can have single channel conductances from <1 pS up to >150 pS [Hille, 2001]. Membrane capacitance was set to 0.75 $\mu F/cm^2$ and axial resistivity to 150 Ωcm [Mainen and Sejnowski, 1996]. For models of neurons that are known to have dendritic spines (all models except the parvalbumin-expressing interneurons), the dendritic membrane capacitance and the number of dendritic ion channels were doubled to account for the extra membrane area (and presumed extra ion channels). The morphology did not contain an axon. For each model neuron, membrane potential was recorded at the soma and at all dendritic locations 100 μm, 200 μm, 300 μm, etc., from the soma. All reported results were obtained from at least 3 s of simulated biological time. The simulation time step was 10 μs.

The simulations of a detailed model of CA1 pyramidal neuron (Sections 3.2.4–3.2.8) used previously published ion channels, morphology and channel distributions [Jarsky et al., 2005]. In this model voltage-dependent ion channels are distributed in the soma, axon and dendrites according to previous experimental measurements. The only modification to the model was the addition of Ih conductance and channel distribution taken from a different publication from the same group [Golding et al., 2005] and consistent with data from other groups [Magee, 1998]. The densities of Na^+ and K^+ leak channels were automatically adjusted to achieve a resting potential of approximately -70 mV throughout the cell, while maintaining a total leak conductance consistent with the original model. The single channel conductance of the delayed rectifier K^+ channels and voltage-dependent Na^+ channels were set to 20 pS, which is similar to estimates from single channel recordings [Magistretti et al., 1999, Chen and Johnston, 2004]. For simplicity, the single channel conductance of A/D type K^+ channels and leak channels were also set to 20 pS, which is similar to experimental measurements for D-type channels [Chen and Johnston, 2004], somewhat larger than estimates for dendritic A-type channels [Chen and Johnston, 2004] and towards the low end of the range of single-channel conductance reported for leak channels [Hille, 2001]. Thus, our simulations of models with only stochastically gating voltage-dependent Na^+ and delayed rectifier K^+ channels can be considered as fully constrained predictions given currently available data, while our simulations of the fully stochastic model likely estimate a lower limit for the consequences of stochastic ion channel gating. This is because our results from simulations when A/D type K^+ channels are deterministic, but voltage-dependent Na^+ or delayed rectifier K^+ channels are stochastic, nevertheless demonstrate highly probabilistic spike firing, indicating that a smaller single channel conductance for A/D type K^+ channels would have little impact on the results, while a possible larger single channel conductance for the leak channels would be expected to increase the impact of stochastic gating. Our simulations of A/D type stochastic gating alone should be considered as setting an upper limit for stochastic effects based on known properties of these channels, whereas the simulations of leak channels alone are less well constrained and serve as an illustrative example. Unlike other ion channels, the single channel conductance of Ih channels is set at 1 pS, which is consistent with noise-analysis of dendritic Ih recorded from cortical neurons [Kole et al., 2006] and the absence of step-like single channel waveforms from measurements of Ih obtained with cell-attached recordings from CA1 pyramidal neurons [Magee, 1998]. Synapses were modeled as bi-exponential conductance changes of rise time 0.2 ms, decay time

2 ms and peak conductance 0.18 nS. Synapses were distributed randomly across all dendrites >30 μm from the soma at an average density of 0.1/μm^2 (1502 in total). Each synapse was activated independently according to a Poisson process with a mean frequency of 5.5 Hz. For analysis dendritic spike times were calculated as upward voltage crossings above a -60 mV threshold. Visual inspection of traces confirmed that this threshold successfully isolated all-or-nothing dendritic events. Comparisons of group data use ANOVAs.

3.3 Results

3.3.1 Resting membrane potential noise in dendritic neurons depends on cell morphology

Dendritic morphology is one of several features commonly used to describe neurons of a given type, both because it is amenable to experimental measurement and is sufficiently distinct between neural types to serve as a useful marker. However, it is also known that the electrical properties of the neuron depend on dendritic morphology. These differences in electrical properties between neurons could differentially shape the membrane potential fluctuations from stochastic ion channel gating. We investigated how heterogeneities in dendritic morphology lead to differences in membrane noise by simulating model neurons from each of six different neural types: cortical layer V pyramidal neurons, cerebellar Purkinje neurons, dopaminergic neurons of the substantia nigra, hippocampal parvalbumin-positive interneurons, hippocampal CA1 pyramidal neurons and hippocampal dentate gyrus granule cells (see Methods for details). For each cell type we simulated five example morphologies (except four for the dopaminergic neurons of the substantia nigra), because individual cells of the same type can show heterogeneities in morphologies great enough to result in substantially different electrical properties [Scorcioni et al., 2004, Szilágyi and De Schutter, 2004]. To isolate the effect of dendritic morphology only for channel noise, we distribute an identical set of membrane ion channels with fixed densities on each cell type, even though in reality it is likely that different cell types express different numbers and types of ion channels to each other. For these simulations we include stochastic fast Na^+, non-inactivating K^+, high-voltage Ca^+, and Na^+ and K^+ leak channels.

Fluctuations in the membrane potential were apparent in all neurons simulated using stochastically gating ion channels (Figure 3.1). However, the amplitude of these fluctuations varied significantly both between neurons of the same morphological class ($p<0.01$ for all classes, ANOVA), between neurons of different morphological classes ($p<1e-9$, ANOVA) (Figure 3.1b), and as a function of dendritic location within neurons ($p<1e-9$, ANOVA). For example, neocortical pyramidal neurons demonstrate relatively small amplitude membrane potential fluctuations (Figure 3.1a). This is consistent with previous modeling and experimental studies of stochastic ion channel activity in layer V pyramidal neurons [Diba et al., 2006, Jacobson et al., 2005, Yaron-Jakoubovitch et al., 2008]. In contrast, membrane potential fluctuations could be substantially larger

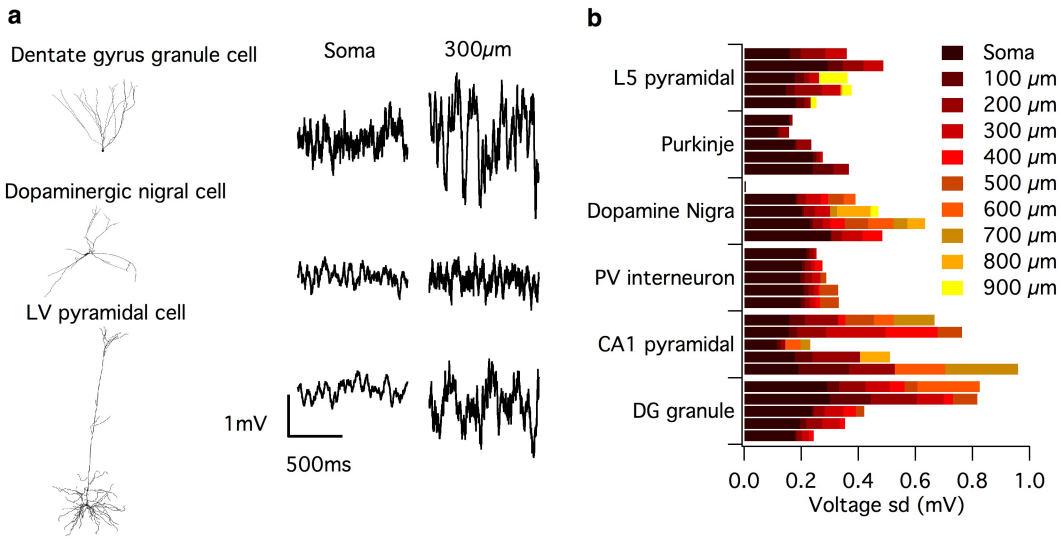

Figure 3.1: Membrane potential fluctuations from stochastic ion channel gating differ between morphologically distinct neuronal cell types. **a**: Example resting membrane potential traces (right) from three model neurons with dendritic arbours from different cell types (left). Traces are from soma and at a dendritic location 300 μm from soma. **b**: Resting voltage s.d. from 29 reconstructed neurons from 6 different cell types. Colour indicates dendritic distance from soma. Note that the amplitude of fluctuations depend on cell type, and are generally larger in the dendrites than at the soma.

in hippocampal dentate gyrus granule cells (Figure 3.1a). In summary, the impact of stochastic gating of dendritic ion channels on neuronal electrical properties is determined by neuronal morphology and can vary according to dendritic location.

3.3.2 Membrane potential influences the magnitude of channel noise

From the binomial model of channel gating outlined in the previous chapter, we expect the fluctuations in ion channel open number, and hence their contribution to channel noise, to be greater when channel open-probability is closer to 0.5. Because most of the ion channels in our simulation are voltage-gated, a straightforward method to simultaneously vary multiple ion channel population's open probabilities is to vary the membrane potential. Experimentally, this is most simply achieved by injecting prolonged positive or negative currents at the cell soma. However, in neurons with extended dendritic arbours, it is likely that currents injected at the soma have only limited control over membrane potential at more distal dendritic locations [Williams and Mitchell, 2008]. To circumvent this, we instead vary membrane potential of the model neuron by modifying the ratio of leak potassium to leak sodium channels. This adjustment is done on a compartment-by-compartment basis to ensure steady-state membrane potential is as close as possible to the desired value at all locations within the model neuron. Note that the cell morphology did not include an axon, or sufficient conductances in the soma, to induce full action potentials.

We varied the resting membrane potential from -70 mV to -50 mV in a CA1 pyramidal neuron model and found prominent increases in the amplitude of membrane potential fluctuations with depolarisation ($p<0.01$ at all dendritic locations, ANOVA) (Figure 3.2). Hence, measurements of membrane noise at resting membrane potential may underestimate noise at more depolarised levels closer to spike threshold.

3.3.3 Channel kinetics influences magnitude of membrane noise from stochastic channel gating

In the previous chapter we found that the kinetics of ion channel gating is one factor which determines the influence of stochastic channel gating. We ask here if this is also the case in the models based on reconstructed neurons. We focus on models of cortical layer V pyramidal neurons and on models of granule cells from the dentate gyrus of the hippocampus. When the fast gating leak channels used for the simulations in Figure 3.1 are replaced with an equivalent deterministic conductance, we find almost no dif-

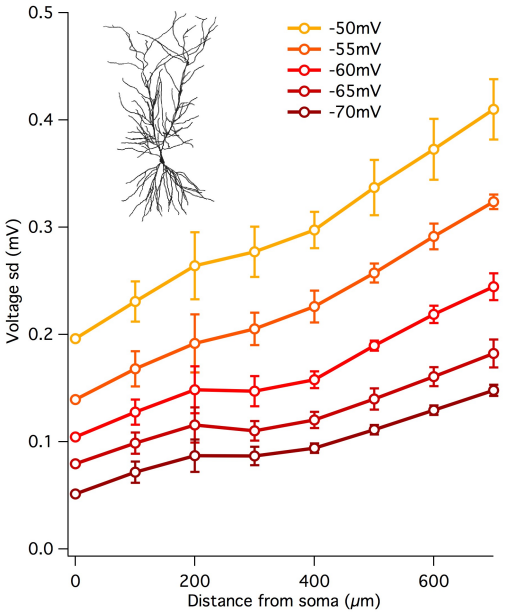

Figure 3.2: The magnitude of voltage channel noise increases with increasing cell membrane potential. The voltage standard deviation is plotted as a function of distance from the soma for a range of resting membrane potentials.

ference in the amplitude of membrane potential fluctuations recorded from somatic or dendritic locations (DG neurons average 1.11 fold difference, p = 0.02; Layer V neurons, average 1.14 fold difference, p = 1.5e-6, ANOVA) (Figure 3.3). Thus, in the configuration used for simulations in Figure 3.1, the membrane potential fluctuations are primarily driven by stochastic gating of voltage-gated ion channels, but not by the leak channels. By contrast, when we replace the fast gating leak channels with otherwise identical slow gating leak channels, the membrane potential fluctuations were approximately three-fold larger than fluctuations recorded from models containing deterministic or fast-gating stochastic leak channels (DG neurons average 3.13 fold difference, p<1e-9; Layer V neurons, average 3.08 fold difference, p<1e-9, ANOVA) (Figure 3.3). Thus, slow gating leak channels can increase the amplitude of spontaneous membrane potential fluctuations due to decreased filtering by the membrane capacitance.

3.3.4 Stochastic ion channels corrupts timing and reliability of synaptically driven action potential firing in dendritic neurons

Although stochastic ion channel gating can corrupt spike timing and reliability from current injection in single-compartment HH models [Schneidman et al., 1998] and

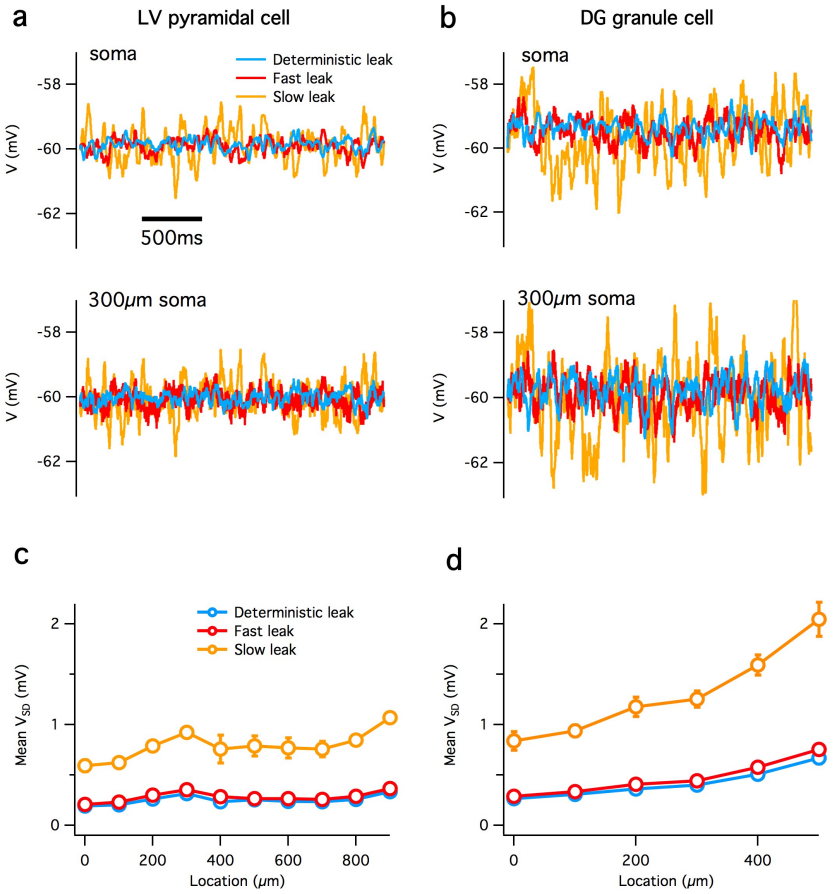

Figure 3.3: Channel kinetics determine the magnitude of membrane noise from stochastic ion channel gating. **a–b**: Example membrane potential traces from model LV pyramidal cell (a) and dentate gyrus granule cell (b) at soma (top) and 300μm from soma (bottom) with either deterministic leak conductance, fast stochastic leak channels or slow stochastic leak channels. **c–d**: Average voltage standard deviation over five model neurons as a function of dendritic distance from soma for LV pyramidal cells (c) and DG granule cells (d). Error bars are $\pm$sd. err.

multi-compartment retinal ganglion cells [van Rossum et al., 2003], it is not clear if channel noise is great enough to disrupt physiologically plausible synaptic integration and subsequent spiking in a morphologically realistic central neuron. To test this, we adapt a previously published CA1 pyramidal neuron model that can account well for *in vitro* axonal and dendritic action potential firing data [Jarsky et al., 2005]. We distribute 1502 synapses across the basal and apical dendrites, and activate each according to an independent Poisson process with a mean rate of 5.5 Hz. We choose the Poisson process because it carries a minimal number of assumptions: each synaptic input occurs with a fixed probability, is independent of all other inputs, and is uncorrelated with the previous input to that synapse. Because synapses are stimulated independently and distributed over a large region of the dendritic arbour, the net drive to the axonal spiking region is mostly tonic, likely similar to the activity during the theta state in awake rodents [Gasparini and Magee, 2006]. This stimulation results in the neuron firing at a rate of approximately 20 Hz, towards the upper end of these neuron's firing rate range *in vivo* [Ahmed and Mehta, 2009].

We first compare the axonal spiking behaviour of the deterministic version of the model to multiple realisations of the stochastic version of the model. The stochastic model displayed three phenomena: 1) 'dropped' spikes that were present in the deterministic model; 2) 'extra' spikes that had no counterpart in the deterministic model; and 3) jitter in spike timing from trial-to-trial (Figure 3.4).

Each of these three phenomena have implications for neural coding. Dropped spikes, by definition, happen when a spike in the deterministic model has no counterpart in a stochastic run. Because spikes are dropped only on some, but not all, stochastic trials, these spike events can be considered probabilistic. Similarly, extra spikes appear aligned in time between stochastic trials, and are present only on a fraction of trials. Hence, all spikes have a certain reliability (probability of occurrence), here ranging from 0.1 to 1 (Figure 3.4c). This unreliability is also evident in the trial-to-trial spike count (3.4e). Events with high probability in the stochastic runs were generally associated with an event in the deterministic simulation (Figure 3.4c). These results demonstrate that stochastic ion channel gating makes the neural input-output transformation necessarily probabilistic.

What are the implications of spike time jitter for neural coding? Jitter of spike event i can be defined as the standard deviation σ_i over the N stochastic runs where the spike appeared, $\sigma_i = \sqrt{\frac{1}{N}\sum_j^N (t_{i,j} - \bar{t}_i)^2}$, where $t_{i,j}$ is the time of spike event i on trial j and $\bar{t}_i$ is the mean time of spike event i. Here jitter ranges from 0.19 ms to 4.68

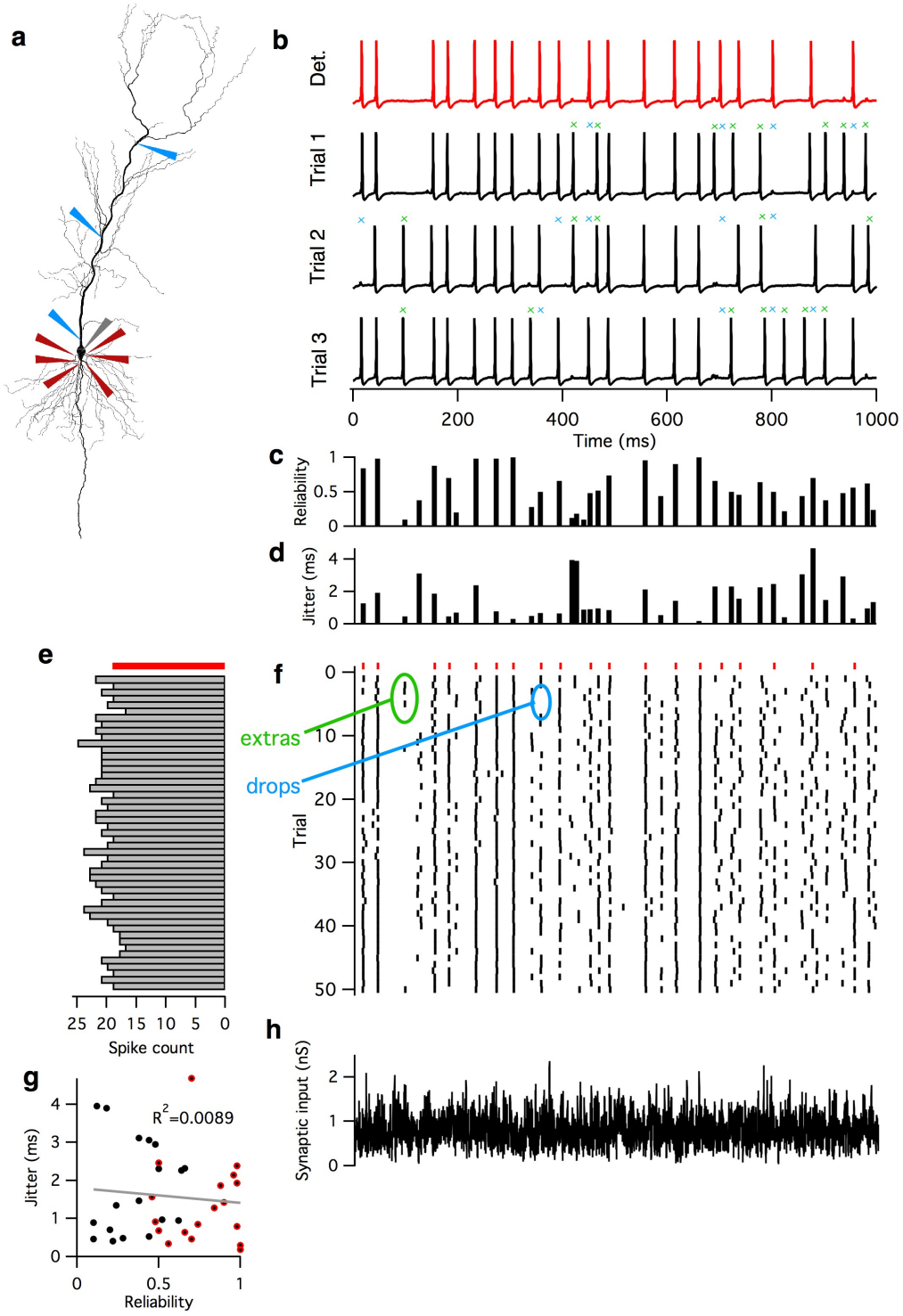

Figure 3.4: Channel noise corrupts synaptic integration in a morphologically realistic neuron model. **a**: Morphology of the CA1 neuron model. Arrows indicate position of recording electrodes; grey is soma, red is basal dendrites, blue is apical dendrites. **b**: Example voltage traces from deterministic model (red), and stochastic trials 1, 2 and 3 (black). Crosses mark 'dropped' spikes (blue) and 'extra' spikes (green). **c-d**: Reliability (c), jitter (d) for each spike event. **e**: Spike count for each trial in f. **f**: Raster plot of action potential times recorded at soma from 1s model time. One deterministic trial in red ticks and fifty stochastic trials in black ticks. **g**: Spike jitter vs reliability. Red dots indicate spikes that appeared in the deterministic simulation. **h**: Summed synaptic input conductance, identical for each trial.

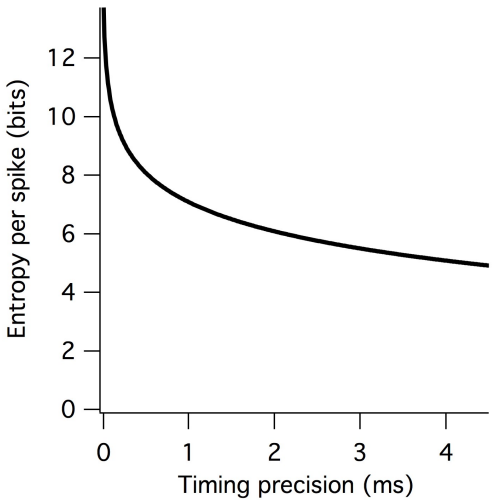

Figure 3.5: Entropy rate decreases with decreasing spike timing precision. Entropy rate calculated at 20Hz and then divided by firing rate to give units of bits/spike. Adapted from Rieke et al. [1999].

ms (Figure 3.4d). By limiting the precision of the neural code, intrinsic spike time jitter sets an upper limit on the maximum amount of information a neuron can convey about its inputs through spike timing. Lower spike timing precision results in lower information transmission rates. We demonstrate this using concepts from information theory [Shannon and Weaver, 1964]. Entropy is a statistical measure that is closely related to information (not to be confused with the concept of entropy in thermodynamics). Roughly speaking, entropy measures how "surprising" a set of responses of a system is, given the knowledge of the likelihood of all possible responses of that system [Dayan and Abbott, 2001]. Surprising in this sense means that the response occurs with a low probability. The rate of entropy of a signal can serve an upper bound on rate of information that that signal can potentially carry. The entropy rate of a spike train, S, can be approximated [MacKay and McCulloch, 1952, Rieke et al., 1999] as

$$S \approx \bar{r} \log_2 \left(\frac{e}{\bar{r} \Delta\tau} \right)$$

where $\bar{r}$ is the mean firing rate and $\Delta\tau$ is the spike timing precision (Figure 3.5). Hence, decreasing spike time precision leads to a decrease in entropy rate. At a timing precision of 1ms (Figure 3.4g) the maximum entropy rate a 20 Hz spike train can transmit is $\sim$7 bits/spike. It would be interesting to compare this value to the information rates estimated from recordings from sensory neurons.

3.3.5 Dropped and extra axonal action potentials are mostly derived from probabilistic dendritic spiking

Where does the probabilistic spiking behaviour arise from? The dendrites of hippocampal and cortical pyramidal neurons can generate local action potentials which forward propagate (either actively or passively) to the soma, often then triggering full-blown axonal action potentials [Spruston et al., 2008]. It is not clear if the probabilistic axonal spiking in the CA1 pyramidal neuron model above is due to 1) probabilistic dendritic spiking, 2) probabilistic conversion of dendritic spikes to axonal spikes, or 3) probabilistic axonal spiking from graded dendritic depolarisation. To clarify this we examine more closely the membrane potential at dendritic locations $\sim 10\mu$m proximal to the soma immediately preceding axonal spike events in the above simulations. We choose to record at proximal locations instead of distal locations because it reduces the possibility of missing dendritic events that originate near the soma.

In all observed cases, axonal action potentials were preceded by dendritic depolarisation. In a small fraction of cases (<10%) these dendritic depolarisations had rapid onset and large amplitude (>-20mV), characteristic of self-regenerative dendritic spikes [Spruston et al., 2008] (Figure 3.6). When these dendritic spikes reached the proximal recording electrodes, they reliably triggered axonal action potentials, contrary to possibility 2 above. Dendritic spike generation, however, was stochastic (Figure 3.6a,b), hence accounting for a portion of probabilistic axonal spiking (possibility 1 above).

The majority of axonal spikes were triggered by more modest dendritic depolarisations ($\sim$10mV). However, on stochastic simulations these modest depolarising events also appeared all-or-none in all examined cases, suggesting that they are dendritic spikes that had decay en route to the soma (Figure 3.6c,d). Not all of these events trigger axonal action potentials, in line with possibility 3 above.

To determine if axonal spike jitter arises from jitter in dendritic events or jitter introduced in the axonal spike initiation process, we plot the two measurements against each other. If dendritic jitter accounted fully for axonal jitter, the two should be exactly correlated. Here we include all dendritic depolarisations, both clear spikes and more modest depolarisations. We find that dendritic event jitter accounts for the majority of axonal spike jitter ($R^2 = 0.919$).

In summary, in this model all-or-none dendritic events appear either 1) as full-blown dendritic spikes that reliably trigger somatic action potentials, or 2) as more modest events that probabilistically trigger somatic action potentials. No axonal action

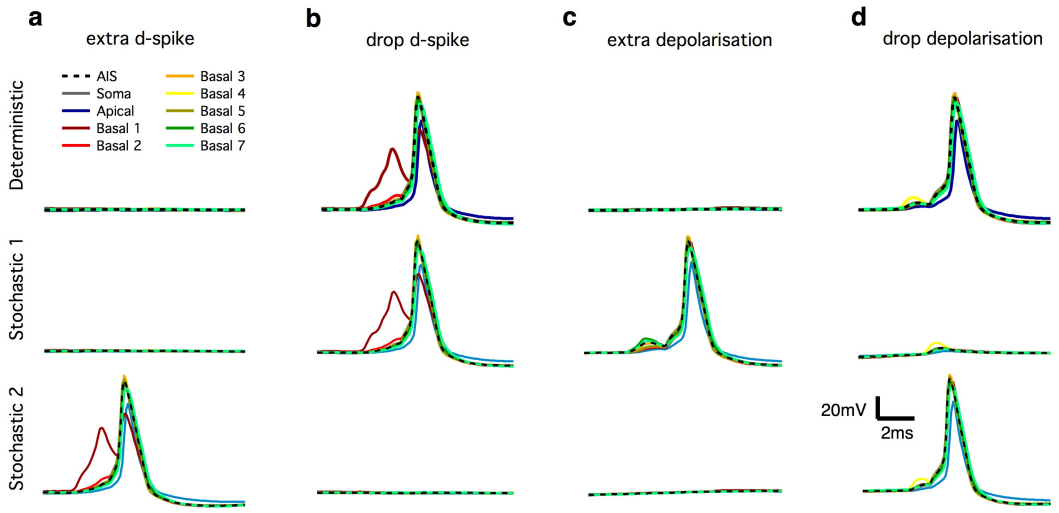

Figure 3.6: Probabilistic dendritic events underlie probabilistic axonal firing. Rows are example voltage traces from deterministic (top), stochastic trial 1 (middle) and stochastic trial 2 (bottom) simulations. **a-b**: Extra (a) and dropped (b) axonal action potentials from probabilistic dendritic spikes. **c-d**: Extra (c) and dropped (d) axonal action potentials from modest but all-or-none dendritic depolarisations.

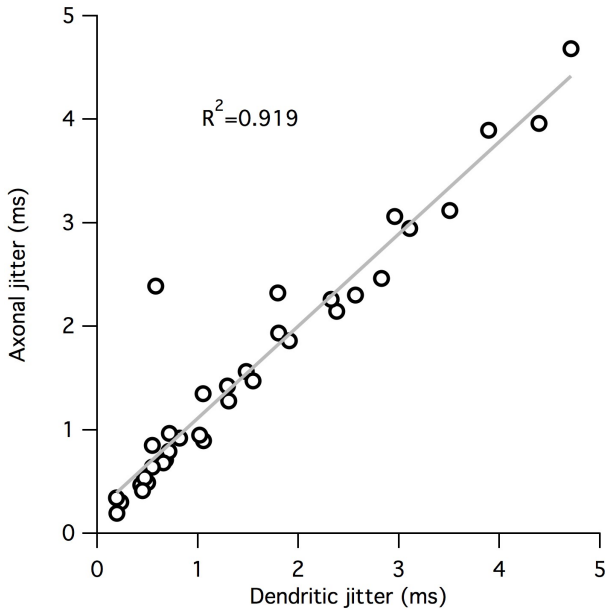

Figure 3.7: Dendritic jitter accounts for almost all axonal spike jitter.

potentials were observed without one of these dendritic events.

3.3.6 Ion channel subcellular location determines their contribution to channel noise

The above results demonstrate that channel noise is strong enough to make synaptic integration in dendritic neurons probabilistic, at least from Poissonian synaptic input. However, channels are distributed throughout the dendrites, soma and axon. It is not clear whether it is the ion channels in the dendrites or in the soma/axon region which most influence probabilistic action potential firing.

To investigate this problem, we repeat the above simulations while allowing stochastic channel gating only in a specified neural region (dendrites or soma/axon), while other conductances are deterministic.

Stochastic channel gating in either the soma/axon or dendrites alone was sufficient to induce unreliable axonal and dendritic spiking and jitter (Figure 3.8). However, channel noise in the axon alone causes less drops and extra axonal spikes ($p<1e-6$, ANOVA) and dendritic events ($p<1e-6$, ANOVA) than the fully stochastic simulation. In contrast, dendritic channel noise alone is sufficient to reproduce the dropped and extra axonal spikes found in the full stochastic model ($p=0.99$ for drops, $p=0.85$ for extras, ANOVA) (Figure 3.8b). Dendritic channel noise did not have a significantly different number of extra dendritic events than that found in the fully stochastic simulation ($p=0.81$, ANOVA), but surprisingly produced more dropped dendritic events than the fully stochastic simulation ($p<1e-6$, ANOVA). Dendritic noise always led to more dropped and extra axonal spikes and dendritic events than axonal/somatic noise ($p<1e-6$, ANOVA) (Figure 3.8b).

Somatic/axonal channel noise introduced little spike time jitter in both axonal spikes and dendritic events (~ 0.5 ms), while dendritic channel noise could account for most of the jitter found in the fully stochastic simulation (~ 1.5 ms) (Figure 3.8c).

These results suggest that although somatic/axonal channel noise can corrupt spike timing and reliability, dendritic channel noise accounts for most of the effects found in the fully stochastic model [van Rossum et al., 2003].

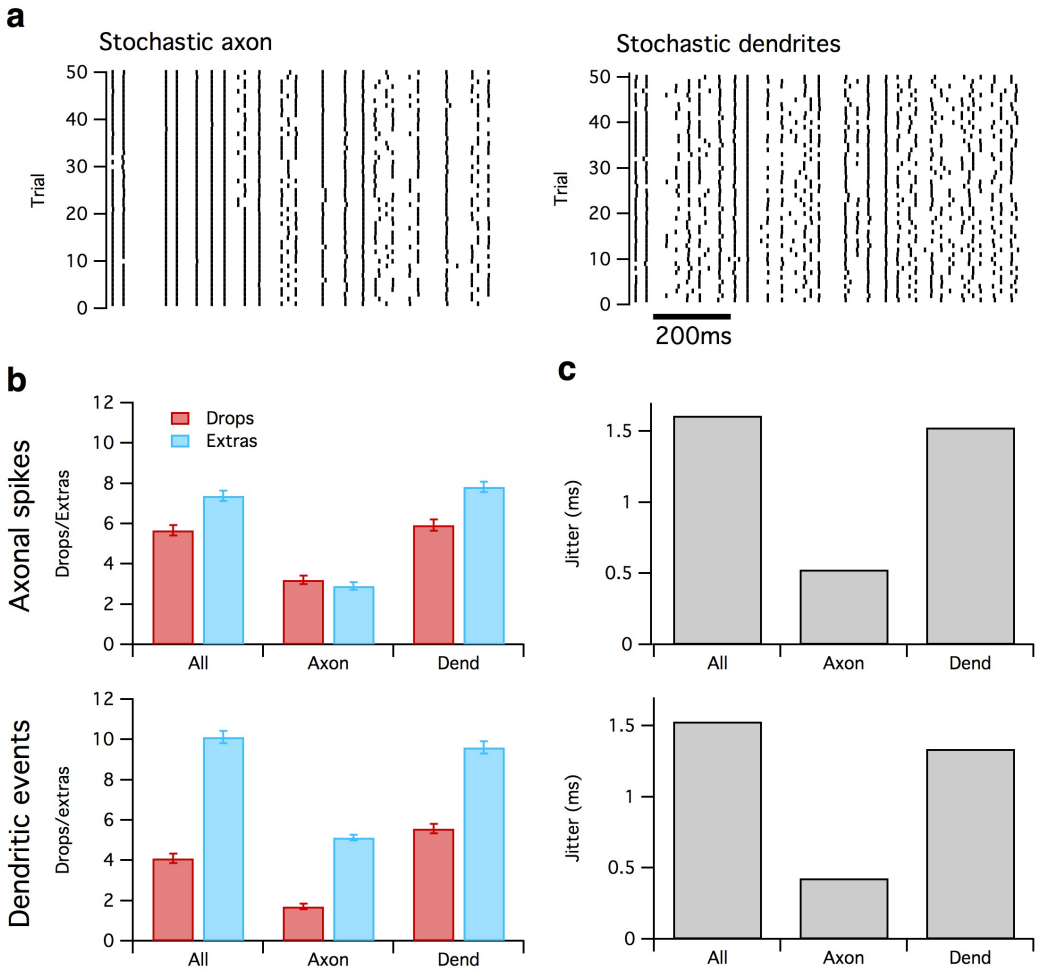

Figure 3.8: Channel location determines their contribution to spike unreliability and jitter. **a**: Raster plots of axonal action potentials while stochastic channel gating was implemented only in the soma/axon (left) or dendrites (right). **b**: Mean number of dropped and extra axonal spikes (top) or dendritic events (bottom) during 1s simulation for each source of stochastic ion channel gating. **c**: Mean jitter in axonal spikes (top) and dendritic events (bottom) for each experimental condition.

3.3.7 Ion channel type determines their contribution to channel noise

The CA1 pyramidal cell model includes several distinct ion channel types (Na_V, K_{Dr}, K_A, H, and both Na^+ and K^+ leak channels) which differ in their voltage-dependence, kinetics and single-channel conductance. To explore which of the channel types contribute most to spike unreliability and jitter, we repeat the above simulations while allowing stochastic gating only for one channel population at a time, while other conductances are deterministic (Figure 3.9).

The stochastic gating of any of the ion channel types included was sufficient to induce some dropped and extra spikes, and spike time jitter. However, no one channel type could alone account fully for the probabilistic spiking and jitter found in the full stochastic simulation. The relative channel contributions in order from most to least, as measured by axonal spike jitter, were: Na_V, K_A, K_{Dr}, leak and H (Figure 3.9c). Of these, stochastic Na_V channels could reproduce the number of dropped axonal spikes ($p = 0.98$, ANOVA) and dendritic events ($p = 0.3$, ANOVA) seen in the full stochastic model, but led to fewer extra events than the full model ($p<1e-4$, ANOVA). All other channel types produced significantly less dropped and extra events than the full model ($p<1e-3$, ANOVA).

These results demonstrate that the stochastic gating of many different channel types, to different degrees, can induce unreliability and jitter into synaptically-driven axonal spike trains, at least under conditions of Poissonian synaptic input.

3.3.8 Channel noise can mediate stochastic resonance of dendritic spiking to oscillatory inputs in a model hippocampal pyramidal neuron

The addition of noise can be of benefit for certain non-linear signal-processing systems. In general, this phenomenon is referred to as stochastic resonance (SR) [McDonnell and Abbott, 2009]. SR is commonly defined for input-output systems as a peak in the ability of the system to transmit information for a non-zero amplitude of added noise. One example of SR can be found in detection systems that threshold weak analog input signals into binary outputs. Here, noise triggers probabilistic but signal-locked threshold crossings that do not occur in the noise-free case, so transmitting information about the signal. Optimal SR in this case occurs when the noise amplitude

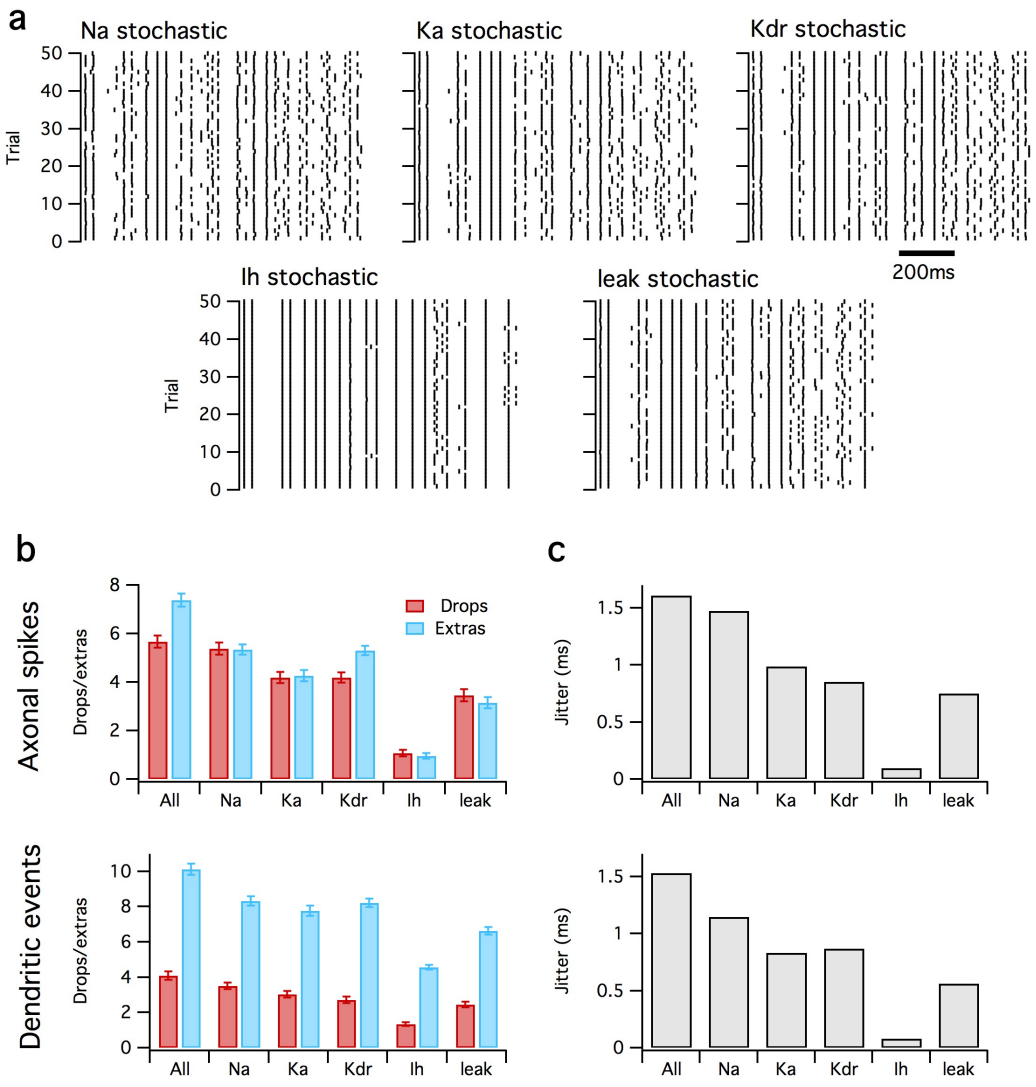

Figure 3.9: Ion channel type determines their contribution to spiking unreliability and jitter. **a**: Raster plots of axonal spike trains from 50 trials with stochastic gating confined to a single channel type in turn. **b**: Dropped and extra axonal spikes (top) and dendritic events (bottom) for each of the stochastic channel conditions. **c**: Axonal spike (top) and dendritic event (bottom) jitter for each condition.

is comparable to the signal amplitude. If noise is too weak, it is not great enough to enhance threshold crossings. If noise is too strong, it overrides the signal.

A single-compartment stochastic Hodgkin-Huxley model suggested that ion channel noise could in principle mediate stochastic resonance in small membrane patches [Goychuk and Hänggi, 2001]. Kole et al. [2006] also found that stochastic Ih channel gating could mediate SR in compartmental models of cortical pyramidal neurons, but only to subthreshold somatic current injection. It is not clear if the membrane noise from stochastic channel gating in a full multi-compartmental model of a central neuron, with realistic ion channel type and number, and dendritic morphology, can also mediate stochastic resonance to synaptic inputs. We address this issue using the CA1 pyramidal neuron model from above. We stimulate the neuron with 500 distributed synaptic inputs. Each synapse is activated according to an inhomogeneous Poisson process where the mean firing rate is a sinusoidal function of time (5 Hz). We choose the Poisson process to ensure decorrelated inputs, and to avoid synchronicity which might trigger dendritic spikes. The mean peak and trough synaptic input frequencies are 3 Hz and 0 Hz, respectively (Figure 3.10a). The peak frequency is chosen so that the stimulus is just slightly too weak to cause axonal spiking in the deterministic version of the model. Hence, the cell transmits no information about its inputs in the absence of noise.

We record the axonal and dendritic spike trains at the soma, and quantify the output signal-to-noise ratio (SNR) for both as follows [Stacey and Durand, 2000]. We first calculate the power spectral density (PSD) of the spike train. We measure the signal as the power at 5 Hz, because the synaptic inputs are periodic with a frequency of 5 Hz. The noise is measured as the mean power over two windows either side of 5 Hz (here measured at the discrete frequencies of 4, 4.5, 5.5 and 6 Hz). Perfect output SNR would correspond to a PSD with a single peak at 5 Hz. We vary the magnitude of channel noise by varying the single-channel conductance γ of all membrane ion channels over a physiological range (2-200 pS), while inversely varying the number of channels so as to keep the total conductance of each channel population constant.

Increasing the magnitude of membrane noise from stochastic ion channel gating (by increasing single-channel conductance) increased the number of both axonal and dendritic spikes (e.g. Figure 3.10b), and the mean power of both spike trains (Figure 3.10c). The SNR for dendritic spikes driven by the periodic synaptic stimulus increased as a function of γ over the entire range (2-200 pS) (Figure 3.10d). However, for $0 < \gamma < 100$ pS no axonal spikes were evoked, so SNR remained 0 in this range

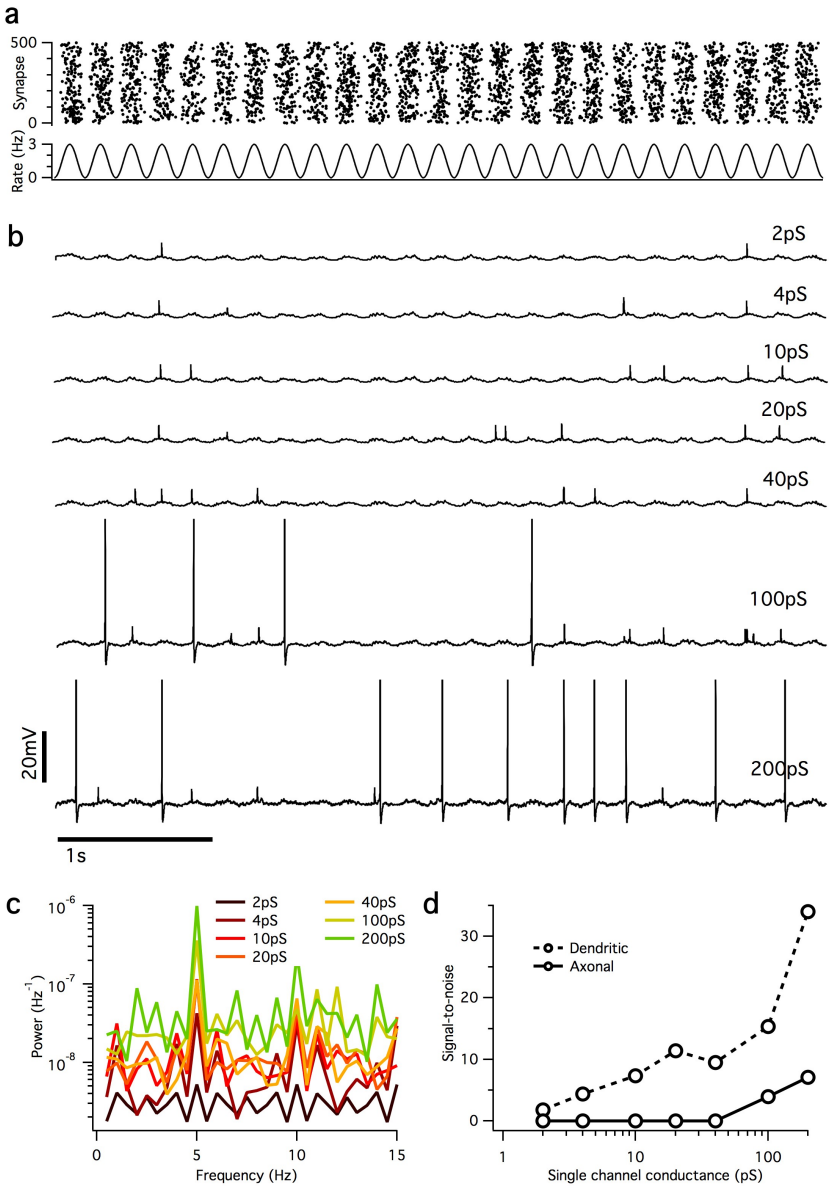

Figure 3.10: Stochastic resonance of dendritic events but not axonal spiking from channel noise in a CA1 pyramidal neuron. **a**: Synaptic input. Raster (top) and firing rate envelope (bottom) of inputs to 500 synapses on model cell. Rate envelope is modulated at 5Hz. **b**: Example somatic voltage traces from single trials for a physiological range of single-channel conductances(2-200pS). **c**: Power spectral density of dendritic event times for single-channel conductances from a. **d**: Signal-to-noise ratio for axonal (solid) and dendritic (dashed) spikes as function of single-channel conductance.

(Figure 3.10c). For $\gamma \geq 100$ pS, SNR increased monotonically. This is within the upper range of single-channel conductances measured physiologically [Hille, 2001]. Of course, these results are highly dependent on stimulus and ion channel properties, but these results demonstrate a proof-of-principle for a physiologically realistic parameter set.

In summary, these results demonstrate that in principle membrane noise from stochastic ion channel gating can mediate SR of dendritic spikes, and may facilitate SR of axonal spiking if channel conductances are large.

3.4 Discussion

3.4.1 Dendritic morphology influences the magnitude of voltage noise from stochastic ion channel gating

By including an identical set of ion channels on the dendritic morphologies of several different example cells from six different neural types, we show that the magnitude of channel noise depends strongly on neuronal morphology (Figure 3.1). Channel noise was significantly different between different cell types. These differences can only be due to the differences in local membrane impedance imposed by the differences in dendritic anatomy — cable diameter, length and branching structure — because the set and distribution of ion channels was identical in each model. This behaviour is predicted because membrane voltage noise variance σ_V^2 is the product of injected current noise variance σ_I^2 (identical in each case) with the squared membrane impedance (different in each case): $\sigma_V^2 = |Z|^2\sigma_I^2$.

Similarly, voltage noise from stochastic channel gating was significantly different in different cells of the same type. This result underscores the importance of repeating simulations of multi-compartmental model neurons in multiple example morphologies of the same cell type before drawing general conclusions in any study [Scorcioni et al., 2004, Szilágyi and De Schutter, 2004].

The amplitude of voltage noise also differed significantly with dendritic distance from soma in all cell types. In general, voltage noise increased at increasingly distal dendritic locations. This is to be expected for three reasons: first, the soma acts as a substantial current sink, so dendritic locations which are electrotonically decoupled from the soma are likely to have larger local impedance than dendritic locations near the soma. Second, dendritic diameter in most neurons tends to decrease with branch order, so that the most distal dendritic branches have narrowest diameters and the largest membrane impedance (except for Purkinje neurons which do not taper). Third, terminal dendrites tend to have a higher impedance than more proximal dendrites because of the boundary conditions at the sealed end of the dendrite, as discussed in the previous chapter [see also Rall, 1959].

This result complements and builds upon several previous studies which have used similar methods to isolate the effects of dendritic morphology on AP firing patterns [Mainen and Sejnowski, 1996], AP backpropagation and dendritic spike initiation [Vetter et al., 2001], AP burst firing [van Elburg and van Ooyen, 2010] and tempo-

ral discrimination of synaptic inputs [Branco et al., 2010, Branco and Häusser, 2011]. Our results are not pre-empted by any of these studies because they consider only deterministic aspects of neural dynamics. Together with our results, they demonstrate the importance of dendritic morphology in single-neuron computation. Hence, it is becoming increasingly clear that there are many aspects of single neural computation that are not reproduced by simplified single-compartment models.

3.4.2 Membrane potential and channel kinetics regulate the magnitude of channel noise

We demonstrate that the magnitude of ion channel noise depends upon membrane potential by varying the resting potential of a model CA1 pyramidal neuron (Figure 3.2). This finding is expected from binomial statistics which predicts that the variance of current fluctuations σ_I^2 from a population of N ion channels depends parabolically on channel open probability p_o: $\sigma_I^2 = N(V_m - E)^2\gamma^2 p_o(1-p_o)$. Hence, current fluctuations are maximal when $p_o = 0.5$. For most ion channel types in our model, $p_o \ll 1$ at -70mV. When we depolarise the model neurons towards -50 mV, p_o increases towards 0.5, so increasing membrane noise. The only exceptions to this are leak channels which have a fixed $p_o = 0.7$, independent of voltage. Their current fluctuations are fixed.

By modifying the transition rates of the leak channels, we also demonstrate that channel kinetics can influence the magnitude of channel noise. Although inclusion of 'fast' leak channels made no difference to the amplitude of membrane noise when compared to simulations with deterministic leak channels, we find that simply slowing leak channel transition rates 10-fold increases membrane voltage noise approximately 3-fold. Again, this is expected from basic biophysical theory because the membrane capacitance acts as a low-pass filter with $1/f$ frequency dependency. Slowing channel transition rates reducing the attenuation of this current noise source and leads to greater membrane potential fluctuations despite no change in mean membrane potential. Hence, channel kinetics can have a large impact on a channel population's contribution to membrane noise.

3.4.3 Stochastic ion channel gating makes synaptic integration probabilistic

We demonstrate that the channel noise is powerful enough to corrupt synaptic integration in a realistic model of a CA1 pyramidal cell which has been previously shown to account for dendritic and axonal spiking observed *in vitro* [Jarsky et al., 2005]. Stochastic simulations displayed *dropped* spikes that appeared during the deterministic simulation, *extra* spikes that did not appear during the deterministic simulation, and *jitter* of spike timing (range 0.1–4.5 ms) (Figure 3.4). Reliability of individual spikes ranged from 0.2–1. Action potentials that appeared in the deterministic simulation were associated with APs that had a high reliability in the stochastic simulations (Figure 3.4c,g).

These findings have important implications for neural codes when viewed at three different temporal scales:

1. If information were to be coded in the precise timing of individual action potentials, then the spike time jitter introduced by stochastic channel gating (Figure 3.4d,g) sets an intrinsic upper limit on the amount of information such a code could carry (Figure 3.5).

2. If information were to be coded by the presence or absence of a spike over a given short time interval ($\lesssim$10 ms) but not in the precise time, then the probabilistic spiking introduced by channel noise would corrupt such a signal. Two potential ways to overcome this limitation could be: a) tune the neuron's membrane ion channels or synaptic receptors according to the statistics of its input so that spike probabilities for important stimuli are driven towards 0 and 1, so minimising the corruptive effects of channel noise; or b) encode information in the probability of a spike event. Although this method would increase the information capacity of such a code, reading out the information would require either averaging over multiple trials (for repeating stimuli) or averaging over multiple parallel neurons simultaneously. The upper limit on the information capacity of this code would be set by the number of trials or neurons involved and the spike probabilities.

3. If information were to be coded not by single spikes but by firing rate as measured over some time interval, stochastic ion channel gating would still corrupt such a code by introducing probabilistic single spike events. Spike count in our

model neuron was variable even over 1 s simulation time (Figure 3.4e). The variance of the spike count estimator for such a code would monotonically decrease with increasing measurement time, and would be minimised for spike probabilities furthest from 0.5 (binomial variance is maximal if $p_{spike} = 0.5$).

Finally, it should be noted that stochastic ion channel gating is but one of many sources of neural variability. Hence, any estimates of the impact of stochastic channel gating on the information carrying capacity of a neural code should be regarded as a lower limit on the impact of neural noise in general.

Both Mainen and Sejnowski [1995] and Nowak et al. [1997] reported an inverse relationship between jitter of spike timing and reliability of spiking from somatic current injection to neocortical pyramidal neurons *in vitro*. This relationship was not reproduced here (R^2= 0.0089, Figure 3.4g). The discrepancy may arise from the type of stimuli used. In our model all stimulation was synaptic, leading to dendritic spike-driven axonal spiking, whereas both experimental papers injected current stimuli directly into the cell body. When current is injected into the cell body there is less chance for jitter to accumulate compared to a dendritic spike which must propagate several 100s of μm's to the soma. Consistent with this explanation, we find that the axonal spiking mechanism adds little jitter to existing dendritic spike jitter (Figure 3.7).

3.4.4 The effects of channel noise on neural input-output variability arises primarily from dendritic sources

Two lines of evidence suggest that the probabilistic input-output behaviour of our CA1 pyramidal neuron model was primarily mediated by channel noise from dendritic sources, but less so by somato-axonal sources:

1. Axonal action potentials were almost always preceded by either moderate amplitude (~10 mV) or large amplitude (>20 mV) dendritic depolarisations which reliably triggered axonal action potentials. It is likely that both of these types dendritic events were dendritic spikes, because they exhibited all-or-none behaviour (Figure 3.6). The moderate amplitude events (~10 mV) likely began as full-blown dendritic spikes that simply attenuated en route to the soma, while the large amplitude events (>20 mV) were likely actively propagated for the entire distance. The probability of axonal spiking was almost fully conditional on these dendritic events. Consistent with this explanation, almost all axonal jitter was accounted for by dendritic jitter (Figure 3.7).

2. When we repeat simulations with stochastic channel gating only in axonal and somatic regions, while dendritic conductances are deterministic, there is a significant and dramatic drop in the number of dropped and extra axonal and dendritic spikes, and a reduction in dendritic and axonal spike time jitter (Figure 3.8). In contrast, when we simulate with only dendritic channel noise, the number of dropped and extra axonal spikes are not significantly different from the fully stochastic case. In addition, dendritic noise could reproduce almost all dendritic and axonal spike time jitter.

These results are consistent with previous findings that spike time irregularity from channel noise in retinal ganglion cell models is primarily accounted for by dendritic channel noise [van Rossum et al., 2003].

3.4.5 The magnitude of channel noise depends on ion channel type

When we run simulations with only one channel type in stochastic mode but all others in deterministic mode, we find that the magnitude of noise effects (spike probability and jitter) depends on channel identity. Our model included six different channel types, which, in order of contribution to axonal spike jitter, were: Na_V, K_A, K_{Dr}, leak and H.

The sum of the effects of individual channel types on stochastic spiking behaviour (4.17 ms axonal jitter) is much greater than the effects in the 'all stochastic' case (1.61 ms axonal jitter). This sublinear behaviour is surprising only if expectations are derived from linear systems. In a linear system, the variances of independent noise sources add to linearly to contribute to the total noise. This model is broken here on two counts. First, noise sources here are not independent because they are coupled through the membrane potential. Second, the axonal and dendritic spiking mechanisms are inherently nonlinear. Hence, even if subthreshold noise sources were to add linearly, their contributions need not be propagated in a linear fashion through the spiking non-linearity. This does not mean that the contributions from individual ion channel populations do not sum at all — adding a stochastic channel population will always increase noise at some level — but how this noise manifests in total system behaviour depends on the nonlinearities involved.

3.4.6 Channel noise is likely too weak to mediate stochastic resonance to periodic synaptic input in a CA1 pyramidal neuron model

A vast body of literature has now demonstrated that the injection of noise to certain non-linear input-output systems can have the surprising effect of enhancing signal transmission — a phenomenon termed stochastic resonance (SR) [Moss et al., 2004, McDonnell and Abbott, 2009]. Previously, channel noise has been proposed as one mechanism through which neurons might enable SR [Bezrukov and Vodyanoy, 1995]. However, it is not clear that a model neuron with realistic morphology, ion channel set and synaptic inputs could mediate this phenomenon. In contrast, Goychuk and Hänggi [2001] demonstrated SR from ion channel noise in HH model membrane patches. Kole et al. [2006] demonstrated SR from stochastic Ih channel gating in a model of a neocortical pyramidal neuron, but to somatic current injection. [Stacey and Durand, 2001] demonstrated that variable background synaptic could mediate SR in model and *in vitro* CA1 pyramidal neurons to a periodic synaptic stimulation. However, they suggest that noise in their experiments arose from synaptic sources. We tested the idea that channel noise can mediate SR by repeating a simulation similar to Stacey and Durand [2001]. We found that ion channel noise alone was too weak to mediate SR of axonal action potential firing from synaptic input. However, channel noise did mediate SR in dendritic spiking events. From earlier simulations (above) we expect that dendritic events can have strong influence on the probability of axonal firing. Hence, it is possible that SR in dendritic spiking from channel noise could be translated to SR in axonal spiking in the presence of additional suitably timed inputs which brought the axon to spike threshold. We did not test this possibility here.

It is also possible that channel noise was too weak to mediate SR in our specific model CA1 pyramidal neuron, but might nonetheless be able to mediate SR in other cell types, or if the cell had more or different ion channels. These possibilities remain to be tested.

Chapter 4

Dendritic spine dynamics regulate the long-term stability of synaptic plasticity

4.1 Background

4.1.1 Spine structural plasticity

Long-term synaptic plasticity is believed to underlie learning in the brain [Hebb, 1949, Bliss and Collingridge, 1993a, Milner et al., 1998, Morris et al., 2003]. Synaptic plasticity in central neurons is initiated by changes in dendritic spine Ca^{2+} concentration driven by pre- and post-synaptic neuronal activity. The Ca^{2+} signals are detected by molecular machinery within the spine, triggering a biochemical cascade that leads to potentiation or depression of synaptic efficacy (Figure 4.1a) [Zucker, 1999, Malenka and Bear, 2004]. Because successful memory storage requires that synaptic strength modifications persist over time, the synaptic plasticity machinery must somehow also remain insensitive to Ca^{2+} fluctuations that arise from ongoing neuronal activity. Understanding how dendritic spines and their synapses solve this trade-off between plasticity and stability is a fundamental problem for the neuroscience of memory.

Several observations suggest that dendritic spine structural plasticity might be functionally linked to synaptic plasticity. Dendritic spine size is actively regulated during synaptic plasticity so that large spines consistently host stronger synapses than small spines [Matsuzaki et al., 2001, 2004]. Because of their differences in volume, small spines also exhibit greater Ca^{2+} concentration changes during synaptic activation than

large spines [Nimchinsky et al., 2004, Noguchi et al., 2005, Sobczyk et al., 2005]. In addition, large spines are more stable in vivo than small spines [Grutzendler et al., 2002, Trachtenberg et al., 2002, Holtmaat et al., 2005, Zuo et al., 2005, Knott et al., 2006]. Despite these data, the function and consequences of the tight spine size to synaptic strength relationship remain poorly understood.

We analyze the consequences of dendritic spine structural plasticity for synaptic Ca^{2+}-signaling. Although a previous study [Kalantzis and Shouval, 2009] explored the effects of spine size changes on spike-timing dependent synaptic plasticity rules, we generalize their results to find that the exact form of the Ca^{2+}-influx to spine-size relationship is a crucial factor which determines long-term synaptic stability, synaptic strength distribution, and whether synapses store information as a binary or continuous variable. We use a detailed biophysical model to predict that hippocampal CA3-CA1 pyramidal neuron synapses fall into the stabilizing, continuous category, unifying several disparate experimental findings and offering a novel mechanism for rapid but robust synaptic information storage.

4.2 Methods

All simulations performed with Matlab (The Mathworks), except for nanodomain model (Section 4.3.7), performed using MCell 3.0 [Stiles et al., 1996, Stiles and Bartol, 2000]. Analysis done using Matlab and Igor Pro (Wavemetrics).

Ca^{2+}-signaling-dependent plasticity rule

Throughout the study, we model the Ca^{2+}-dependence of synaptic plasticity as follows. Low or baseline spine Ca^{2+} concentration cause no change in synaptic strength, Ca^{2+} concentrations above a moderate threshold trigger depression and Ca^{2+} concentrations above a higher threshold cause potentiation (Figure 4.1b) [Cummings et al., 1996, Hansel et al., 1997, Yang et al., 1999, Cormier et al., 2001, Cho et al., 2001, Shouval et al., 2002, Ismailov et al., 2004]. We formulate this plasticity rule as the difference of two sigmoid functions:

$$\Delta w([Ca^{2+}]) = \frac{\eta_p}{1+e^{-([Ca^{2+}]-\theta_p)/\sigma_p}} - \frac{\eta_d}{1+e^{-([Ca^{2+}]-\theta_d)/\sigma_d}}$$

where Δw is the change in synaptic strength, η sets the magnitude of plasticity events, $[Ca^{2+}]$ is the spine Ca^{2+} concentration, and θ and σ set the offset and steepness of

the sigmoids respectively. The subscripts p and d denote potentiation and depression respectively. The properties of the molecular Ca^{2+} detectors and plasticity machinery are independent of synaptic strength.

Integrate-and-fire model

The subthreshold voltage of the leaky integrate-and-fire neuron (Figs. 4.2c and 4.2) was modeled as

$$\frac{dV}{dt} = (-V + R_{in} I_{syn})/\tau_m$$

where V is the membrane potential, R_{in} is the input resistance (1GΩ), $I_{syn} = \sum_{n=1}^{N_{syn}} i_{syn}$ is the summed synaptic input current and τ_m is membrane time constant (10 ms). When the voltage reaches threshold, $V_{th} = 20$ mV, a spike is fired and the voltage reset to zero. We use current-based synapses where single synaptic input currents were modelled as $i_{syn} = w(e^{-t/\tau_{decay}} - e^{-t/\tau_{rise}})$ where w is the synaptic weight and τ_m =0.18 ms and $\tau_{decay} = 1.8$ ms set the waveform timecourse.

In this simplified model, synaptic Ca^{2+} signals arose solely from NMDARs (N-methyl D-aspartate receptors) [Sabatini et al., 2002, Shouval et al., 2002]. The Ca^{2+} influx through NMDARs was modeled as $Ca_{NMDA} = \rho \times \nu$; it is the instantaneous product of a dimensionless variable representing the amount of bound glutamate, ρ, which is synapse specific, with a dimensionless voltage variable v, representing post-synaptic membrane potential change from an action potential, which is identical for all synapses [Shouval et al., 2002]. Both ρ and v were constrained between 0 and 1, and evolved as $dx = -x/\tau$ ($\tau_\rho = 50$ ms and $\tau_v = 5$ ms). When the synapse is activated, $\rho_{t+\Delta t} = \rho_t + (1 - \rho_t)/2$, ensuring eventual NMDAR saturation upon repeated activation. When a postsynaptic spike occurs, $v \to 1$. The amount of spine Ca^{2+}, Ca_{sp}, from the Ca^{2+} influx through NMDARs follows $\frac{dCa_{sp}}{dt} = (Ca_{NMDA} - Ca_{sp})/\tau_{Ca}$ ($\tau_{Ca} = 20$ ms).

To model each of the three Ca^{2+} influx scenarios, we set the magnitude of Ca_{NMDA} to be a function of spine volume: $Ca_{NMDA}(V_{sp}) = A(V_{sp})^\alpha$ where A is a constant of proportionality ($A_{comp} = 8.33$, $A_{under} = 0.06$ and $A_{over} = 1000$; found by tuning so that spine Ca^{2+} transients were in the range of 0–10 μM) and α determines the scenario, as explained below. The spine volume-averaged Ca^{2+} concentration is related to the absolute amount of Ca^{2+} by

$$[Ca^{2+}] = \frac{Ca_{sp}}{V_{sp}} = \frac{A(V_{sp})^\alpha}{V_{sp}} = A(V_{sp})^{\alpha-1}$$

If $\alpha = 1$, then spine [Ca^{2+}] is independent of spine volume. This corresponds to the compensating scenario. In contrast, if $\alpha < 1$, then spine [Ca^{2+}] is a decreasing function of spine volume, corresponding to the undercompensating scenario. If $\alpha > 1$, then spine [Ca^{2+}] is an increasing function of spine volume, corresponding to the overcompensating scenario. For the presented simulations we set α equal to 1, 0 and 2 for the compensating, undercompensating and overcompensating scenarios, respectively. Synaptic weights, w, were instantaneously updated at each timestep according to the Ca^{2+}-dependent plasticity rule.

For Figure 4.3, all 500 synapses were initially set to approximately the same strength, close to the steady-state weight and continuously stimulated at a low rate (~5 Hz). A subset (fifty) of these synapses were then stimulated with either one or three bursts of 40 spikes at 80 Hz. The inter-burst interval was 1000 ms. The results in Figure 4.3B are the average from 5 simulation runs. The drift rate, D, (Figure 4.3c) was calculated as the difference between the mean stimulated synaptic strength at two time points, $D = (\bar{w}_{stim}(t) - \bar{w}_{stim}(t + \Delta t))/\Delta t$ and was always plotted as a function of the initial mean strength, $\bar{w}_{stim}(t)$. Δt here was 1000 s of simulation time.

Fokker-Planck model

Under certain conditions, the Fokker-Planck equation describes the time evolution of a probability density function. Here, it is

$$\frac{\partial P(V_{sp},t)}{\partial t} = -\frac{\partial}{\partial V_{sp}} A(V_{sp}) P(V_{sp},t) + \frac{1}{2}\frac{\partial^2}{\partial V_{sp}^2} B(V_{sp}) P(V_{sp},t)$$

where $P(V_{sp},t)$ is the time-dependent spine volume probability distribution, V_{sp} is the spine head volume, and $A(V_{sp})$ and $B(V_{sp})$ are the drift and diffusion terms, respectively. We numerically evaluate A and B as follows. First, we use a discretized Ca^{2+} concentration probability distribution. In the implementation described here the distribution is exponential. We choose the exponential distribution because it is the positive distribution with the smallest number of tunable parameters (the mean). Qualitatively similar results were found with either uniform or log-normal distributions, or when a limit of 20 μM is imposed on the amplitude of the exponential distribution, because of the saturation in the plasticity rule at high [Ca^{2+}]. The Ca^{2+}-dependent plasticity rule to calculate the discrete probability distribution of plasticity jump sizes for a given spine volume, $Q(\Delta V_{sp})$. From this we calculate the average jump, $\langle \Delta V_{sp} \rangle = \sum_i V_{sp,i} Q_i$ and its mean square $\langle (\Delta V_{sp})^2 \rangle = \sum_i (V_{sp,i})^2 Q_i$. The average jump size as a function

of spine volume gives the drift term, $A(V_{sp})$, while the mean square jump gives the diffusion term, $B(V_{sp})$ [van Kampen, 1992]. To incorporate intrinsic fluctuations we add a volume dependent term to the diffusion term, based on data demonstrating that the magnitude of spine size fluctuations increases linearly with spine head volume [Yasumatsu et al., 2008]. Hence the final diffusion term, $B'(V_{sp})$, is given by

$$B'(V_{sp}) = B(V_{sp}) + (2 \times 10^{-8})(1 + 20 V_{sp} \mu m^{-3})$$

For simulation, we discretize the spine volume probability distribution, $P(V_{sp}, t)$, at resolution Δt and ΔV. We use the drift and diffusion terms to build a Markov transition matrix, M, so that $P(t + \Delta t) = \Delta t M P(t)$. It is important that Δt and ΔV are kept small for the Fokker-Planck assumptions to hold. If we let $a_i = A_i / 2\Delta V$ and $b'_i = B'_i / 2(\Delta V)^2$, then M is the tridiagonal matrix

$$M = \begin{pmatrix} -a_1 - b_1 & -a_2 + b_2 & 0 & \dots & 0 & 0 \\ a_1 + b_1 & -2b_2 & -a_3 + b_3 & \dots & 0 & 0 \\ 0 & a_2 + b_2 & -2b_3 & \dots & 0 & 0 \\ \vdots & \vdots & \vdots & \ddots & \vdots & \vdots \\ 0 & 0 & 0 & \dots & -2b_{n-1} & -a_n + b_n \\ 0 & 0 & 0 & \dots & a_{n-1} + b_{n-1} & a_n - b_n \end{pmatrix}$$

Because the columns of M sum to zero, it has at least one eigenvalue equal to zero, λ_0. The eigenvector associated with λ_0 corresponds to the steady-state probability distribution, π_0 (Figure 4.4). For Figure 4.4a-b, left (the compensating scenario) we set depression to be slightly more likely than potentiation so that the synaptic strength probability distribution always drifts to the minimum strength, no matter what the initial strength is. For Figure 4c, we measure the time to steady-state (the lifetime) as the time it takes for the median of the spine volume probability distribution to reach $\pm 20\%$ of the steady-state median strength. We choose the median instead of the mean because the distributions were often bimodal and plotting the median more clearly represented the simulation findings, although the results were qualitatively the same in either case. For Figure 4.4d, we define the probability of a spontaneous transition from the weak to strong stable strength as $p_{flip} = \sum_i P(V_{sp,i} > V_{max}/2)$ following a fixed simulation time, t_{flip}. Here $t_{flip} = 5000$ s, but varying this choice does not change the qualitative shape of the curve in Figure 4.4d.

Biophysical CA1 pyramidal neuron spine model

The biophysical spine model (Figure 4.6a and Table 4.1) includes both Ca^{2+} and electrical dynamics and consists of three compartments: a spherical head (volume range 0.01–0.3 μm^3; Harris and Stevens, 1989), a spine neck (diameter 0.1 μm, length 0.5 μm; Harris and Stevens, 1989), and a single-compartment cylindrical dendrite segment (diameter 2 μm, length 795.77 μm, surface area 5000 μm^2). The values of the model parameters are given in Table 1. The electrical component contained AMPARs (α-amino-3- hydroxy-5-methyl-4-isoxazole propionic acid receptors), NMDARs, an R-type voltage gated Ca^{2+} conductance and a leak conductance. The timecourse of AMPAR and NMDAR glutamate binding was expressed as the dimensionless quantity G and modeled as the difference between two exponentials: $G_{ampar/nmdar} = e^{-t/\tau_{decay}} - e^{-t/\tau_{rise}}$, but the NMDAR model also contained a voltage-dependent Mg+ block [Jahr and Stevens, 1990], so the total NMDAR conductance is

$$g_{nmdar} = \frac{\bar{g}_{nmdar} \times G_{nmdar}}{1 + e^{-0.063 V_m}([Mg^+]/3.57)}$$

where $\bar{g}_{nmdar}$ is the peak NMDAR conductance, V_m is the spine membrane potential in mV and $[Mg^+]$ is the extracellular magnesium concentration in mM, here taken as 1 mM [Jahr and Stevens, 1990]. For all presented simulations, the post-synaptic voltage in both spine and dendrite was clamped to a fixed value. The three-compartment circuit was simulated using standard compartmental modeling methods [Segev and Koch, 1998].

The Ca^{2+} dynamics had parameters hand-tuned to reproduce the data from Sabatini et al. [2002]. Ca^{2+} entered the spine head through NMDARs and R-type Ca^{2+} channels and was buffered, extruded through membrane pumps or diffused to the dendrite. Spine head Ca^{2+} concentration, $[Ca^{2+}]_{sp}(t)$, followed:

$$\begin{aligned}
\frac{d[\mathrm{Ca}^{2+}]_{\mathrm{sp}}(\mathrm{t})}{dt} &= \frac{-I_{Ca}}{zFV_{sp}} \\
&\quad - \left([\mathrm{Ca}^{2+}]_{\mathrm{sp}}(\mathrm{t}) - [\mathrm{Ca}^{2+}]_0\right) \frac{\beta_{sp} S_{sp}}{V_{sp}} \\
&\quad - D \frac{\left([\mathrm{Ca}^{2+}]_{\mathrm{sp}}(\mathrm{t}) - [\mathrm{Ca}^{2+}]_{\mathrm{neck}}\right) A_{neck}}{l_{neck} V_{sp}} \\
&\quad - k_f \left([B]_{sp}(t)[\mathrm{Ca}^{2+}]_{\mathrm{sp}}(\mathrm{t})\right) + k_b \left([B]_{Tsp} - [B]_{sp}(t)\right)
\end{aligned}$$

The first term on the right-hand side represents Ca^{2+} influx; I_{Ca} is the total Ca^{2+} current influxing to the spine ($I_{Ca} = I_{Rtype} + 0.1 I_{nmdar}$), z is the Ca^{2+} ionic charge, 2, and

F is the Faraday constant. We assume that one-tenth of the NMDAR current is carried by Ca^{2+} ions [Segev and Koch, 1998]. The second term represents extrusion through the membrane; $[Ca^{2+}]_0$ is the resting Ca^{2+} concentration, β_{sp} is the extrusion rate, S_{sp} is the spine head surface area. The third term is diffusion through the spine neck; D is the Ca^{2+} cytoplasmic diffusion constant, $[Ca^{2+}]_d$ is the dendritic Ca^{2+} concentration, A_{neck} is the cross-sectional area of the spine neck and l_{neck} is the length of the spine neck. The fourth and fifth terms represent Ca^{2+} binding and unbinding with endogenous buffer respectively, k_f and k_b are the forward and backward Ca^{2+} buffer binding rate constants respectively, $[B]_{Tsp}$ is the fixed total concentration of endogenous Ca^{2+} buffer and $[B]_{sp}(t)$ is the dynamic concentration of unbound endogenous Ca^{2+} buffer. An analogous equation governs Ca^{2+} dynamics in the dendrite.

The Ca2+ to Ca2+ buffer reaction was modeled according to the kinetic equation $[Ca]_{sp} + [B]_{sp} \leftrightarrow [BCa]$ where $[BCa]$ is the concentration of Ca^{2+}-bound buffer, $[BCa] = [B]_{Tsp} - [B]_{sp}$. The free buffer, $[B]_{sp}$, evolves as

$$\frac{d[B]_{sp}}{dt} = -k_f\left([B]_{sp}[Ca]_{sp}\right) + k_b\left([B]_{Tsp} - [B]_{sp}\right)$$

In this model the spine's endogenous buffer capacity $\kappa_E \approx [B]_{Tsp}(t)k_f/k_b = 100\mu\text{M} \times 10^8\text{M}^{-1}\text{s}^{-1}/500\text{s}^{-1} = 20$, implying that $\sim 95\%$ of the Ca2+ influxing to the spine is initially buffered [Sabatini et al., 2002]. The remainder of the Ca^{2+} is rapidly extruded and only a small fraction ($< 1\%$) diffuses to the dendrite [Sabatini et al., 2002]. Hence, the spine neck plays only a negligible role in Ca^{2+} dynamics.

The peak AMPAR conductance, $\bar{g}_{ampa}$, was proportional to spine head volume, $\bar{g}_{ampa} = 2000V_{sp}$ pS/μm^3, while peak NMDAR conductance, $\bar{g}_{nmda}$, was independent of spine head volume, $\bar{g}_{nmda} = 60$ pS (Figure 4.6b). This relationship models the data from [Noguchi et al., 2005], and is crucial for the predictions of the biophysical model. We obtained qualitatively similar results if we assumed an NMDAR conductance that weakly increased with spine size ($\bar{g}_{nmda} = 35 + 250V_{sp}$ pS/μm^3). Should higher resolution data from future studies appear, it could be incorporated in to the model to help to further constrain its predictions.

The stimulation protocol for Figure 4.6 was a burst of 100 synaptic inputs at 100 Hz with the post-synaptic voltage driven to the described potential by a tonic current to the dendrite. Although R-type VGCCs are included in the model, they become inactivated by the sustained depolarization and so contribute only minimally to Ca^{2+} influx.

Molecular-level MCell spine model

The model is adapted from Keller et al. [2008] and implemented with the MCell simulator [Stiles et al., 1996, Stiles and Bartol, 2000]. The spine head is represented as a single cube with edge length scaled to achieve the desired volume. One side of the cube is chosen as the post-synaptic density (PSD) and contains 20 NMDARs, independent of spine volume. NMDARs were here represented as simple Ca^{2+} sources which released Ca^{2+} ions into the spine at a fixed rate, governed by the Mg^{+}-voltage block equation [Jahr and Stevens, 1990]. To simulate elevated post-synaptic activity and common synaptic plasticity protocols [Lee et al., 2009], the post-synaptic membrane potential is set to -30 mV. The spine bulk contains three Ca^{2+} buffers: mobile calbindin (45 μM), immobile calmodulin (10μM) and a generic fast immobile endogenous buffer (5 μM). The spine membrane uniformly contains plasma membrane Ca^{2+} ATPases (PCMA) pumps, Na^{+}-Ca^{2+} exchangers (NCX), and a constant low-rate Ca^{2+} influx to maintain resting Ca^{2+} concentration [Keller et al., 2008]. The base of the spine contains a square patch of membrane $0.15 \times 0.15 \mu m^2$ that is transparent to Ca^{2+}, modelling Ca^{2+} escape by diffusion through the spine neck to the dendrite. The Ca^{2+} nanodomain signals are measured around a single L-type Ca^{2+} channel [Magee and Johnston, 1995] that is inserted into the centre of the PSD. We choose the L-type Ca^{2+} channel because it has been implicated in local postsynaptic Ca^{2+} signaling involved in synaptic plasticity [Yasuda et al., 2003, Lee et al., 2009].

C_m	Membrane capacitance	0.75 μF/cm^2	
r_a	Axial resistivity	200 Ωcm	
$\bar{g}_{Leak}$	Leak conductance density	1 pS/μm^2	Tuned parameter
E_{leak}	Leak reversal potential	-70 mV	
$\bar{g}_{Rsp}$	Spine R-type conductance density	200 pS/μm^2	
$\bar{g}_{Rdend}$	Dendrite R-type conductance density	10 pS/μm^2	
E_{Ca}	Ca^{2+} reversal potential	+10 mV	
$lneck$	Spine neck length	0.5 μm	
d_{neck}	Spine neck diameter	0.15 μm	
$ldend$	Dendrite length	795.77 μm	
d_{dend}	Dendrite diameter	2 μm	
τ_{rise}^{AMPA}	AMPAR rise time constant	0.18 ms	
τ_{decay}^{AMPA}	AMPAR decay time constant	1.8 ms	
τ_{rise}^{NMDA}	NMDAR rise time constant	2 ms	
τ_{decay}^{NMDA}	NMDAR decay time constant	89 ms	
E_{syn}	AMPAR and NMDAR reversal potential	0 mV	
$[Ca]_0$	Resting Ca^{2+} concentration	50 nM	
D	Ca^{2+} diffusion constant	0.009×10^{-9} m^2/s	
β_{sp}	Spine extrusion rate	0.8×10^{-4} /s	Tuned parameter
β_{dend}	Dendrite extrusion rate	3.2×10^{-4} /s	4$\times$ spine extrusion
k_f	Endogenous buffer forward binding rate	100×10^6 /M/s	
k_b	Endogenous buffer backward binding rate	500 /s	
B_{Tsp}	Spine total buffer concentration	100 μM	
B_{Tdend}	Dendrite total buffer concentration	500 μM	
η_p	Potentiation rate	5×10^{-10}	Tuned parameter
θ_p	Offset for potentiation sigmoid	5 μM	Tuned parameter
σ_p	Slope for potentiation sigmoid	0.3 μM	Tuned parameter
η_d	Depression rate	2.5×10^{-10}	Tuned parameter
θ_p	Offset for depression sigmoid	3.5 μM	Tuned parameter
σ_p	Slope for depression sigmoid	0.3 μM	Tuned parameter

Table 4.1: Parameters for biophysical spine model.

4.3 Results

4.3.1 The spine-size to Ca^{2+}-influx relationship is critical factor in synaptic plasticity

How does the relationship between spine size and Ca^{2+} influx mechanisms affect synaptic plasticity? We consider the case of a single dendritic spine attached to a parent dendrite. Fast electrical excitatory post-synaptic currents are primarily mediated by AMPA receptors (AMPARs). The number and state of the synaptic AMPARs is one important factor underlying the strength of excitatory synapses. Throughout this study we assume that synaptic AMPAR number is proportional to spine head volume (Figure 4.1b right) [Takumi et al., 1999, Matsuzaki et al., 2001, Ganeshina et al., 2004, Noguchi et al., 2005].

Ca^{2+} influx to spines arises primarily from NMDARs and voltage-gated Ca^{2+} channels, and is determined by both pre- and post-synaptic activity patterns. Intracellular [Ca^{2+}] changes of sufficient amplitude can trigger synaptic plasticity [Lynch et al., 1983]. We assume that the Ca^{2+} concentration within the spine directly determines both the magnitude and polarity of synaptic plasticity [Cummings et al., 1996, Hansel et al., 1997, Yang et al., 2008, Cho et al., 2001, Cormier et al., 2001, Shouval et al., 2002, Ismailov et al., 2004]. Low or baseline spine [Ca^{2+}] causes no change in synaptic strength. Intermediate [Ca^{2+}] triggers synaptic depression, while high [Ca^{2+}] triggers synaptic potentiation, with corresponding changes in spine size (Figure 4.1b left).

Once given these assumptions, there are three possible scenarios (Figure 4.1c-f). First, Ca^{2+} concentration in a spine may be independent of spine volume (Figure 4.1c-f, left column). This scenario can only be achieved if Ca^{2+} influx and outflux mechanisms are continuously scaled to exactly counter changes in spine head volume (Figure 4.1c). We refer to this case as the compensating scenario. In this case, because Ca^{2+} concentration does not depend upon spine size, then the direction and magnitude of synaptic plasticity is dictated only by neuronal activity and not by synaptic strength. Although possible in principle, exact compensation is unlikely because it requires the rapid and precise tuning of multiple spine Ca^{2+} properties. For example, to compensate Ca^{2+} influx for changes in spine volume, the spine would need to scale the density of its Ca^{2+}-permeable channels and receptors proportional to $r^{3/2}$ (where r is the spine head radius).

Second, when spines increase in size, they might not have a corresponding increase in the number of Ca^{2+}-permeable channels and receptors. We refer to this case as the undercompensating scenario (Figure 4.1c–f, centre column). For example, if the number of Ca^{2+}-permeable channels and receptors was independent of spine head volume, then small spines would experience greater magnitude $[Ca^{2+}]$ changes than large spines would from similar stimuli (Figure 4.1e, centre). Given the Ca^{2+}-dependent plasticity rule, in this situation a single stimulus might trigger potentiation at small spines, but depression at larger spines. In addition, very large spines might have $[Ca^{2+}]$ changes too dilute to trigger synaptic plasticity at all. Hence, undercompensation can make strong synapses on sufficiently large spines immune to synaptic plasticity from ongoing neural activity.

Third, when spines increase in size, the number of Ca^{2+}-permeable channels they gain may be greater than that required for exact compensation. We refer to this situation as the overcompensating scenario (Figure 4.1c–f, right column). For example, a spine might double its volume following synaptic potentiation while trebling its number of voltage-gated calcium channels. In this case, large spines experience greater magnitude $[Ca^{2+}]$ changes from synaptic stimulation than small spines. Hence, according to the Ca^{2+}-dependent plasticity rule, overcompensation makes strong synapses on large spines more susceptible to potentiation, and makes weak synapses on small spines more susceptible to depression (Figure 4.1f).

In summary, there are only three possible Ca^{2+}-influx scenarios which can exist when spine volume is changed during synaptic plasticity: compensation, undercompensation or overcompensation. The primary factor that determines which of the three scenarios occurs for a given synapse is the relationship between spine volume and its number of Ca^{2+}-permeable channels or receptors (Ca^{2+}-outflux mechanisms also play an important role). If the magnitude of Ca^{2+}-influx J_{Ca} is known to be strict function of spine volume, $J_{Ca}(V_{sp})$, then the identity of the scenario can be determined by examining whether a small increase in volume ΔV_{sp} is matched by a sufficient proportional increase in Ca^{2+}-influx ΔJ_{Ca}. Exact compensation is achieved only when $\frac{\Delta J_{Ca}}{J_{Ca}} = \frac{\Delta V_{sp}}{V_{sp}}$. Undercompensation occurs if there is not a sufficient increase in Ca^{2+}-influx to counter the fractional change in spine volume, $\frac{\Delta J_{Ca}}{J_{Ca}} < \frac{\Delta V_{sp}}{V_{sp}}$. Analogously, overcompensation occurs when the fractional increase in Ca^{2+}-influx is greater than the fractional change in spine volume: $\frac{\Delta J_{Ca}}{J_{Ca}} > \frac{\Delta V_{sp}}{V_{sp}}$.

Consider the following example of a spine with a spherical head, surface area A_{sp} and volume V_{sp}. If the number of spine Ca^{2+}-channels scales proportionally to spine

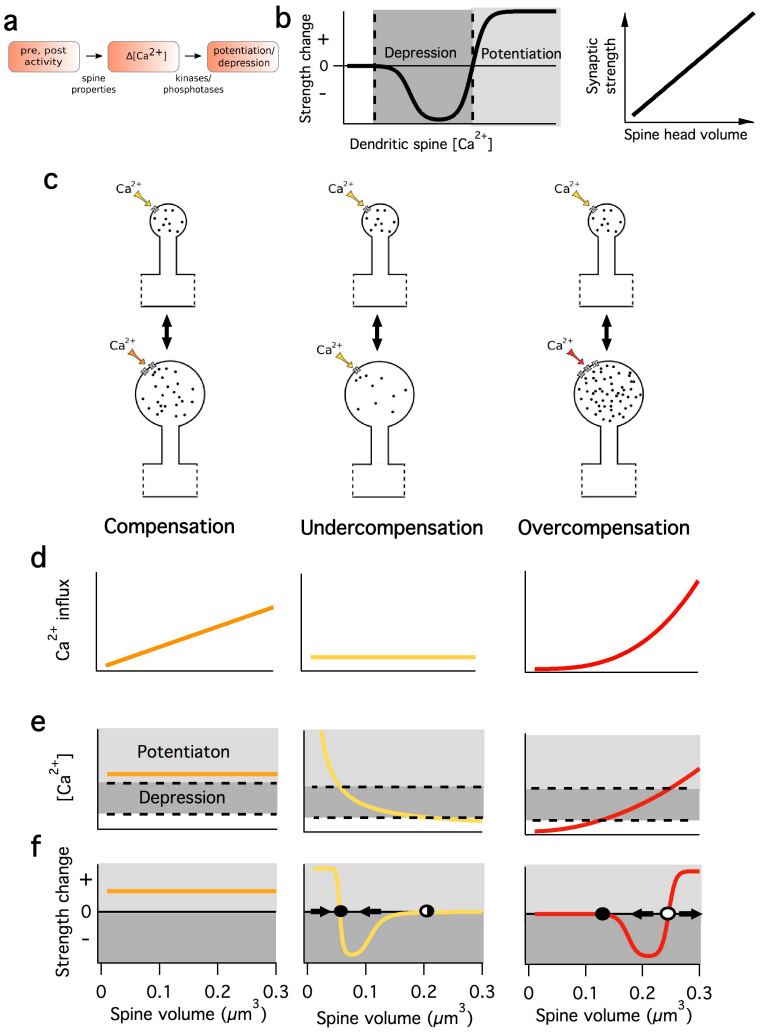

Figure 4.1: Imperfect coupling between spine size and Ca^{2+} profoundly affects synaptic plasticity. **a**: The synaptic plasticity cascade. Pre- and post-synaptic activity triggers postsynaptic Ca^{2+} signals, shaped by dendritic spine properties. Ca^{2+} signals trigger kinase and phosphotase-based molecular cascades, resulting in long-term potentiation/depression. **b**: Left: the change in synaptic strength as a function of spine Ca^{2+} concentration, $[Ca^{2+}]$. Right: spine size is proportional to synaptic strength. **c**: Depending on how the sources of Ca^{2+} influx scale as spine volume changes, the spine is said to compensate (left), undercompensate (centre) or overcompensate (right). **d-f**: The absolute amount of Ca^{2+} influx (**d**), Ca^{2+} concentration (**e**) and the change in synaptic strength (**f**) following a plasticity-inducing stimulus are plotted as a function of synaptic strength. Filled circles mark stable fixed points, open circles mark unstable fixed points. The right and left pointing arrows indicate potentiation and depression, respectively. Compensation results in spine size-independent Ca^{2+} signals for a given stimulus. Undercompensation biases small spines to large Ca^{2+} signals and large spines to weak Ca^{2+} signals. A plasticity-inducing stimulus drives spines of most sizes towards a single target strength (filled circle). Overcompensation causes a plasticity-inducing stimulus to potentiate large spines and depress small spines (separated by an unstable threshold, open circle).

surface area at 10 channels/μm^2, then

$$\begin{aligned} J_{ca}(V_{sp}) &= 10 j_{Ca} A_{sp} \\ &= \left(10(36\pi)^{1/3} j_{Ca}\right) V_{sp}^{2/3} \\ &= \alpha V_{sp}^{2/3} \end{aligned}$$

where j_{Ca} is the Ca^{2+} influx through a single Ca^{2+}-channel and $\alpha = 10(36\pi)^{1/3} j_{Ca}$. The slope of this function is

$$\frac{dJ_{Ca}}{dV_{sp}} = \left(\frac{2\alpha}{3}\right) V_{sp}^{-1/3}$$

For a small change in spine volume ΔV_{sp}, ΔJ_{Ca} can be approximated as $\Delta J_{Ca} \approx \frac{dJ_{Ca}}{dV_{sp}} \Delta V_{sp}$, giving

$$\begin{aligned} \frac{\Delta J_{Ca}}{J_{Ca}} &= \frac{\left(\frac{2\alpha}{3} V_{sp}^{-1/3}\right) \Delta V_{sp}}{J_{Ca}} \\ &= \frac{\left(\frac{2\alpha}{3} V_{sp}^{-1/3}\right) \Delta V_{sp}}{\alpha V_{sp}^{2/3}} \\ &= \frac{2}{3} \frac{\Delta V_{sp}}{V_{sp}} \\ &< \frac{\Delta V_{sp}}{V_{sp}} \end{aligned}$$

Therefore in this case a fractional increase in spine volume is not accompanied by a matched fractional increase in Ca^{2+} influx. Hence, scaling Ca^{2+}-channel number proportional to spine surface area leads to undercompensation.

This method can be readily applied to any Ca^{2+}-influx to spine volume relationship to determine the applicable scenario. It is not clear *a priori* which of the three scenarios applies to biological synapses.

4.3.2 Undercompensation leads to continuous synapses and overcompensation leads to binary synapses

How do the three spine Ca^{2+}-handling scenarios affect long-term synaptic strength dynamics? To address this, we consider the same spine model as in Figure 4.1, but we now also consider what happens as the stimulus magnitude (pre- and post-synaptic activity levels) is varied. In general we assume the amplitude of spine Ca^{2+}-influx to be a monotonically increasing function of stimulus magnitude. For example, increasing the

pre-synaptic firing rate leads to increased numbers of glutamate-bound NMDARs, or increasing post-synaptic voltage leads to increased Mg^{+} unblock of NMDARs, both of which cause greater Ca^{2+}-influx to the spine. Figure 4.2a schematically illustrates this effect for the three scenarios of exact, under and over compensation (Figures 4.2a left, centre and right, respectively). In all cases, the thin to thick curves indicate $[Ca^{2+}]$ in spines for stimuli of greater and greater magnitude. In spines of all size and in all three scenarios, increasing stimulus magnitude increases spine $[Ca^{2+}]$. Figure 4.2b shows schematic maps of the direction of synaptic change as a function of both spine volume and stimulus magnitude for each scenario. These illustrate how the mechanisms of under (Figure 4.2b centre) and overcompensation (Figure 4.2b right) shape the rules of synaptic plasticity as compared to the compensating scenario, where the direction of synaptic plasticity is independent of synaptic strength (Figure 4.2b left). Finally, to explore how stimulus magnitude influences long-term synaptic strength dynamics, we simulate a model integrate-and-fire neuron with simplified plastic synapses and spines that obey either compensating, undercompensating or overcompensating plasticity rules. We stimulate all synapses on the neuron with spike trains of a given average firing rate, and observe how their synaptic strengths evolve. Eventually synaptic strengths settle to steady-state values (plotted for each scenario as a function of presynaptic firing rate in Figure 4.2c). Now we discuss the three scenarios individually in turn.

If synapses exactly compensate their Ca^{2+}-influx following spine size changes, then the direction of a plasticity event is determined solely by pre- and post-synaptic activity (Figure 4.2a–b, left). Weak activity causes no change, intermediate activity causes depression and high activity causes potentiation (thin, medium and thick lines respectively in Figure 4.2a left). If a compensating synapse repeatedly receives a potentiating or depressing stimulus, it will continue to potentiate/depress without limit because there is no inherent mechanism in the plasticity rule to provide an upper or lower limit to its strength. In our integrate-and-fire model simulations we impose hard upper and lower limits on synaptic strength to avoid unphysiologically strong or weak synapses. In these simulations, following repeated stimulation synaptic strengths converge to either the maximum or minimum strengths. Whether a synapse settles to the maximum or minimum strength depends only on the frequency of its synaptic inputs, and not on their initial synaptic strength. Hence, exact compensation does not endow any particular initial synaptic strength with extra stability over other strengths. Therefore, exactly compensating synapses can store information as a continuous variable,

but if potentiation and depression are not finely balanced, they will eventually lose this information by drifting to their maximum or minimum strengths (Figure 4.2c left)[Fusi and Senn, 2006, Fusi and Abbott, 2007].

In the undercompensating scenario, because a plasticity-inducing stimulus induces potentiation at weak synapses but depression at strong synapses, then it acts to drive synapses towards a stable target strength at the crossover point between potentiation and depression (Figure 4.2a–b, centre). Hence, repeating the same plasticity-inducing stimulus at an undercompensating synapse will eventually saturate plasticity at a fixed synaptic strength [McNaughton et al., 1978, Dudek and Bear, 1993, O'Connor et al., 2005] (although this could also be implemented by additional mechanisms). In contrast, at compensating synapses a plasticity-inducing stimulus leads to a fixed jump in synaptic strength. Importantly, because increasing the stimulus strength (pre-synaptic firing frequency or postsynaptic voltage) increases $[Ca^{2+}]$ in synapses of all strength, stronger stimuli to undercompensating synapses shift the target strength to greater values (thin to thick lines in Figure 4.2a centre), as observed experimentally [McNaughton et al., 1978]. In our integrate-and-fire model simulations, the steady-state synaptic strength is a monotonic increasing function of presynaptic firing frequency (Figure 4.2c centre). Consequently, undercompensating synapses can store information as a continuous variable. In the undercompensating scenario, the plasticity rule naturally regulates synaptic strength so that no externally imposed limits on synaptic strength are necessary.

In the third scenario, overcompensation, a plasticity-inducing stimulus will depress weak synapses but potentiate strong synapses (Figure 4.2a–b right). Hence, all stimuli drive synapses towards their either their minimum or maximum limits. As for the compensating case, these minimum and maximum strengths must be imposed by some additional mechanism. Whether a given synapse potentiates or depresses depends on whether its initial synaptic strength is greater or less than a certain threshold (Figure 4.2b right and dotted grey line, Figure 4.2c right). The magnitude of the stimulus determines the threshold so that stronger stimuli lower the threshold (Figure 4.2b–c right). In the integrate-and-fire neuron model synapses converge towards either the maximum or minimum strengths, depending both on their stimulation frequency and their initial strengths. This suggests that in this scheme the synapse is effectively binary because only the minimum and maximum synaptic strengths are stable. Although in general binary synapses cannot store as much information as multi-state synapses [Barrett and van Rossum, 2008], binary storage is robust because small, undesired changes

in synaptic strength are automatically corrected and random transitions between the strong and weak states are unlikely.

In summary, we find the Ca^{2+}-influx to spine size scenario crucially determines the long-term dynamics of synaptic strength and the form of synaptic information storage. Compensation leads to binary information storage which is not robust, undercompensation leads to stable continuous-variable information storage, and overcompensation leads to robust binary information storage. Here we have considered only idealized scenarios, but later we will also consider the effect of intrinsic fluctuations in synaptic strength on stability.

4.3.3 Spine plasticity determines the influence of ongoing neural activity on synaptic strength stability

Ongoing neural activity might degrade stored memories by occasionally causing spine $[Ca^{2+}]$ fluctuations great enough to trigger synaptic plasticity. Therefore, we ask: how does the relationship between spine size and Ca^{2+} influx affect memory storage in the presence of ongoing neural activity? To address this question we compare how well each of the three scenarios can store information about a previous activity pattern in the synaptic strengths of an integrate-and-fire model neuron, similar to that presented in Figure 4.2c. Now we consider a neuron with 500 synapses that are tonically active at a rate just sufficient to keep the post-synaptic neuron active (both pre and post firing rates are ~ 5 Hz). To simulate weak and strong memory events we subject 50 of the synapses to either $1\times$ or $3\times$ brief high-frequency trains of input, respectively (see Methods). These high-frequency input events potentiate the stimulated synapses. After the input events, synapses are left to evolve their strengths in the presence of baseline neural activity. Because the baseline presynaptic inputs arrive randomly in time (but with a fixed average firing rate), occasionally multiple inputs arrive simultaneously by chance. If they are of large enough amplitude, these chance events can trigger spontaneous synaptic plasticity. These spontaneous synaptic strength changes will accumulate over time, and might eventually 'wash out' the potentiation initially induced by our high-frequency stimulus. However, in general we find that the stability of the memory depends on both the magnitude of the initial high-frequency stimulus ($1\times$ or $3\times$) and on the Ca^{2+}-influx to spine size scenario. We now examine each scenario in turn.

In the exactly compensating scenario, in the presence of baseline activity the synaptic strengths drift in a direction determined by the ratio of total spontaneous potentia-

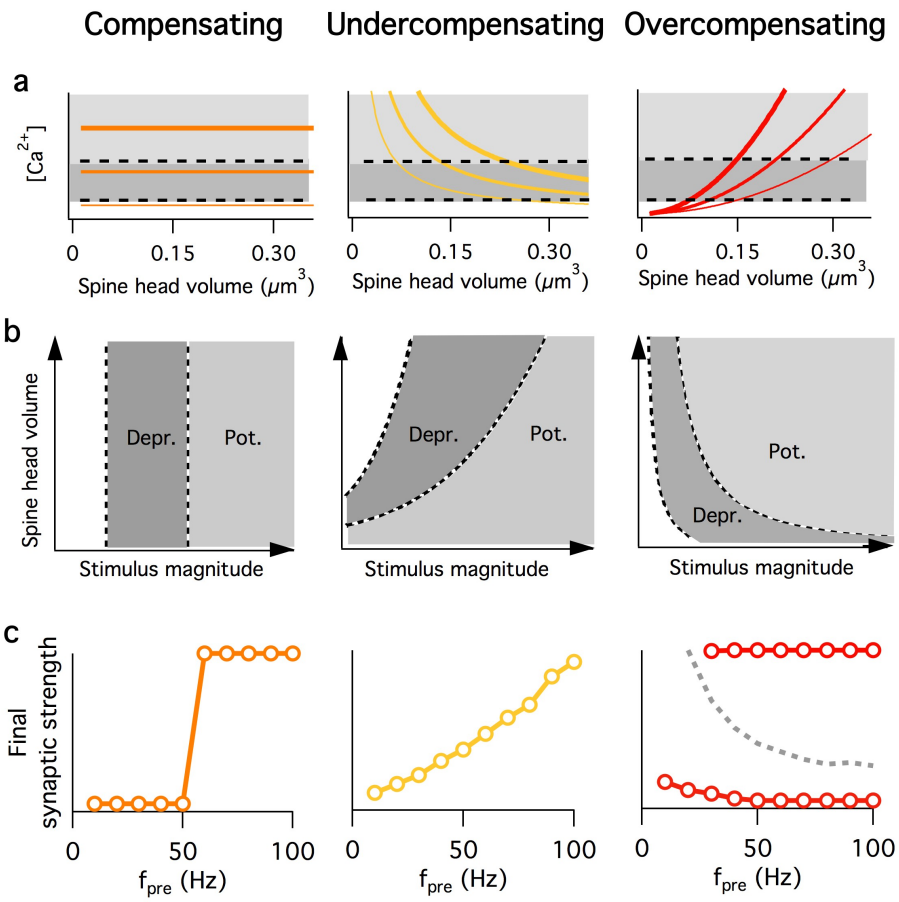

Figure 4.2: Undercompensation leads to analog information storage while overcompensation leads to binary information storage. **a**: Increasing the stimulus strength (from thinner to thicker lines) increases the Ca^{2+} influx across all spine volumes in all three cases. For the compensating rule (left), the direction of synaptic plasticity is independent of spine volume. Stronger stimuli for the undercompensating rule (centre) shift the stable point to greater spine volumes. For the overcompensating rule (right), stronger stimuli shift the unstable threshold between depression and potentiation to smaller spine sizes. **b**: Plasticity direction as a function of both stimulus strength (horizontal axis) and spine head volume (vertical axis). Dashed black curves indicate thresholds for LTD and LTP. **c**: Final synaptic strengths following prolonged stimulation, as a function of presynaptic firing rate. With the compensating rule, synapses eventually drift to their maximum or minimum strength, depending on their stimulation rate. Undercompensation yields synapses that represent their stimulation strength as a continuous variable. Overcompensation again leads to either maximal or minimal strengths, but whether a synapse ends up strong or weak depends not only on the stimulus strength, but also on the initial synaptic strength. Above the separatrix (dashed grey curve) the synapse will potentiate, but below it will depress. Simulations from an integrate-and-fire neuron.

tion to total spontaneous depression. If baseline activity is high, then large amplitude [Ca^{2+}] fluctuations are frequent and potentiation dominates over depression. In the example shown (Figure 4.3a–b left), the baseline activity triggers more depression than potentiation so that all synapses experience net depression over time. Synapses eventually drift towards their minimum strength (5 pA) (Figure 4.3a–b, left). Importantly, the rate and direction of drift are independent of synaptic strength, such that no particular initial synaptic strength is more stable than any other (Figure 4.3c left).

In contrast, for the undercompensating scenario strong synapses stay potentiated for the duration of the simulation, because the large volumes of their spines dilutes [Ca^{2+}] transients so that spontaneous depression is rarely triggered. At the same time, intermediate strength synapses are occasionally spontaneously depressed, causing their synaptic strengths to eventually drift back to baseline (Figure 4.3a–b centre). The rate of drift is slower for strong synapses than for weak synapses (Figure 4.3c centre) because [Ca^{2+}] at undercompensating synapses is a decreasing function of spine volume (Figure 4.1e centre). In this way, undercompensating synapses protect stronger memory traces from plasticity due to ongoing activity and allow them to persist for longer.

In the third, overcompensating scenario the behavior of synapses is qualitatively different to both of the two previous cases (Figure 4.3 right column). After initial potentiation, strong synapses are continually potentiated by ongoing activity until reaching the maximum strength (25 pA), because overcompensation makes larger spines have greater [Ca^{2+}] transients and therefore more susceptible to potentiation. Once these synapses reach the maximum strength, they are fixed there indefinitely. Weaker synapses, in contrast, are subject to net depression and drift back toward baseline strength. The net drift from spontaneous potentation and depression is positive for strong synapses and negative for weak synapses (Figure 4.3c right). Thus, overcompensating synapses threshold memory events into two categories: either strong and persistent or weak and transient.

4.3.4 Spine plasticity increases synaptic lifetimes in the presence of intrinsic fluctuations

In addition to spontaneous synaptic plasticity due to ongoing neural activity, dendritic spines have intrinsic fluctuations in their size [Yasumatsu et al., 2008, Minerbi et al., 2009], while post-synaptic densities show intrinsic fluctuations in both their size and shape [Mysore et al., 2007, Blanpied et al., 2008]. Because these fluctuations are

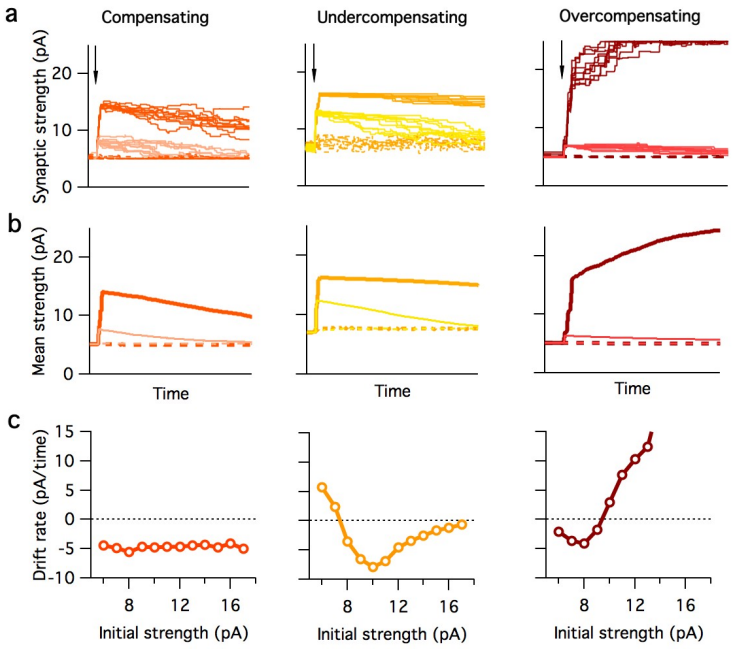

Figure 4.3: Memory induction and retention in an integrate-and-fire neuron depends on the relationship between spine size and Ca^{2+} influx. **a**: Synapses potentiate in response to a strong stimulus (vertical arrows) and then drift over time due to weak ongoing activity that occasionally triggers plasticity. Dark and light colors indicate strong and weak memory stimuli respectively for the compensating (left), undercompensating (centre) and overcompensating (right) learning rules. **b**: Mean synaptic strength over time for five repetitions of experiment in a. **c**: Drift rate as a function of initial synaptic strength. The drift rate is independent of synaptic strength in the compensating case, decreases for strong synapses in the undercompensating case, and is large and negative for weak synapses and large and positive for strong synapses in the overcompensating case.

thought to be random [Yasumatsu et al., 2008], over time they may corrupt information encoded in the synapse's strength. To examine the impact of these fluctuations, we use a reduced mathematical model, based on the Fokker-Planck equation, where synaptic strength is described by a probability distribution. The intrinsic fluctuations are simplified to a net diffusive effect on this probability distribution. We set the amplitude of intrinsic fluctuations to scale proportionally to spine size [Minerbi et al., 2009]. Together, the activity-dependent plasticity and intrinsic fluctuations probabilistically determine the synapse's evolution (see Methods). This abstract model's key strength over more detailed models is that it contains only a small number of free parameters that are all based on clear assumptions. It therefore allows general properties to be established that would be difficult to uncover using either a biophysical or integrate-and-fire model neuron.

Using this model, we change the strength of a single synapse and then follow the time evolution of its synaptic strength probability distribution when the synapse is subject to $[Ca^{2+}]$ transients from ongoing neural activity. We measure how long the synapse takes to return to baseline equilibrium (Figure 4.4). Once this equilibrium has been reached the synapse has lost any information that it was storing, because it has become indistinguishable from other synapses. We measure the equilibration time as a function of initial synaptic strength for each of the three spine Ca^{2+}-handling scenarios in the presence of intrinsic spine size fluctuations.

For the compensating scenario, the drift rate towards equilibrium is independent of synaptic strength (parallel curves in Figure 4.4b left). As a result, the retention time of compensating synapses is poor, but scales linearly with initial strength (Figure 4.4c left). When we increase the relative amplitude of intrinsic fluctuations, we find that synapses of all strength have roughly similar decreases in their retention time (Figure 4.4d left).

In contrast to the compensating scenario, in the undercompensating scenario the rate of decay of a potentiated synapse depends non-linearly on its strength. All synapses eventually drift towards a single stable strength, but, because strong synapses are less susceptible to plasticity, they decay more slowly than weak synapses (Figure 4.4b–c centre). This relationship saturates only for very strong synapses where plasticity events are uncommon and intrinsic fluctuations begin to dominate (Figure 4.4c right). As we increase the amplitude of intrinsic fluctuations (Figure 4.4d right), synaptic retention time drops dramatically for synapses of all strength, because fluctuations are so large that they corrupt the synapse's ability to remain potentiated. If we decrease

the amplitude of fluctuations, the retention time of strong synapses diverges to infinity because their spines are so large that the [Ca^{2+}] fluctuations from ongoing activity is never strong enough to trigger depression.

The overcompensating scenario causes the synaptic probability distribution to drift either to the minimum or maximum limit, depending both on neural activity and initial strength (Figure 4.4a–b right). Small excursions from the stable minimum or maximum strengths quickly disappear. If intrinsic fluctuations are small, the synapse persists at the stable strengths indefinitely. If fluctuations are large, random transitions between the strong and weak states become likely (Figure 4.4e). As a consequence memory storage is degraded.

These results demonstrate that intrinsic fluctuations effect on compensating synapses are independent of their size, whereas the effects of undercompensation reduces the sensitivity of large spines to intrinsic fluctuations, and overcompensation stabilizes spines that are already close to their maximum or minimum size. Thus, imperfect matching of Ca^{2+} dynamics and spine size may facilitate long-term storage of information by dendritic spines in the presence of moderate intrinsic fluctuations.

4.3.5 Undercompensation reproduces experimental synaptic strength distributions

The shape of synaptic strength distributions can provide information on the form of synaptic memory storage [Barbour et al., 2007]. The synaptic strength distributions measured from hippocampus, neocortex and cerebellum appear qualitatively similar [Barbour et al., 2007]. They are typically continuous, unimodal, have a peak at low strength and a long tail. What is the relationship between the three spine size-to-Ca^{2+} influx scenarios described above and the actual in vivo distribution of spine sizes or synaptic strengths? To address this question, we calculate equilibrium synaptic strength distributions directly from the Fokker-Planck model introduced above (see Methods).

Of the three learning rules, only the undercompensating case predicts a unimodal synaptic strength distribution with a central peak (Figure 4.5). If synapses compensate or overcompensate, strength distributions are either unimodal or bimodal with peaks at the minimum and/or maximum strengths but not at intermediate strengths.

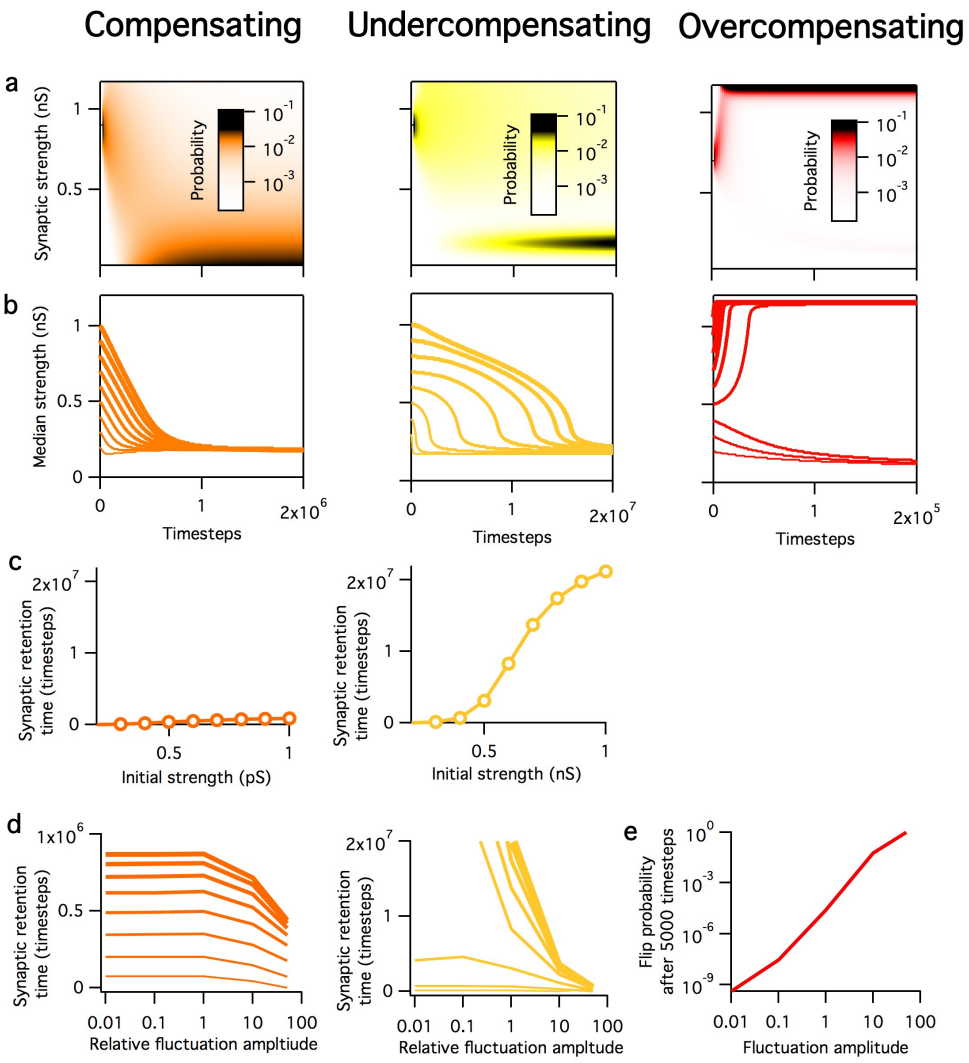

Figure 4.4: Spine plasticity increases the lifetime of undercompensating and overcompensating synapses in a Fokker-Planck model. **a**: Synaptic strength probability distributions over time. Darker color indicates higher probability. In each case the synapse is initialized at a particular strength but then drifts probabilistically over time. Note different timescales on x-axis of each panel. **b**: Median synaptic strength against time for the three learning rules for a range of different initial size spines. **c**: The synaptic retention time for the compensating and undercompensating learning rules as a function of initial synaptic strength. **d**: Synaptic retention time for compensating and undercompensating synapses of increasing initial strength (thin to thick lines) as a function of relative amplitude of fluctuations. **e**: Probability of overcompensating synapse spontaneously transitioning from lower to upper stable strength as a function of intrinsic spine volume fluctuation magnitude. Fluctuation strengths are reported relative to the value used for all other simulations.

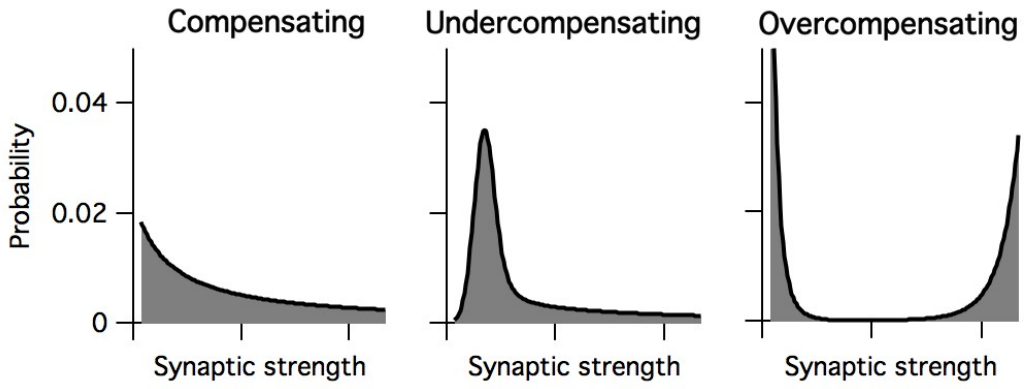

Figure 4.5: The steady-state synaptic strength distributions predicted by the compensating (left), undercompensating (center) and overcompensating (right) learning rules using a Fokker-Planck model. Only the undercompensating rule reproduces the central, unimodal synaptic strength distributions reported experimentally.

4.3.6 A biophysical hippocampal spine model predicts stable and undercompensating synapses

To determine if the properties of real dendritic spines are consistent with under, over or exact compensation we construct a model of a CA1 pyramidal neuron spine using available biophysical data as a test case.

Dendritic spine Ca^{2+} handling has been intensively studied in CA1 pyramidal neurons. Their main source of Ca^{2+} influx from synaptic activation is the N-methyl-D-aspartate receptor (NMDAR) [Sabatini et al., 2002]. In the model, NMDAR conductance is independent of spine volume in accordance with experimental data [Nimchinsky et al., 2004, Noguchi et al., 2005, Sobczyk et al., 2005, Takumi et al., 1999, Racca et al., 2000, Ganeshina et al., 2004]. In contrast, AMPA receptor (AMPAR) conductance is directly proportional to spine volume [Matsuzaki et al., 2001, Noguchi et al., 2005, Nusser et al., 1998, Takumi et al., 1999, Ganeshina et al., 2004] (Figure 4.6b; see Methods).

Most CA1 pyramidal dendritic spine heads have volumes of approximately 0.01–0.06μm^3, but there is a sub-population of large spines with head volumes ranging up to at least 0.3μm^3 [Harris and Stevens, 1989, Mishchenko et al., 2010]. For our simulations we select three spine sizes spanning this distribution: 0.01, 0.05 and 0.15μm^3 (Figure 4.6b). We subject the synapses on these spines to a typical experimental plasticity protocol used to induce long-term potentiation and spine head enlargement: a tetanic presynaptic stimulus (100 pulses at 100Hz) coupled with a steady post-synaptic

current stimulus [Cummings et al., 1996, Kauer et al., 1988, Ngezahayo et al., 2000, Harvey and Svoboda, 2007]. Varying the postsynaptic voltage regulates the amount of Mg^{+}-block of the synaptic NMDARs [Jahr and Stevens, 1990], and therefore the amount of Ca^{2+} influx to the spine. Synaptic plasticity is triggered by the Ca^{2+}influx from the stimulus (Figure 4.6d-e).

At a moderate holding potential of -50mV the small synapse potentiates, the medium synapse depresses and the large synapse does not change (Figure 4.6d). Importantly, the small and medium synapses converge to the same final strength, as expected for an undercompensating synapse (Figure 4.1, center). The Ca^{2+} concentration in the large spine does not reach the threshold for LTD, making it resistant to this plasticity protocol.

Upon repeating the experiment at a more depolarized postsynaptic holding potential of -30mV, all three synapses converge to the same strength (Figure 4.6e). The final stable synaptic strength is greater than that found for the -50mV holding potential, as predicted for undercompensating synapses (Figure 4.2, center). The large synapse's depression demonstrates how strong persistent synapses could still be reset under this scheme if given a suitably strong stimulus. We repeat the simulations for a large range of postsynaptic holding potentials (Figure 4.6f-g). The weakest synapse is plastic over the entire stimulus range, while the strongest synapse is mostly resistant to change. Notably, an identical stimulus can result in different plasticity outcomes depending on the initial synaptic strength (Figure 4.6g).

4.3.7 Dendritic spine size can influence nanodomain Ca^{2+} signaling

Some experimental data has indicated a role for local Ca^{2+}-signaling in some forms of synaptic plasticity [Hoffman et al., 2002, Yasuda et al., 2003, Lee et al., 2009]. We explored the possibility that dendritic spine size could regulate Ca^{2+} nano-domain signaling in a detailed molecular-level model of a hippocampal CA1-pyramidal neuron dendritic spine. The model (Figure 4.7a) was adapted from [Keller et al., 2008] and implemented using the MCell 3.0 simulator. The spine head was represented as a single cube with edge length scaled to achieve the desired volume. One side of the cube was chosen as the PSD and contained 20 NMDARs, independent of spine volume. Unlike Keller et al. [2008], NMDARs were here represented as simple Ca^{2+} sources which released Ca^{2+}+ ions into the spine at a fixed rate, governed by the Mg^{+}-voltage

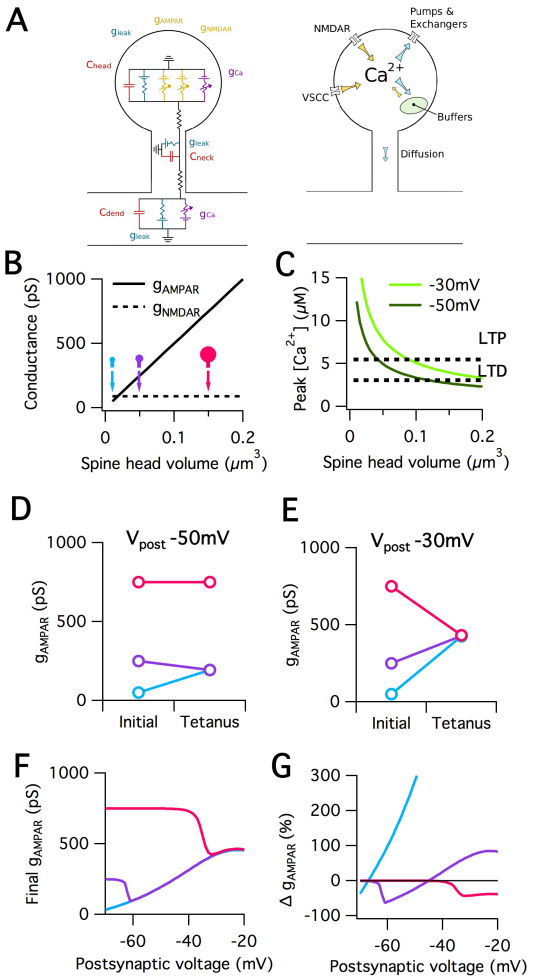

Figure 4.6: A biophysical spine model predicts that CA1 pyramidal synapses undercompensate. **a**: The spine model includes electrical dynamics (left) and Ca^{2+} dynamics (right). **b**: The spine's AMPAR and NMDAR conductances plotted as a function of spine head volume. **c**: The peak spine head Ca^{2+} concentration obtained during burst stimulation is plotted as a function of spine head volumes. Post-synaptic holding potentials of –30mV and –50mV are in light and dark green, respectively. **d-e**: AMPAR conductance of three synapses of different initial strength following a tetanic stimulus for post-synaptic holding potentials of -50mV (d) and -30mV (e). The small, medium and large synapses had initial spines head volumes of 0.01μm, 0.05μm3 and 0.15μm3 respectively. **f**: Final AMPAR conductance for small, medium and large synapses following a single tetanic plasticity-inducing stimulus for a range of post-synaptic holding potentials. **g**: Relative change in AMPAR conductance for same data as **f**.

block equation [Jahr and Stevens, 1990]. The voltage was set to -30mV, representing elevated post-synaptic activity. The spine bulk contained three Ca^{2+} buffers: mobile calbindin (45μM), immobile calmodulin (10μM) and a generic fast immobile endogenous buffer (5μM). The spine membrane uniformly contained PCMA Ca^{2+} pumps, NCX Na^{+}-Ca^{2+} exchangers, and a constant leak Ca^{2+} influx to maintain resting Ca^{2+} concentration. The base of the spine contained a square patch of membrane 0.15 x 0.15 μm2 that was transparent to Ca^{2+} to represent Ca^{2+} escape by diffusion through the spine neck to the dendrite. A single L-type Ca^{2+} channel [Magee and Johnston, 1995] was inserted into the centre of the PSD from which the Ca^{2+} nanodomain signals were measured. We choose the L-type Ca^{2+} channel because it has been implicated in postsynaptic local Ca^{2+} signaling [Yasuda et al., 2003, Lee et al., 2009].

Nanodomain signaling was tested as follows. Initially, we allow NMDARs to influx Ca^{2+} for 3 ms. This sets a baseline Ca^{2+} concentration in the spine. Then, the L-type Ca^{2+} channel is opened for 0.5 ms. This influxes Ca^{2+} ions at a rate of s^{-1}, rapidly causing a localized elevation of Ca^{2+} concentration near the channel pore, where Ca^{2+} buffers are not in their equilibrium binding state. We measure Ca^{2+} concentration as a function of distance from the channel (averaged over ten stochastic realizations), and repeat for several spine volumes over a physiological range. Decreasing the spine volume increased the Ca^{2+} concentration at all distances from the channel (Figure 4.7b-c), because the instantaneous bulk Ca^{2+} concentration was large enough to substantially add to the local concentration. The effect was greatest for small spine volumes, $<0.05\mu m^3$.

These simulation results suggest that even in the case that synaptic plasticity relies on microdomain Ca^{2+} signaling, spine volume could still implement the undercompensating mechanisms described here by enabling smaller spines to experience larger nanodomain Ca^{2+} signals than large spines.

4.4 Discussion

4.4.1 Hippocampal and neocortical spines appear to undercompensate

Our biophysical simulation of a model hippocampal CA1 pyramidal neuron spine suggests that these synapses likely undercompensate. This prediction unifies several disparate pieces of evidence: 1) NMDAR immunoreactivity [Takumi et al., 1999, Racca

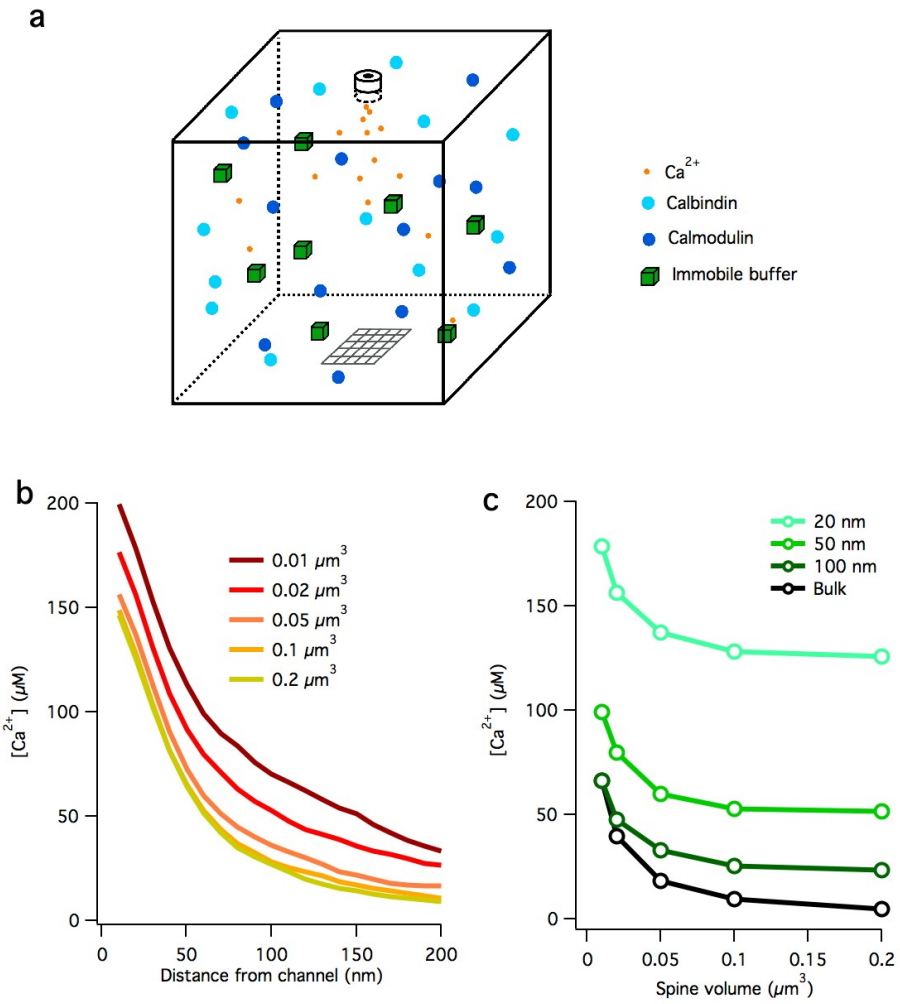

Figure 4.7: Spine size influences Ca^{2+} nano-domain signaling in a molecular model of a CA1 pyramidal neuron dendritic spine. **a**: Schematic diagram of molecular spine model (MCell simulator). Shown are Ca^{2+} ions, calbindin, calmodulin and a fast immobile endogenous buffer. L-type Ca^{2+} channel at top of spine, Ca^{2+} transparent patch (grey mesh) at bottom allowing Ca^{2+} escape to spine neck and dendrite. Not shown are 20 NMDARs (distributed randomly across top surface of spine), PCMA Ca^{2+} pumps, NCX Na+-Ca^{2+} exchangers, and leak Ca^{2+} influx channels (distributed randomly across entire surface of spine). **b**: Local Ca^{2+} concentration as a function of distance from the mouth of an open L-type Ca^{2+} channel. Each curve represents a different spine volume. **c**: Local Ca^{2+} concentration as a function of spine volume at varying distances from the mouth of an L-type Ca^{2+} channel. Same data as b. 'Bulk' indicates mean Ca^{2+} concentration over the entire spine volume.

et al., 2000, Ganeshina et al., 2004] and NMDAR excitatory post-synaptic potential (EPSC) amplitude [Nimchinsky et al., 2004, Noguchi et al., 2005, Sobczyk et al., 2005] do not increase with spine size; 2) focal glutamate uncaging causes larger Ca^{2+} fluorescence transients in small spines than in large spines [Nimchinsky et al., 2004, Noguchi et al., 2005, Sobczyk et al., 2005]; 3) synapses on small spines are easier to potentiate than synapses on large spines [Matsuzaki et al., 2004]; 4) weak synapses potentiate more than strong synapses [Larkman et al., 1992, Bi and Poo, 1998, Debanne et al., 1999, Montgomery et al., 2001]; 5) potentiated synapses become 'locked in' at high strength [O'Connor et al., 2005]; 6) repeated LTP saturates [McNaughton et al., 1978, Dudek and Bear, 1993, O'Connor et al., 2005]; 7) spine size and synaptic strength distributions are unimodal with a non-zero peak [Yasumatsu et al., 2008, Minerbi et al., 2009, Harris and Stevens, 1989; but see Mishchenko et al., 2010] and 8) longitudinal studies in hippocampal cultures find a negative correlation between momentary synaptic strength and subsequent change in synaptic strength [Yasumatsu et al., 2008, Minerbi et al., 2009]. Nevertheless, our model's prediction is strongly dependent on the assumed relationship between spine head volume and NMDAR number. If future data on NMDAR number, VGCCs, extrusion mechanisms and endogenous buffers becomes available, our model can be refined to make more quantitative predictions.

Although less well studied, neocortical synapses also show the properties of undercompensation: 1) the magnitude of synaptic plasticity events are negatively correlated with initial synaptic strength [Volgushev et al., 1997, Sjöström et al., 2001, Hardingham et al., 2007, Sáez and Friedlander, 2009]; 2) small spines fluctuate in size while large spines persist in vivo [Grutzendler et al., 2002, Trachtenberg et al., 2002, Holtmaat et al., 2005, Zuo et al., 2005, Knott et al., 2006] and 3) cortical synapses have unimodal synaptic strength distributions [Holmgren et al., 2003, Song et al., 2005, Feldmeyer et al., 2006].

4.4.2 Spine structural plasticity provides a potential solution to the plasticity-stability problem

There is no known mechanistic reason why spine structural plasticity should necessarily be tethered to synaptic plasticity. The two processes are mediated by signaling pathways that are at least partly independent from one another [Cingolani and Goda, 2008], suggesting that they are instead co-regulated for functional reasons. Our theory proposes that the spine size to synaptic efficacy relationship is maintained in order to

imprint a strength-dependence on the synaptic plasticity rule that preferentially stabilizes some synaptic strengths. Evolution may have favored this mechanism because of its simplicity and robustness.

4.4.3 Generalising the model's assumptions

Our analysis assumes that the amplitude of bulk Ca^{2+}-concentration changes in dendritic spines is the sole signal that triggers synaptic plasticity. However, there are data suggesting that the timecourse of Ca^{2+} signals [Wang et al., 2005] and nanodomain Ca^{2+} signaling [Hoffman et al., 2002, Yasuda et al., 2003, Lee et al., 2009] could also play a role.

The Ca^{2+} timecourse

Our model assumes that synaptic plasticity is triggered instantaneously by the amplitude of spine Ca^{2+} concentration. However, the timecourse of synaptic Ca^{2+} signals might also influence the direction of synaptic plasticity [Malenka et al., 1992, Yang et al., 1999, Wang et al., 2005, Nevian and Sakmann, 2006, Wittenberg and Wang, 2006]. In particular, potentation may be initiated by fast events, while depression may require more prolonged (>70 ms) events [Wang et al., 2005, Rubin et al., 2005].

In our current model, synaptic strength is tied to spine head size and NMDAR conductance, parameters which mainly influence spine $[Ca^{2+}]$ amplitude without substantially influencing Ca^{2+}-timecourse. Therefore, the model applies the stability mechanisms of undercompensation or overcompensation only to the amplitude component of spine $[Ca^{2+}]$ signals, but not the timecourse component. If the influence of $[Ca^{2+}]$ timecourse on synaptic plasticity is found to be comparable to the influence of $[Ca^{2+}]$ amplitude, our model could be extended to incorporate these effects. For example, undercompensating the Ca^{2+}-timecourse might require a mechanism that made Ca^{2+}-transients at small spines faster than Ca^{2+}-transients at large spines. Notably, dendritic spines possess multiple mechanisms that can differentially modulate the amplitude and timecourse of their $[Ca^{2+}]$ signals, including the kinetics of Ca^{2+} sources, the Ca^{2+}-permeability of ion channels and glutamate receptors, the efficiency of extrusion pumps and exchangers, spine neck morphology and the concentration and affinity of endogenous Ca^{2+} buffers [Bloodgood and Sabatini, 2007]. Hence, spines can possibly implement the stability mechanisms we describe above on both the amplitude and timecourse components of Ca^{2+}-signals simultaneously by tying multiple spine

properties to synaptic strength in parallel.

Local Ca^{2+} signaling

In our model we assume that the volume-averaged Ca^{2+} concentration in the spine is the signal read by the Ca^{2+}-sensing molecules, hence negating any role for Ca^{2+} nano- or micro-domain signaling in plasticity induction. Evidence supporting this assumption include findings that EGTA, a Ca^{2+} chelator which binds too slowly to affect nanodomains, blocks hippocampal LTP [Lynch et al., 1983] and perirhinal LTD [Cho et al., 2001]. EGTA and BAPTA are also equally effective at blocking neocortical LTD [Egger et al., 1999], spike-timing-dependent plasticity [Nevian and Sakmann, 2006] and NMDAR-dependent CaMKII activation [Lee et al., 2009]. Furthermore, NMDARs unbind glutamate at a relatively slow rate (100ms), much longer than the <2ms equilibration time of the spine Ca^{2+} concentration [Yuste and Denk, 1995, Cornelisse et al., 2007]. Accordingly, photo-activating Ca^{2+} buffers up to one second after synaptic stimulation can block hippocampal LTP [Malenka et al., 1992], indicating a Ca^{2+} integration timescale much longer than the fast equilibration time. Finally, postsynaptic Ca^{2+}-uncaging, predicted to be more dilute than physiological Ca^{2+} microdomains, is sufficient to induce both LTP and LTD [Yang et al., 1999].

Nevertheless, there are also data indicating a role for microdomain interactions in some forms of synaptic plasticity [Hoffman et al., 2002, Yasuda et al., 2003, Lee et al., 2009]. Even in this case, there are several mechanisms through which spine head size could continue to shape synaptic plasticity by regulating local Ca^{2+} signaling. First, spine volume determines the bulk spine Ca^{2+} concentration upon which the local Ca^{2+} concentration changes are superimposed. Theoretical models and Ca^{2+}-uncaging experiments at presynaptic boutons estimate that Ca^{2+} concentrations near ion channel pores reach 10-100 μM [Augustine et al., 2003], while dendritic spine Ca^{2+} concentrations reach ~10 μM [Sabatini et al., 2002]. Hence, bulk Ca^{2+} concentration modulate local Ca^{2+} signals through simple addition. Second, the bulk Ca^{2+} concentration sets the level of endogenous buffer saturation. Hence, if bulk Ca^{2+} concentrations are sufficiently elevated, there is less free buffer available to restrict the Ca^{2+} influxing through the channel pore, so elevating microdomain Ca^{2+} signals — a mechanism originally proposed to explain activity-dependent presynaptic facilitation [Neher, 1998]. Third, because small spines have a greater surface-to-volume ratio than large spines, any mobile Ca^{2+}-sensing molecules are statistically more likely to diffuse closer to membrane-bound Ca^{2+} sources in smaller spines than in larger spines.

The role of internal Ca^{2+} stores, buffering, pumping and diffusion mechanisms

Many factors contribute to the dynamics of Ca^{2+} within the dendritic spine: influx from NMDARs, VGCCs, release from internal Ca^{2+} stores, the concentrations and affinities of endogenous Ca^{2+} buffers, diffusion through the spine neck, and efflux through membrane pumps and exchangers [Bloodgood and Sabatini, 2007]. However, in our models we assume that the alterations in Ca^{2+} dynamics with synaptic strength are due only to the relationship between synaptic strength and spine size and NMDAR number. We focus on spine size and NMDAR number for two reasons: first, they are both strong determinants of spine Ca^{2+} signaling [Sabatini et al., 2002], and second, the relationship between both these factors and synaptic strength has been well studied for hippocampal synapses [Nusser et al., 1998, Takumi et al., 1999, Racca et al., 2000, Matsuzaki et al., 2001, Ganeshina et al., 2004, Matsuzaki et al., 2004, Nimchinsky et al., 2004, Noguchi et al., 2005, Sobczyk et al., 2005]. Although the relationship between the other factors and synaptic strength is not well understood, it is important to note that if they are also found to scale with synaptic strength, then they could in principle also determine whether spine Ca^{2+} dynamics falls into the compensating, undercompensating or overcompensating scenario. Indeed, spine-to-spine differences in many of these properties have already been shown to influence the induction of synaptic plasticity, even for different synapses on the same neuron: Ca^{2+} extrusion mechanisms [Holthoff et al., 2002, Simons et al., 2009], VGCC regulation [Yasuda et al., 2003, Humeau et al., 2005] and internal Ca^{2+} stores [Holbro et al., 2009]. Future experimental studies might help uncover potential relationships between these properties and synaptic strength.

4.4.4 Relation to previous models

Our results are consistent with a previous study [Kalantzis and Shouval, 2009] which suggested that dendritic spine structural plasticity could modulate synaptic plasticity rules by scaling spine Ca^{2+} concentrations. Here, we generalize these findings by clearly delineating the three scenarios of Ca^{2+} over, under, or exact compensation (Figure 4.1). In addition, the present study examines the consequences of these three scenarios for the form of synaptic information storage (Figure 4.2), the long-term dynamics of synaptic strength (Figure 4.3), the robustness of memory storage to intrinsic synaptic strength fluctuations (Figure 4.4), and the distributions of synaptic strength (Figure 4.6). These general issues have not been addressed previously.

Although the undercompensating mechanism helps to prevent runaway synaptic plasticity, it is not homeostatic. Homeostatic plasticity is commonly defined as a global feedback mechanism which counteracts long-term changes in post-synaptic activity [Yeung et al., 2004], while here there is no such feedback.

The undercompensating mechanism is also very distinct to the classic BCM plasticity rule [Bienenstock et al., 1982]. Although the qualitative shape of the post-synaptic activity dependence of the BCM rule is similar to the Ca^{2+} dependence of the plasticity rule we employ here, the mechanisms underlying synaptic stability in the two rules differ greatly. The sliding threshold in BCM leads both to stabilisation of post-synaptic firing rates and competition between synapses. In contrast, the undercompensating rule we propose here stabilises synaptic dynamics through a purely local mechanism: each individual synapse's plasticity rule depends only on its strength, not on past post-synaptic activity levels. As a result, undercompensation does not induce competition between synapses, unlike BCM.

Our theory is mostly complementary to previous phenomenological models of synaptic plasticity [van Rossum et al., 2000, Rubin et al., 2001, Gütig et al., 2003, Zou and Destexhe, 2007]. However, these phenomenological models often predict that strong synapses are the least stable [van Rossum et al., 2000, Rubin et al., 2001, Gütig et al., 2003, Zou and Destexhe, 2007] (but see [Shouval, 2005]), whereas experimental data suggests that strong synapses and large spines are the most stable [Grutzendler et al., 2002, Trachtenberg et al., 2002, Holtmaat et al., 2005, Zuo et al., 2005, Knott et al., 2006]. This stability is successfully explained by the mechanisms from spine structural plasticity that we propose here.

A second class of models of synaptic strength stability rely on complex molecular cascades with multiple stable states [Lisman and Zhabotinsky, 2001, Hayer and Bhalla, 2005, Graupner and Brunel, 2007]. Although our theory is compatible with these previous models, it also successfully incorporates two important biological observations that existing models do not. First, although spines in vivo can exist stably for many months [Grutzendler et al., 2002, Trachtenberg et al., 2002, Holtmaat et al., 2005, Zuo et al., 2005, Knott et al., 2006], the spine and PSD are tiny devices (volume < 1fL), implying that the molecular reactions at the synapse involve a small number of particles and may therefore be noisy [Franks and Sejnowski, 2002, Keller et al., 2008]. When LTP cascades are modeled stochastically, spontaneous transitions are found to occur between states that are stable in an equivalent deterministic model [Bhalla, 2004]. Changing parameters to reduce the spontaneous transitions also makes the sys-

tem insensitive to stimuli (but see [Miller et al., 2005]). In contrast, under- and over-compensating synapses can both override the effects of noise on stability (Figure 4.4). Second, the impact of changes in spine size on the concentration of spine constituents is typically not included in current biophysical models of synaptic plasticity (although see [Kalantzis and Shouval, 2009]). The effects of including these experimentally observed changes in spine size in existing molecular models for synaptic stabilization are unclear. One possibility is that molecular stability mechanisms act in concert with the stability mechanisms from spine structural plasticity we propose here. For example, calcium/calmodulin-dependent kinase II (CaMKII), a molecule critical for many forms of synaptic plasticity, is rapidly activated ($\sim$5s) and inactivated ($\sim$1min) during LTP, while spine enlargement occurs more slowly ($\sim$1min) and is long-lasting (> 30min) [Lee et al., 2009]. It is possible that the two mechanisms cooperate as part of a larger system that mediates synaptic plasticity over several timescales.

4.4.5 Experimental predictions

Given sufficient data on the spine size to Ca^{2+}-influx relationship for a population of synapses to determine their scaling scenario, our model makes specific experimental predictions. Undercompensating synapses should show the following properties collectively:

1. Stable strong synapses but plastic weak synapses.
2. Synaptic retention time should increase dramatically with synaptic strength.
3. A plasticity-inducing stimulus should drive all stimulated synapses towards a single common strength.
4. The stable synaptic strength should be an increasing, continuous function of stimulus strength.
5. The stable strength can be varied by enhancing or reducing Ca^{2+} influx to the spine.
6. The distribution of synaptic strengths should be unimodal with a central non-zero peak.

Overcompensating synapses, in contrast, should show collectively that:

1. Individual synapses should be most stable at a maximum or minimum strength but not at intermediate strengths.

2. A plasticity-inducing stimulus should potentiate all synapses with a strength greater than a certain threshold and depress all synapses with a strength weaker than the same threshold.

3. The threshold should be a continuously increasing function of stimulus strength.

4. The threshold can be varied by enhancing or reducing Ca^{2+} influx to the spine.

5. There should be some additional mechanism to limit synaptic strength at its maximum and minimum values.

6. Synaptic strength distributions should appear bimodal.

Another powerful approach to test our model's predictions is pharmacological or genetic dissociation of spine size from synaptic strength [Zhou et al., 2004, Wang et al., 2007b]. For example, manipulations that permit synaptic plasticity while blocking spine structural plasticity would make synapses behave as if in the compensating mode where our model predicts: 1) individual synaptic strengths drift at an elevated rate that is independent of synaptic strength; 2) potentiated synapses rapidly decay to naïve strengths; 3) synaptic strength distributions spread. A further critical experiment would be the tracking of individual synaptic strengths over time in vivo. Correlating spine and synaptic strength changes with physiological neural activity patterns could uncover strength-dependent plasticity rules.

Chapter 5

Summary and beyond

This thesis theoretically explored the consequences of two separate neurobiological processes: the stochastic gating of ion channels and dendritic spine structural plasticity. Here we summarise our findings, then discuss possible future directions for the work.

First, we found that the stochastic gating of membrane ion channels introduces an inescapable source of variability into the electrical dynamics of neurons. Through simulation, we examined in detail cases where this microscopic variability has macroscopic consequences. In Chapter 2 we found that channel noise can trigger spontaneous action potentials in small compartments or thin cables. We proposed that this mechanism underlies the spontaneous firing of thin peripheral nerves during certain neuropathic pain conditions. In Chapter 3 we quantified the magnitude of channel noise in multicompartmental models of central neurons with complex dendritic arbours. We found that channel noise is of sufficient magnitude to introduce stochasticity into the process of synaptic integration and leads to probabilistic spiking and jitter of spike timing. Because this source of variability is intrinsic, it sets a fundamental physical limit on the ability of neurons to propagate information.

Second, we found that the relationship between dendritic spine size and synaptic strength very likely introduces a strength-dependence into the rules of synaptic plasticity. In Chapter 4 we delineated the three qualitatively different scenarios that can occur, and demonstrated their implications for the long-term stability of synaptic information storage. When given biological data on spine Ca^{2+} handling properties, the framework makes specific testable predictions. We used a detailed biophysical model of a CA1 pyramidal neuron dendritic spine to unify several previously disparate experimental findings on the distribution of synaptic strengths, the saturation of synaptic plasticity, and the stability of strong synapses. The model suggests a novel mechanism

through which synapses can simultaneously exhibit both plasticity and robust stability.

5.1 Channel noise extensions

5.1.1 Exploring noise-drive neuropathic pain

We proposed that channel noise underlies the spontaneous activity observed in thin peripheral nerves during certain neuropathic pain states. To test this hypothesis more rigorously would require more work on both experimental and theoretical fronts.

Experimentally, we can both test the theory's qualitative predictions and collect further data to constrain new computational models to generate more quantitative predictions. The qualitative predictions, briefly, are:

- Spontaneous firing patterns should be irregular. At low rates, inter-spike-intervals should be Poisson distributed, after adjusting for refractory period [Chow and White, 1996].
- Spontaneous spikes should preferentially emerge from axon terminals, both because the cable end has the lowest current threshold [Jack et al., 1975, Koch, 1999] and ion channels are known to accumulate there following nerve injury [Black et al., 2008]. However we have studied only the case where channels are distributed homogeneously.
- Spontaneous firing rate should be negatively correlated with axon diameter.
- Spontaneous firing rate should be positively correlated with cable length.
- The presence of channels with large single channel conductance, slow kinetics or elevated resting open probability should correlate with increased spontaneous firing rates.

Intracellular electrophysiology at peripheral nerve fibre terminals may prove difficult or impossible due to their tiny dimensions ($< 1\mu$m diameter). However, computational models could still be built based on DRG recordings of membrane currents from specific channel populations, combined with quantitative imaging of the same fluorescent-tagged channels at the nerve terminals. It is likely, although absolutely not certain, that the ion channels expressed at the cell body are similar to those also expressed further

down the axon. Particularly useful data could be gathered from single-channel recordings which can provide information crucial to stochastic channel gating models, such as single-channel conductance and open time distribution.

Theoretical work could initially proceed by analysing the current noise expected from ion channel types known to be expressed by peripheral nerves, in a manner similar to the analysis we presented in Chapter 2 on the HH Na^+ and K^+ conductances. Such an analysis might suggest which channel types are most likely to contribute to membrane voltage noise. This work should be backed by Markov simulations to make quantitative predictions for comparison with experimental data.

This novel hypothesis also makes several immediate suggestions for therapeutic interventions to neuropathic pain, listed in the Discussion to Chapter 2. Briefly, they are: 1) dilate thin spontaneously active fibres by altering osmolarity; 2) reduce axoplasmic resistivity; 3) introduce ion channels with small conductance or fast kinetics, or conversely block ion channels with large conductance or slow kinetics; 4) increase nerve temperature.

5.1.2 Understanding the impact of stochastic ion channel gating on synaptic integration

Although we demonstrate that the magnitude of membrane noise from stochastic ion channel gating depends on neuronal morphology, our simulations employed identical sets of ion channels on each cell type. In reality, each cell type likely has different sets and distributions of ion channels. Quantitative estimates of the magnitude of channel noise should be based on neural models that are specifically designed on a cell-type by cell-type basis. This, combined with knowledge of a given cell type's circuit function, could be used to estimate the importance of channel noise *in vivo*.

It is possible that, for some cell types, channel noise is an undesirable source of noise which should be minimised. For example, if the task of a neuron is to convey maximum information about stimuli in the external environment, then channel noise would likely be a hindrance [e.g. van Rossum et al., 2003]. It is important to note, however, that the addition of noise is only necessarily detrimental to signal-to-noise ratios in linear systems. In nonlinear systems, noise can sometimes have a beneficial role, as we discuss next.

The second possibility is that channel noise is used in certain cell types in a constructive manner. Three positive examples might be: stochastic resonance to weak

signals (see section 3.3.8), reliable propagation of firing rates through layers of neurons [van Rossum et al., 2002], and the probabilistic coding of information in neural populations [Ma et al., 2006].

These possibilities remain to be determined. The relative benefit of studying noise from stochastic channel gating, as opposed to generic noise sources, is that its magnitude is determined entirely by biophysics. The process of stochastic channel gating is itself well understood [Hille, 2001]. The only ambiguity arises from imprecise or inaccurate experimental data for building single channel kinetic schemes, or channel number and distribution in cell membrane. Even without hard numbers, however, these parameters can be given reasonable physiological bounds. The second limitation, computing power, is becoming less and less of a problem, thanks both to the ever-growing power of modern microprocessors and to the development of new tools for efficient simulation [Cannon et al., 2010]. Hence, the implications of channel noise may soon become one of best understood noise problems in neurobiology.

5.2 Consequences of the spine plasticity model

We demonstrate theoretically that dendritic spine structural plasticity can introduce a weight-dependence into Ca^{2+}-dependent synaptic plasticity rules. The form of the weight dependence is dictated by the relationship between spine size and Ca^{2+} influx mechanisms. We characterised the three possible weight-dependencies that can arise from this phenomenon. Each case has different implications for the long-term dynamics of synaptic strength. Our biophysical simulations predict that CA1 pyramidal neuron spines fall into the undercompensating category. Here, the weight dependence biases weak synapses towards potentiation, biases intermediate strength synapses towards depression, and makes strong synapses relatively immune to change (Figure 5.1). Crucially, the weight-dependence is non-monotonic. This feature contrasts with all other previously studied weight-dependent learning rules, which have been exclusively monotonic [van Rossum et al., 2000, Rubin et al., 2001, Gütig et al., 2003].

What are the functional consequences of this novel non-monotonic weight-dependent plasticity rule? We first examine what the existing literature might tell us about this question, then discuss possible future extensions of the model.

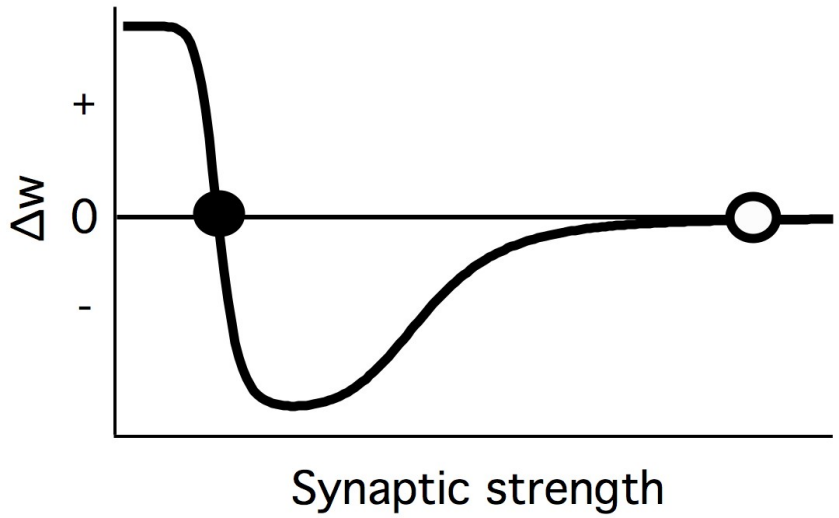

Figure 5.1: Non-monotonic weight-dependence of the plasticity rule in the undercompensating scenario.

5.2.1 Existing studies of weight-dependent synaptic plasticity

Hints towards the importance of the weight-dependent plasticity rule we describe can be gathered from previous studies of non-weight-dependent and monotonic weight-dependent learning rules. The plasticity rule's weight-dependence has several important effects on synaptic strength dynamics and synaptic memory storage:

Stabilisation or destabilisation of long-term synaptic strength dynamics.

It is well known that all purely Hebbian plasticity rules are, if left unchecked, inherently unstable. Correlated pre- and post-synaptic activity leads to potentiation, which leads to increased post-synaptic activity, leading to further potentiation, causing to synaptic weights potentiate *ad infinitum*. The simple introduction of a rule for long-term synaptic depression does not lead to an immediate solution to this problem. Stability of synaptic strength might be achieved in this case if there was an exact long-term balance between potentiation and depression events. Even then, incidental changes in synaptic strength will accumulate over time so that the synaptic strength undergoes a random walk [Sejnowski, 1977]. Ultimately, however, such a system suffers from the weakness of being very sensitive to changes in input statistics. If presynaptic activity levels are increased or decreased over time, potentiation or depression begins to dominate, driving synapses to their maximum or minimum strengths, respectively [Miller, 1996]. Weight dependent synaptic plasticity rules offer one solution to this problem.

If there is a negative relationship between the degree of potentiation or depression and the synapse's current strength (so-called 'soft bounds'), synaptic strengths are limited to a functional range without ever reaching either their maximum or minimum limits, so preventing the problem of runaway synaptic strengths [van Rossum et al., 2000, Rubin et al., 2001, Gütig et al., 2003, Fusi and Abbott, 2007]. Because the undercompensating scenario involves a negative weight-dependence in the plasticity rule, it too imposes soft bounds on synaptic weights. Interestingly, because the limits introduced by the undercompensating mechanism arise from the effect of spine volume changes on Ca^{2+} dynamics, other processes that modulate Ca^{2+} signaling, such as neuromodulation or the location of internal calcium stores, could potentially also modulate the soft bounds on synaptic strength.

The presence of the soft, saturating upper bound might however introduce an additional problem which has not been previously studied. Because of the 'squashing' form of the weight-dependence at the upper end of the plasticity rule, large plasticity-triggering events which differ greatly in magnitude might result in only small eventual differences in synaptic strength. If the differences between these synaptic strengths are small compared to the resolution of the read-out mechanism for recalling the memory, then this saturating non-linearity might have the effect of limiting information storage, because the synapse possesses fewer effective states than it would otherwise have without the saturating non-linearity. Hence, although the saturating non-linearity might be beneficial from a physiological or energy-budget perspective, it might prove detrimental from an information-storage perspective. Resolution of this dilemma would be an interesting problem for future theoretical studies.

Presence or absence of competition between synapses.

Competition between synapses implies that if one synapse potentiates, other synapses onto the same cell are depressed, or are at least biased to depression [reviewed by Miller, 1996]. The same concept can be applied to competition between groups of synapses with correlated inputs. One example of robust system-level competition in the nervous system is the formation of ocular dominance columns in the visual system [Wiesel and Hubel, 1965].

Early theoretical models of synaptic competition did not employ weight-dependent synaptic plasticity rules, but typically invoked either weight normalisation (ensuring the sum of the synaptic strengths on to a single neuron remains constant; [reviewed by Miler and MacKay, 1994]) or a cell-wide sliding plasticity threshold [Bienenstock

et al., 1982]. Both of these types of models share the fact that the stabilisation of synaptic strength is accompanied by competition between synapses. In the first case, the process of weight normalisation ensures that if any given synapse is potentiated, all others are depressed. In the second case, synaptic potentiation leads to an increase in postsynaptic activity levels, which raises the cell-wide threshold for potentiation, which makes depression more likely for all other synapses. Recent models of spike-timing dependent plasticity (STDP) have also shown that competition between synapses can emerge from simple, local rules when plasticity is either independent or only weakly dependent on synaptic weight [Song et al., 2000, Gütig et al., 2003]. Competition in this case arises through a 'rich-get-richer' mechanism, as long as the additional assumption that depression slightly dominates over potentiation is fulfilled [Song et al., 2000]. Here, the arrival of strong presynaptic input results in the temporary increase in the probability of a postsynaptic spike. Hence, a strong synapse has an elevated probability of further potentiation. In contrast, all other synapses, if uncorrelated with this strong synapse, are subject to net depression. Importantly, introduction of a strong weight-dependence in to the STDP rule, in accordance with experimental data, destroys competition because all synapses are driven to similar weights, regardless of input activity levels or correlation strength [van Rossum et al., 2000, Rubin et al., 2001]. This is consistent with unimodal weight distributions observed experimentally [reviewed by Barbour et al., 2007]. Competition can be reintroduced in the weight-dependent case if additional mechanisms are added, such as slow homeostatic plasticity or lateral inhibition between cells [van Rossum et al., 2000, Billings and van Rossum, 2009]. In the undercompensating model, synapses have a negative weight-dependence in the lower-strength range but a reduction of the magnitude of synaptic plasticity in the higher-strength range. Hence, it is likely that the undercompensation rule will, on its own, reduce competition for weaker synapses, but the effects of the reduction in plasticity for strong synapses remain unclear.

Stabilisation of firing rates

A problem related to that of stabilisation of synaptic strength is stabilisation of cell firing rate. Neurons possess both upper and lower limits to their firing rate range. The upper limit, typically in the hundreds of Hz range, is determined both by cell morphology and its suite of membrane ion channels. The trivial lower limit is that of zero spiking. To be both computationally useful and metabolically efficient, neurons must keep their firing rates within some subset of this range. The level of synaptic input

to a neuron, however, might be beyond its control. Hence, a neuron should possess mechanisms to counteract any changes in its input statistics that would otherwise drive its output firing rates out of its 'desired' operating range. One well studied mechanism to achieve this is homeostatic synaptic plasticity (or 'synaptic scaling'). Here, the strengths of all synapses on a single neuron are regulated on a slow timescale to ensure its mean firing rate is neither too high or too low [Pozo and Goda, 2010]. Superficially, the undercompensating plasticity rule might appear similar. However, this rule is not homeostatic. Unlike homeostatic mechanisms, here, increased levels of postsynaptic activity lead to further increases synaptic strength. However, it might be that the stabilisation of synaptic strength from undercompensation discussed above also ensures stabilisation of postsynaptic firing rate. Whether firing rate stability is ensured depends on the relationship between the neuron's input-output function and the degree of stability introduced by undercompensation. If undercompensation is sufficiently strong, then it can always limit synaptic strength, and hence limit post-synaptic firing rate (assuming limited pre-synaptic input rate). However, if the neuron has a steep input-output function (small changes in input firing rate lead to large changes in postsynaptic firing rate), or a steep Ca^{2+} influx-to-postsynaptic firing rate relationship, then it might be that the braking mechanism introduced by undercompensation is insufficient to counter the increased Ca^{2+} influx introduced by elevated post-synaptic activity. Hence, although undercompensation is potentially capable of stabilising cell firing rate, its presence alone is insufficient to guarantee firing rate stability in all circumstances.

5.2.2 Extensions of the spine plasticity model

Here we suggest several possible directions to orient future work at several levels of biological detail.

Biophysical models of synaptic plasticity including spine size plasticity

As discussed above, several groups have constructed biochemical models of known aspects of synaptic plasticity cascades [Manninen et al., 2010]. To our knowledge, none so far have investigated the effects of spine size plasticity on these cascades. Spine size is likely to play an important role in these models because it is one factor which determines the local concentration of any mobile species, including, Ca^{2+}, protein kinases and phosphotases. For example, often the aim of these models is to investigate

the conditions necessary for multiple stable states of the system to exist (e.g. a naive synapse vs a potentiated synapse), and whether external stimuli (e.g. Ca^{2+}-influx from synaptic stimulation) can switch the system between these states. Because the stability of the fixed points in these systems, and the systems' sensitivity to external stimuli, depend on the relative concentration of the system components, changes in spine size that alter the concentration of some of these components might substantially alter the system properties.

An interesting future research project would be to implement spine size changes in parallel with synaptic potentiation/depression in a biochemical model synapse, and to investigate whether the biochemical cascades are either: a) robust to this perturbation, b) vulnerable to this perturbation, or c) perhaps use this mechanism constructively for some function.

The implications for spike-timing-dependent plasticity

It has proved a challenge for theorists to reproduce the phenomenological features of spike-time-dependent synaptic plasticity from computational models based on lower-level components such as biochemical cascades, or even Ca^{2+} dynamics [reviewed by Graupner and Brunel, 2010]. The issue remains unresolved. Nevertheless, one study did examine the effects of varying dendritic spine size on the shape of the STDP window in a Ca^{2+}-dependent synaptic plasticity rule, similar to the rule employed in our study above [Kalantzis and Shouval, 2009]. They found that varying spine size had a substantial effect on the shape of the STDP curve. The exact changes in the shape of the curve depended on how NMDAR number scaled with spine size — they considered cases where NMDAR number was either independent of spine size, scaled proportionally to spine surface area, or scaled proportionally to spine volume. However, the authors did not investigate the consequences of this scaling in a dynamical model.

Although several previous phenomenological studies of STDP have included a weight-dependence [van Rossum et al., 2000, Rubin et al., 2001, Gütig et al., 2003, Morrison et al., 2007, Billings and van Rossum, 2009], none have considered the non-monotonic weight-dependence predicted by the undercompensating or overcompensating spine models. An interesting project would be to examine the implications of this rule in a dynamic STDP model for synaptic competition, synaptic stability, and synaptic strength distribution.

The interaction between undercompensating synapses and homeostatic plasticity

Neither of the compensating, overcompensating or undercompensating synaptic plasticity rules is necessarily sufficient to stabilise synaptic strength dynamics on its own. The compensating and overcompensating rules lead to divergence of synaptic strength in both positive and negative directions. They both require an additional mechanism to limit synaptic strength in the long term. Although undercompensation could potentially limit synaptic strength, it is not guaranteed to (discussed above). Hence, it is likely that additional homeostatic plasticity mechanisms [Davis, 2006] are required to ensure stability of both synaptic strength and cell firing rate in the long term, regardless of the spine plasticity scenario.

Although homeostatic synaptic plasticity was originally postulated simply as a mechanism to keep cell firing rates in a useful range [Turrigiano et al., 1998], several theoretical studies have shown that it can also, in conjunction with Hebbian plasticity, result in many desirable functional properties. Together, the two plasticity mechanisms can 1) facilitate synaptic competition while maintaining synaptic stability [van Rossum et al., 2000]; 2) be reconciled with metaplastic mechanisms through regulation of Ca^{2+} signaling [Yeung et al., 2004]; 3) learn to optimally transmit information about presynaptic inputs [Toyoizumi et al., 2007]; 4) lead to the formation of stable sparse patterns of synaptic strengths distributed throughout a dendritic tree [Rabinowitch and Segev, 2006] and 5) improve memory storage capacity [Wu and Mel, 2009]. It is an open question how homeostatic mechanisms would interact with the learning rules proposed here.

Undercompensating synapses in a neuronal network

In our study we focused only on the consequences of compensation, undercompensation and overcompensation for either a single synapse or, to a limited extent, a population of such synapses on a single neuron. It is much less clear what the effects of these plasticity rules would be when applied to synapses in a recurrent network of multiple neurons.

Superficially, one might expect that the stability mechanisms we find from undercompensation or overcompensation would automatically extend to synapses in a neural circuit. However, the problem is complicated by the fact that the dynamics of electrical activity on the network, and the synaptic connectivity between neurons in the network,

are reciprocally dependent on each other. Hence, changes in synaptic strengths lead to changes in network activity, which in turn lead to further changes in synaptic strengths. It is not trivial to predict how the network will evolve given a certain synaptic plasticity rule [Morrison et al., 2007, Billings and van Rossum, 2009, Gilson et al., 2010]. Part of the difficulty arises from the fact that the input-output function of recurrent networks has a fundamentally different dependence on synaptic weight changes than that of simpler feed-forward networks (including the single neuron model). In a feed-forward network, small changes to synaptic strengths lead to correspondingly small changes in the network's activity patterns. In a recurrent network, small changes in synaptic weight structure can sometimes lead to dramatic changes in network activity patterns, if the network dynamics passes through a bifurcation point [Doya, 1992]. This is one factor which makes the effects of synaptic plasticity in recurrent networks difficult to predict. Hence, an interesting project would be to study the effects of under- and overcompensating plasticity rules in a network of neurons to examine how they affect processes such as network activity patterns, receptive field development, or memory retention.

H Agmon-Snir, C E Carr, and John Rinzel. The role of dendrites in auditory coincidence detection. *Nature*, 393(6682):268–272, 1998.

Omar J Ahmed and Mayank R Mehta. The hippocampal rate code: anatomy, physiology and theory. *Trends in neurosciences*, 32(6):329–338, 2009.

Osvaldo Alvarez, Carlos Gonzalez, and Ramon Latorre. Counting channels: a tutorial guide on ion channel fluctuation analysis. *Advances in physiology education*, 26 (1-4):327–341, 2002.

George J Augustine, Fidel Santamaria, and Keiko Tanaka. Local calcium signaling in neurons. *Neuron*, 40(2):331–346, 2003.

Boris Barbour, Nicolas Brunel, Vincent Hakim, and Jean-Pierre Nadal. What can we learn from synaptic weight distributions? *Trends in neurosciences*, 30(12):622–629, 2007.

Adam B Barrett and Mark van Rossum. Optimal learning rules for discrete synapses. *PLoS computational biology*, 4(11):e1000230, 2008.

F Bezanilla. Single sodium channels from the squid giant axon. *Biophysical journal*, 52(6):1087–1090, 1987.

S M Bezrukov and I Vodyanoy. Noise-induced enhancement of signal transduction across voltage-dependent ion channels. *Nature*, 378(6555):362–364, 1995.

Upinder S Bhalla. Signaling in small subcellular volumes. I. Stochastic and diffusion effects on individual pathways. *Biophysical journal*, 87(2):733–744, 2004.

G Q Bi and M M Poo. Synaptic modifications in cultured hippocampal neurons: dependence on spike timing, synaptic strength, and postsynaptic cell type. *The Journal of neuroscience : the official journal of the Society for Neuroscience*, 18(24):10464–10472, 1998.

E L Bienenstock, L N Cooper, and P W Munro. Theory for the development of neuron selectivity: orientation specificity and binocular interaction in visual cortex. *The Journal of neuroscience : the official journal of the Society for Neuroscience*, 2(1): 32–48, 1982.

Guy Billings and Mark van Rossum. Memory retention and spike-timing-dependent plasticity. *Journal of neurophysiology*, 101(6):2775–2788, 2009.

Joel A Black, Lone Nikolajsen, Karsten Kroner, Troels S Jensen, and Stephen G Waxman. Multiple sodium channel isoforms and mitogen-activated protein kinases are present in painful human neuromas. *Annals of neurology*, 64(6):644–653, 2008.

Thomas A Blanpied, Justin M Kerr, and Michael D Ehlers. Structural plasticity with preserved topology in the postsynaptic protein network. *Proceedings of the National Academy of Sciences of the United States of America*, 105(34):12587–12592, 2008.

T V Bliss and G L Collingridge. A synaptic model of memory: long-term potentiation in the hippocampus. *Nature*, 361(6407):31–39, January 1993a.

T V Bliss and T Lomo. Long-lasting potentiation of synaptic transmission in the dentate area of the anaesthetized rabbit following stimulation of the perforant path. *The Journal of physiology*, 232(2):331–356, July 1973.

Brenda L Bloodgood and Bernardo L Sabatini. Ca(2+) signaling in dendritic spines. *Current opinion in neurobiology*, 17(3):345–351, 2007.

H Blumberg and W Jänig. Discharge pattern of afferent fibers from a neuroma. *Pain*, 20(4):335–353, 1984.

Tiago Branco and Michael Häusser. Synaptic integration gradients in single cortical pyramidal cell dendrites. *Neuron*, 69(5):885–892, 2011.

Tiago Branco, Beverley A Clark, and Michael Häusser. Dendritic discrimination of temporal input sequences in cortical neurons. *Science*, 329(5999):1671–1675, 2010.

Ian C Bruce. Evaluation of stochastic differential equation approximation of ion channel gating models. *Annals of biomedical engineering*, 37(4):824–838, 2009.

James N Campbell and Richard A Meyer. Mechanisms of neuropathic pain. *Neuron*, 52(1):77–92, 2006.

Robert C Cannon, Cian O'Donnell, and Matthew F Nolan. Stochastic ion channel gating in dendritic neurons: morphology dependence and probabilistic synaptic activation of dendritic spikes. *PLoS computational biology*, 6(8), 2010.

Nicholas T Carnevale and Michael L Hines. *The NEURON Book*. Cambridge University Press, Cambridge, 2006.

William A Catterall, Alan L Goldin, and Stephen G Waxman. International Union of Pharmacology. XLVII. Nomenclature and structure-function relationships of voltage-gated sodium channels. *Pharmacological reviews*, 57(4):397–409, 2005.

G A Cecchi, M Sigman, J M Alonso, L Martínez, D R Chialvo, and M O Magnasco. Noise in neurons is message dependent. *Proceedings of the National Academy of Sciences of the United States of America*, 97(10):5557–5561, 2000.

Xixi Chen and Daniel Johnston. Properties of single voltage-dependent K+ channels in dendrites of CA1 pyramidal neurones of rat hippocampus. *The Journal of physiology*, 559(Pt 1):187–203, 2004.

Dmitri B Chklovskii. Synaptic connectivity and neuronal morphology: two sides of the same coin. *Neuron*, 43(5):609–617, 2004.

K Cho, J P Aggleton, M W Brown, and Z I Bashir. An experimental test of the role of postsynaptic calcium levels in determining synaptic strength using perirhinal cortex of rat. *The Journal of physiology*, 532(Pt 2):459–466, 2001.

C C Chow and John A White. Spontaneous action potentials due to channel fluctuations. *Biophysical journal*, 71(6):3013–3021, 1996.

Lorenzo A Cingolani and Yukiko Goda. Actin in action: the interplay between the actin cytoskeleton and synaptic efficacy. *Nature reviews Neuroscience*, 9(5):344–356, 2008.

J R Clay and L J DeFelice. Relationship between membrane excitability and single channel open-close kinetics. *Biophysical journal*, 42(2):151–157, 1983.

C M Colbert, J C Magee, D A Hoffman, and D Johnston. Slow recovery from inactivation of Na+ channels underlies the activity-dependent attenuation of dendritic action potentials in hippocampal CA1 pyramidal neurons. *The Journal of neuroscience : the official journal of the Society for Neuroscience*, 17(17):6512–6521, 1997.

R J Cormier, A C Greenwood, and J A Connor. Bidirectional synaptic plasticity correlated with the magnitude of dendritic calcium transients above a threshold. *Journal of neurophysiology*, 85(1):399–406, 2001.

L Niels Cornelisse, Ronald A J van Elburg, Rhiannon M Meredith, Rafael Yuste, and Huibert D Mansvelder. High speed two-photon imaging of calcium dynamics in

dendritic spines: consequences for spine calcium kinetics and buffer capacity. *PLoS ONE*, 2(10):e1073, 2007.

Roman Cregg, Aliakmal Momin, Francois Rugiero, John N Wood, and Jing Zhao. Pain channelopathies. *The Journal of Physiology*, 588(11):1897–1904, 2010.

J A Cummings, R M Mulkey, R A Nicoll, and R C Malenka. Ca2+ signaling requirements for long-term depression in the hippocampus. *Neuron*, 16(4):825–833, 1996.

T R Cummins and S G Waxman. Downregulation of tetrodotoxin-resistant sodium currents and upregulation of a rapidly repriming tetrodotoxin-sensitive sodium current in small spinal sensory neurons after nerve injury. *The Journal of neuroscience : the official journal of the Society for Neuroscience*, 17(10):3503–3514, 1997.

G Davis. Homeostatic Control of Neural Activity: From Phenomenology to Molecular Design. *Annual Review of Neuroscience*, 2006.

Peter Dayan and L F Abbott. *Theoretical Neuroscience*. MIT Press, Cambridge, MA, 2001.

D Debanne, B H Gähwiler, and S M Thompson. Heterogeneity of synaptic plasticity at unitary CA3-CA1 and CA3-CA3 connections in rat hippocampal slice cultures. *The Journal of neuroscience : the official journal of the Society for Neuroscience*, 19(24):10664–10671, 1999.

Louis J DeFelice. *Introduction to Membrane Noise*. Plenum Press, 1981.

H E Derksen and A A Verveen. Fluctuations of resting neural membrane potential. *Science*, (151):1388–1389, 1966.

Sulayman D Dib-Hajj, Theodore R Cummins, Joel A Black, and Stephen G Waxman. From genes to pain: Na v 1.7 and human pain disorders. *Trends in neurosciences*, 30(11):555–563, 2007.

Sulayman D Dib-Hajj, Theodore R Cummins, Joel A Black, and Stephen G Waxman. Sodium Channels in Normal and Pathological Pain. *Annual Review of Neuroscience*, 33:325–347, 2010.

Kamran Diba, Henry A Lester, and Christof Koch. Intrinsic noise in cultured hippocampal neurons: experiment and modeling. *The Journal of neuroscience : the official journal of the Society for Neuroscience*, 24(43):9723–9733, 2004.

Kamran Diba, Christof Koch, and Idan Segev. Spike propagation in dendrites with stochastic ion channels. *Journal of computational neuroscience*, 20(1):77–84, 2006.

Laiche Djouhri, Stella Koutsikou, Xin Fang, Simon McMullan, and Sally N Lawson. Spontaneous pain, both neuropathic and inflammatory, is related to frequency of spontaneous firing in intact C-fiber nociceptors. *The Journal of neuroscience : the official journal of the Society for Neuroscience*, 26(4):1281–1292, 2006.

Alan D Dorval and John A White. Channel noise is essential for perithreshold oscillations in entorhinal stellate neurons. *The Journal of neuroscience : the official journal of the Society for Neuroscience*, 25(43):10025–10028, 2005.

K. Doya. Bifurcations in the learning of recurrent neural networks. 6:2777–2780 vol.6, 1992.

S M Dudek and M F Bear. Bidirectional long-term modification of synaptic effectiveness in the adult and immature hippocampus. *The Journal of neuroscience : the official journal of the Society for Neuroscience*, 13(7):2910–2918, 1993.

Joshua T Dudman and Matthew F Nolan. Stochastically gating ion channels enable patterned spike firing through activity-dependent modulation of spike probability. *PLoS computational biology*, 5(2):e1000290, 2009.

P J Dyck and A P Hopkins. Electron microscopic observations on degeneration and regeneration of unmyelinated fibres. *Brain : a journal of neurology*, 95(2):233–234, 1972.

D M Egelman and P R Montague. Calcium dynamics in the extracellular space of mammalian neural tissue. *Biophysical journal*, 76(4):1856–1867, 1999.

V Egger, D Feldmeyer, and B Sakmann. Coincidence detection and changes of synaptic efficacy in spiny stellate neurons in rat barrel cortex. *Nature neuroscience*, 2(12): 1098–1105, 1999.

A Faisal, S Laughlin, and J White. How reliable is the connectivity in cortical neural networks? *Neural Networks*, 2002.

A Aldo Faisal and Simon B Laughlin. Stochastic simulations on the reliability of action potential propagation in thin axons. *PLoS computational biology*, 3(5):e79, 2007.

A Aldo Faisal, John A White, and Simon B Laughlin. Ion-channel noise places limits on the miniaturization of the brain's wiring. *Current biology : CB*, 15(12):1143–1149, 2005.

A Aldo Faisal, L Selen, and D Wolpert. Noise in the nervous system. *Nature reviews Neuroscience*, March 2008.

P Fatt and B Katz. Some observations on biological noise. *Nature*, 166(4223):597–598, 1950.

P Fatt and B Katz. Spontaneous subthreshold activity at motor nerve endings. *The Journal of physiology*, 117(1):109–128, 1952.

Dirk Feldmeyer, Joachim Lübke, and Bert Sakmann. Efficacy and connectivity of intracolumnar pairs of layer 2/3 pyramidal cells in the barrel cortex of juvenile rats. *The Journal of physiology*, 575(Pt 2):583–602, 2006.

John C Fiala, Josef Spacek, and Kristen M Harris. Dendrite structure. In Greg Stuart, Nelson Spruston, and Michael Häusser, editors, *Dendrites*. Oxford University Press, Oxford, 2008.

R F Fox. Stochastic versions of the Hodgkin-Huxley equations. *Biophysical journal*, 72(5):2068–2074, 1997.

RF Fox and Yn Lu. Emergent collective behavior in large numbers of globally coupled independently stochastic ion channels. *Physical review E, Statistical physics, plasmas, fluids, and related interdisciplinary topics*, 49(4):3421–3431, 1994.

Kevin M Franks and Terrence J Sejnowski. Complexity of calcium signaling in synaptic spines. *BioEssays : news and reviews in molecular, cellular and developmental biology*, 24(12):1130–1144, 2002.

Kevin M Franks, Charles F Stevens, and Terrence J Sejnowski. Independent sources of quantal variability at single glutamatergic synapses. *The Journal of neuroscience : the official journal of the Society for Neuroscience*, 23(8):3186–3195, 2003.

Stefano Fusi and L F Abbott. Limits on the memory storage capacity of bounded synapses. *Nature neuroscience*, 10(4):485–493, 2007.

Stefano Fusi and Walter Senn. Eluding oblivion with smart stochastic selection of synaptic updates. *Chaos (Woodbury, NY)*, 16(2):026112, 2006.

Olga Ganeshina, Robert W Berry, Ronald S Petralia, Daniel A Nicholson, and Yuri Geinisman. Differences in the expression of AMPA and NMDA receptors between axospinous perforated and nonperforated synapses are related to the configuration and size of postsynaptic densities. *The Journal of comparative neurology*, 468(1): 86–95, 2004.

Sonia Gasparini and Jeffrey C Magee. State-dependent dendritic computation in hippocampal CA1 pyramidal neurons. *The Journal of neuroscience : the official journal of the Society for Neuroscience*, 26(7):2088–2100, 2006.

Matthieu Gilson, Anthony Burkitt, and Leo J van Hemmen. STDP in Recurrent Neuronal Networks. *Frontiers in computational neuroscience*, 4, 2010.

N L Golding and N Spruston. Dendritic sodium spikes are variable triggers of axonal action potentials in hippocampal CA1 pyramidal neurons. *Neuron*, 21(5):1189–1200, 1998.

Nace L Golding, Timothy J Mickus, Yael Katz, William L Kath, and Nelson Spruston. Factors mediating powerful voltage attenuation along CA1 pyramidal neuron dendrites. *The Journal of physiology*, 568(Pt 1):69–82, 2005.

Joshua H Goldwyn, Nikita S Imennov, Michael Famulare, and Eric Shea-Brown. On stochastic differential equation models for ion channel noise in Hodgkin-Huxley neurons. *arXiv*, q-bio.NC, 2010.

Tim Gollisch and Markus Meister. Rapid neural coding in the retina with relative spike latencies. *Science*, 319(5866):1108–1111, 2008.

I Goychuk and P Hänggi. Stochastic resonance as a collective property of ion channel assemblies. *EPL (Europhysics Letters)*, 2001.

Michael Graupner and Nicolas Brunel. STDP in a bistable synapse model based on CaMKII and associated signaling pathways. *PLoS computational biology*, 3(11): e221, 2007.

Michael Graupner and Nicolas Brunel. Mechanisms of induction and maintenance of spike-timing dependent plasticity in biophysical synapse models. *Frontiers in computational neuroscience*, 4, 2010.

Jaime Grutzendler, Narayanan Kasthuri, and Wen-Biao Gan. Long-term dendritic spine stability in the adult cortex. *Nature*, 420(6917):812–816, 2002.

R Gütig, R Aharonov, S Rotter, and Haim Sompolinsky. Learning input correlations through nonlinear temporally asymmetric Hebbian plasticity. *The Journal of neuroscience : the official journal of the Society for Neuroscience*, 23(9):3697–3714, 2003.

C Hansel, A Artola, and W Singer. Relation between dendritic Ca2+ levels and the polarity of synaptic long-term modifications in rat visual cortex neurons. *The European journal of neuroscience*, 9(11):2309–2322, 1997.

Neil R Hardingham, Giles E Hardingham, Kevin D Fox, and Julian J B Jack. Presynaptic efficacy directs normalization of synaptic strength in layer 2/3 rat neocortex after paired activity. *Journal of neurophysiology*, 97(4):2965–2975, 2007.

Kristen M Harris and J K Stevens. Dendritic spines of CA 1 pyramidal cells in the rat hippocampus: serial electron microscopy with reference to their biophysical characteristics. *The Journal of neuroscience : the official journal of the Society for Neuroscience*, 9(8):2982–2997, 1989.

Christopher D Harvey and Karel Svoboda. Locally dynamic synaptic learning rules in pyramidal neuron dendrites. *Nature*, 450(7173):1195–1200, 2007.

Michael Häusser and Bartlett Mel. Dendrites: bug or feature? *Current opinion in neurobiology*, 13(3):372–383, 2003.

Arnold Hayer and Upinder S Bhalla. Molecular switches at the synapse emerge from receptor and kinase traffic. *PLoS computational biology*, 1(2):137–154, 2005.

D.O. Hebb. *The organization of behavior: a neuropsychological theory*. A Wiley book in clinical psychology. Wiley, 1949.

B Hille. Ionic channels in nerve membranes. *Progress in biophysics and molecular biology*, 21:1–32, 1970.

Bertil Hille. *Ion Channels of Excitable Membranes*. Sinauer Associates Inc., USA, 3rd edition, 2001.

Alan Lloyd Hodgkin and Andrew F Huxley. A quantitative description of membrane current and its application to conduction and excitation in nerve. *The Journal of physiology*, 117(4):500–544, 1952.

D A Hoffman, R Sprengel, and B Sakmann. Molecular dissection of hippocampal theta-burst pairing potentiation. *Proceedings of the National Academy of Sciences of the United States of America*, 99(11):7740–7745, 2002.

N Holbro, A Grunditz, and T Oertner. Differential distribution of endoplasmic reticulum controls metabotropic signaling and plasticity at hippocampal synapses. *Proceedings of the National Academy of Sciences of the United States of America*, 106 (35):15055–15060, August 2009.

Carl Holmgren, Tibor Harkany, Björn Svennenfors, and Yuri Zilberter. Pyramidal cell communication within local networks in layer 2/3 of rat neocortex. *The Journal of physiology*, 551(Pt 1):139–153, 2003.

Knut Holthoff, David Tsay, and Rafael Yuste. Calcium dynamics of spines depend on their dendritic location. *Neuron*, 33(3):425–437, January 2002.

Anthony Holtmaat and Karel Svoboda. Experience-dependent structural synaptic plasticity in the mammalian brain. *Nature reviews Neuroscience*, 10(9):647–658, 2009.

Anthony J G D Holtmaat, Joshua T Trachtenberg, Linda Wilbrecht, Gordon M Shepherd, Xiaoqun Zhang, Graham W Knott, and Karel Svoboda. Transient and persistent dendritic spines in the neocortex in vivo. *Neuron*, 45(2):279–291, 2005.

Y Horikawa. Noise effects on spike propagation in the stochastic Hodgkin-Huxley models. *Biological cybernetics*, 66(1):19–25, 1991.

J F Howe, J D Loeser, and W H Calvin. Mechanosensitivity of dorsal root ganglia and chronically injured axons: a physiological basis for the radicular pain of nerve root compression. *Pain*, 3(1):25–41, 1977.

Yann Humeau, Cyril Herry, Nicola Kemp, Hamdy Shaban, Elodie Fourcaudot, Stephanie Bissière, and Andreas Lüthi. Dendritic spine heterogeneity determines afferent-specific Hebbian plasticity in the amygdala. *Neuron*, 45(1):119–131, January 2005.

B Hutcheon and Y Yarom. Resonance, oscillation and the intrinsic frequency preferences of neurons. *Trends in neurosciences*, 23(5):216–222, 2000.

Iskander Ismailov, Djanenkhodja Kalikulov, Takafumi Inoue, and Michael J Friedlander. The kinetic profile of intracellular calcium predicts long-term potentiation and long-term depression. *The Journal of neuroscience : the official journal of the Society for Neuroscience*, 24(44):9847–9861, 2004.

Eugene M Izhikevich. *Dynamical Systems in Neuroscience: The Geometry of Excitability and Bursting*. MIT Press, Cambridge, Massachusetts, 2007.

Julian JB Jack, Denis Noble, and Richard W Tsien. *Electric current flow in excitable cells*. Oxford University Press, Oxford, 1975.

Gilad A Jacobson, Kamran Diba, Anat Yaron-Jakoubovitch, Yasmin Oz, Christof Koch, Idan Segev, and Yosef Yarom. Subthreshold voltage noise of rat neocortical pyramidal neurones. *The Journal of physiology*, 564(Pt 1):145–160, 2005.

C E Jahr and C F Stevens. Voltage dependence of NMDA-activated macroscopic conductances predicted by single-channel kinetics. *The Journal of neuroscience : the official journal of the Society for Neuroscience*, 10(9):3178–3182, 1990.

Tim Jarsky, Alex Roxin, William L Kath, and Nelson Spruston. Conditional dendritic spike propagation following distal synaptic activation of hippocampal CA1 pyramidal neurons. *Nature neuroscience*, 8(12):1667–1676, 2005.

S Johansson and P Arhem. Single-channel currents trigger action potentials in small cultured hippocampal neurons. *Proceedings of the National Academy of Sciences of the United States of America*, 91(5):1761–1765, 1994.

David Julius and Edwin McCleskey. Cellular and molecular properties of primary afferent neurons. In *Wall and Melzack's Textbook of Pain*, pages 35–48. Elsevier, London, 2006.

Georgios Kalantzis and Harel Z Shouval. Structural plasticity can produce metaplasticity. *PLoS ONE*, 4(11):e8062, 2009.

B Katz and R Miledi. Membrane noise produced by acetylcholine. *Nature*, 226(5249): 962–963, June 1970.

B Katz and R Miledi. Further observations on acetylcholine noise. *Nature: New biology*, 232(30):124–126, July 1971.

B Katz and R Miledi. The statistical nature of the acetycholine potential and its molecular components. *The Journal of physiology*, 224(3):665–699, August 1972.

J A Kauer, R C Malenka, and R A Nicoll. A persistent postsynaptic modification mediates long-term potentiation in the hippocampus. *Neuron*, 1(10):911–917, 1988.

Daniel X Keller, Kevin M Franks, Thomas M Bartol, and Terrence J Sejnowski. Calmodulin activation by calcium transients in the postsynaptic density of dendritic spines. *PLoS ONE*, 3(4):e2045, 2008.

Thomas Klausberger and Peter Somogyi. Neuronal diversity and temporal dynamics: the unity of hippocampal circuit operations. *Science*, 321(5885):53–57, 2008.

Graham W Knott, Anthony Holtmaat, Linda Wilbrecht, Egbert Welker, and Karel Svoboda. Spine growth precedes synapse formation in the adult neocortex in vivo. *Nature neuroscience*, 9(9):1117–1124, 2006.

C Koch. Cable theory in neurons with active, linearized membranes. *Biological cybernetics*, 50(1):15–33, 1984.

C Koch. *Biophysics of Computation: Information Processing in Single Neurons*. Oxford University Press, 1999.

Maarten H P Kole, Stefan Hallermann, and Greg J Stuart. Single Ih channels in pyramidal neuron dendrites: properties, distribution, and impact on action potential output. *The Journal of neuroscience : the official journal of the Society for Neuroscience*, 26(6):1677–1687, 2006.

A Larkman, T Hannay, K Stratford, and J Jack. Presynaptic release probability influences the locus of long-term potentiation. *Nature*, 360(6399):70–73, 1992.

M E Larkum, J J Zhu, and B Sakmann. A new cellular mechanism for coupling inputs arriving at different cortical layers. *Nature*, 398(6725):338–341, 1999.

H Lecar and R Nossal. Theory of threshold fluctuations in nerves. I. Relationships between electrical noise and fluctuations in axon firing. *Biophysical journal*, 11 (12):1048–1067, 1971a.

H Lecar and R Nossal. Theory of threshold fluctuations in nerves. II. Analysis of various sources of membrane noise. *Biophysical journal*, 11(12):1068–1084, 1971b.

Seok-Jin R Lee, Yasmin Escobedo-Lozoya, Erzsebet M Szatmari, and Ryohei Yasuda. Activation of CaMKII in single dendritic spines during long-term potentiation. *Nature*, 458(7236):299–304, 2009.

Johannes J Letzkus, Björn M Kampa, and Greg J Stuart. Learning rules for spike timing-dependent plasticity depend on dendritic synapse location. *The Journal of neuroscience : the official journal of the Society for Neuroscience*, 26(41):10420–10429, 2006.

Daniele Linaro, Marco Storace, and Michele Giugliano. Accurate and fast simulation of channel noise in conductance-based model neurons by diffusion approximation. *PLoS computational biology*, 7(3):e1001102, 2011.

B Lindner, J Garcia-Ojalvo, A Neiman, and L Schimansky-Geier. Effects of noise in excitable systems. *Physics Reports-Review Section of Physics Letters*, 392(6): 321–424, 2004.

J E Lisman and A M Zhabotinsky. A model of synaptic memory: a CaMKII/PP1 switch that potentiates transmission by organizing an AMPA receptor anchoring assembly. *Neuron*, 31(2):191–201, 2001.

I Llano, C K Webb, and F Bezanilla. Potassium conductance of the squid giant axon. Single-channel studies. *The Journal of general physiology*, 92(2):179–196, 1988.

Andrea Lörincz and Zoltan Nusser. Cell-type-dependent molecular composition of the axon initial segment. *The Journal of neuroscience : the official journal of the Society for Neuroscience*, 28(53):14329–14340, December 2008.

G Lynch, J Larson, S Kelso, G Barrionuevo, and F Schottler. Intracellular injections of EGTA block induction of hippocampal long-term potentiation. *Nature*, 305(5936): 719–721, 1983.

Wei Ji Ma, Jeffrey M Beck, Peter E Latham, and Alexandre Pouget. Bayesian inference with probabilistic population codes. *Nature neuroscience*, 9(11):1432–1438, 2006.

Donald M MacKay and Warren S McCulloch. The limiting information capacity of a neuronal link. *Bulletin of Mathematical Biology*, 127-135, 1952.

J C Magee. Dendritic hyperpolarization-activated currents modify the integrative properties of hippocampal CA1 pyramidal neurons. *The Journal of neuroscience : the official journal of the Society for Neuroscience*, 18(19):7613–7624, 1998.

J C Magee. Dendritic integration of excitatory synaptic input. *Nature reviews Neuroscience*, 1(3):181–190, 2000.

J C Magee and D Johnston. Characterization of single voltage-gated Na+ and Ca2+ channels in apical dendrites of rat CA1 pyramidal neurons. *The Journal of physiology*, 487 (Pt 1):67–90, 1995.

J C Magee and D Johnston. A synaptically controlled, associative signal for Hebbian plasticity in hippocampal neurons. *Science*, 275(5297):209–213, 1997.

Jeffrey C Magee. Dendritic voltage-gated ion channels. In Greg Stuart, Nelson Spruston, and Michael Häusser, editors, *Dendrites*, pages 225–250. Oxford University Press, Oxford, 2008.

J Magistretti, D S Ragsdale, and A Alonso. Direct demonstration of persistent Na+ channel activity in dendritic processes of mammalian cortical neurones. *The Journal of physiology*, 521 Pt 3:629–636, 1999.

Z F Mainen and T J Sejnowski. Reliability of spike timing in neocortical neurons. *Science*, 268(5216):1503–1506, 1995.

Z F Mainen and T J Sejnowski. Influence of dendritic structure on firing pattern in model neocortical neurons. *Nature*, 382(6589):363–366, 1996.

Z F Mainen, J Joerges, J R Huguenard, and T J Sejnowski. A model of spike initiation in neocortical pyramidal neurons. *Neuron*, 15(6):1427–1439, 1995.

R C Malenka, B Lancaster, and R S Zucker. Temporal limits on the rise in postsynaptic calcium required for the induction of long-term potentiation. *Neuron*, 9(1):121–128, 1992.

Robert C Malenka and Mark F Bear. LTP and LTD: an embarrassment of riches. *Neuron*, 44(1):5–21, 2004.

Tiina Manninen, Katri Hituri, Jeanette Hellgren Kotaleski, Kim T Blackwell, and Marja-Leena Linne. Postsynaptic signal transduction models for long-term potentiation and depression. *Frontiers in computational neuroscience*, 4:152, 2010.

A Manwani and C Koch. Detecting and estimating signals in noisy cable structure, I: neuronal noise sources. *Neural computation*, 11(8):1797–1829, 1999a.

A Manwani and C Koch. Detecting and estimating signals in noisy cable structures, II: information theoretical analysis. *Neural computation*, 11(8):1831–1873, 1999b.

A Manwani and Christof Koch. Detecting and estimating signals over noisy and unreliable synapses: information-theoretic analysis. *Neural computation*, 13(1):1–33, 2001.

E Marder, L F Abbott, G G Turrigiano, Z Liu, and J Golowasch. Memory from the dynamics of intrinsic membrane currents. *Proceedings of the National Academy of Sciences of the United States of America*, 93(24):13481–13486, 1996.

M Matsuzaki, G C Ellis-Davies, T Nemoto, Y Miyashita, M Iino, and H Kasai. Dendritic spine geometry is critical for AMPA receptor expression in hippocampal CA1 pyramidal neurons. *Nature neuroscience*, 4(11):1086–1092, 2001.

Masanori Matsuzaki, Naoki Honkura, Graham C R Ellis-Davies, and Haruo Kasai. Structural basis of long-term potentiation in single dendritic spines. *Nature*, 429 (6993):761–766, 2004.

A Mauro, F Conti, F Dodge, and R Schor. Subthreshold behavior and phenomenological impedance of the squid giant axon. *The Journal of general physiology*, 55(4): 497–523, 1970.

Mark D McDonnell and Derek Abbott. What is stochastic resonance? Definitions, misconceptions, debates, and its relevance to biology. *PLoS computational biology*, 5(5):e1000348, 2009.

B L McNaughton, R M Douglas, and G V Goddard. Synaptic enhancement in fascia dentata: cooperativity among coactive afferents. *Brain research*, 157(2):277–293, 1978.

R A Meyer, S N Raja, J N Campbell, S E Mackinnon, and A L Dellon. Neural activity originating from a neuroma in the baboon. *Brain research*, 325(1-2):255–260, 1985.

Richard A Meyer, Matthias Ringkamp, James N Campbell, and Srinivasa N Raja. Peripheral mechanisms of cutaneous pain. In Stephen B McMahon and Martin Koltzenburg, editors, *Wall and Melzack's Textbook of Pain*, pages 3–34. Elsevier, London, 2006.

KD Miler and DJC MacKay. The role of constraints in Hebbian learning. *Neural computation*, (6):100–126, 1994.

K D Miller. Synaptic economics: competition and cooperation in synaptic plasticity. *Neuron*, 17(3):371–374, 1996.

Paul Miller, Anatol M Zhabotinsky, John E Lisman, and Xiao-Jing Wang. The stability of a stochastic CaMKII switch: dependence on the number of enzyme molecules and protein turnover. *PLoS biology*, 3(4):e107, 2005.

B Milner, L R Squire, and E R Kandel. Cognitive neuroscience and the study of memory. *Neuron*, 20(3):445–468, 1998.

Amir Minerbi, Roni Kahana, Larissa Goldfeld, Maya Kaufman, Shimon Marom, and Noam E Ziv. Long-term relationships between synaptic tenacity, synaptic remodeling, and network activity. *PLoS biology*, 7(6):e1000136, 2009.

Hiroyuki Mino, Jay T Rubinstein, and John A White. Comparison of algorithms for the simulation of action potentials with stochastic sodium channels. *Annals of biomedical engineering*, 30(4):578–587, 2002.

Yuriy Mishchenko, Tao Hu, Josef Spacek, John Mendenhall, Kristen M Harris, and Dmitri B Chklovskii. Ultrastructural analysis of hippocampal neuropil from the connectomics perspective. *Neuron*, 67(6):1009–1020, 2010.

J M Montgomery, P Pavlidis, and D V Madison. Pair recordings reveal all-silent synaptic connections and the postsynaptic expression of long-term potentiation. *Neuron*, 29(3):691–701, 2001.

R G M Morris, E I Moser, G Riedel, S J Martin, J Sandin, M Day, and C O'Carroll. Elements of a neurobiological theory of the hippocampus: the role of activity-dependent synaptic plasticity in memory. *Philosophical transactions of the Royal Society of London Series B, Biological sciences*, 358(1432):773–786, 2003.

Abigail Morrison, Ad Aertsen, and Markus Diesmann. Spike-timing-dependent plasticity in balanced random networks. *Neural computation*, 19(6):1437–1467, 2007.

Frank Moss, Lawrence M Ward, and Walter G Sannita. Stochastic resonance and sensory information processing: a tutorial and review of application. *Clinical neurophysiology : official journal of the International Federation of Clinical Neurophysiology*, 115(2):267–281, 2004.

Shreesh P Mysore, Chin-Yin Tai, and Erin M Schuman. Effects of N-cadherin disruption on spine morphological dynamics. *Frontiers in Cellular Neuroscience*, 1:1, 2007.

E Neher. Usefulness and limitations of linear approximations to the understanding of Ca++ signals. *Cell calcium*, 24(5-6):345–357, 1998.

Erwin Neher and Bert Sakmann. Single-channel currents recorded from membrane of denervated frog muscle fibres. *Nature*, 260(5554):799–802, 1976.

Thomas Nevian and Bert Sakmann. Spine Ca2+ signaling in spike-timing-dependent plasticity. *The Journal of neuroscience : the official journal of the Society for Neuroscience*, 26(43):11001–11013, 2006.

A Ngezahayo, M Schachner, and A Artola. Synaptic activity modulates the induction of bidirectional synaptic changes in adult mouse hippocampus. *The Journal of neuroscience : the official journal of the Society for Neuroscience*, 20(7):2451–2458, 2000.

Esther A Nimchinsky, Ryohei Yasuda, Thomas G Oertner, and Karel Svoboda. The number of glutamate receptors opened by synaptic stimulation in single hippocampal spines. *The Journal of neuroscience : the official journal of the Society for Neuroscience*, 24(8):2054–2064, 2004.

Jun Noguchi, Masanori Matsuzaki, Graham C R Ellis-Davies, and Haruo Kasai. Spine-neck geometry determines NMDA receptor-dependent Ca2+ signaling in dendrites. *Neuron*, 46(4):609–622, 2005.

L G Nowak, M V Sanchez-Vives, and D A McCormick. Influence of low and high frequency inputs on spike timing in visual cortical neurons. *Cereb Cortex*, 7(6): 487–501, 1997.

Z Nusser, R Lujan, G Laube, J D Roberts, E Molnar, and P Somogyi. Cell type and pathway dependence of synaptic AMPA receptor number and variability in the hippocampus. *Neuron*, 21(3):545–559, 1998.

Daniel H O'Connor, Gayle M Wittenberg, and Samuel S-H Wang. Dissection of bidirectional synaptic plasticity into saturable unidirectional processes. *Journal of neurophysiology*, 94(2):1565–1573, 2005.

Charles Pecher. La fluctuation d'excitabilite de la fibre nerveuse. *Arch Intern Physiol*, 49(2):129–152, 1939.

Karine Pozo and Yukiko Goda. Unraveling mechanisms of homeostatic synaptic plasticity. *Neuron*, 66(3):337–351, 2010.

Ithai Rabinowitch and Idan Segev. The endurance and selectivity of spatial patterns of long-term potentiation/depression in dendrites under homeostatic synaptic plasticity. *The Journal of neuroscience : the official journal of the Society for Neuroscience*, 26(52):13474–13484, 2006.

C Racca, F A Stephenson, P Streit, J D Roberts, and P Somogyi. NMDA receptor content of synapses in stratum radiatum of the hippocampal CA1 area. *The Journal of neuroscience : the official journal of the Society for Neuroscience*, 20(7):2512–2522, 2000.

Wilfrid Rall. Branching dendritic trees and motoneuron membrane resistivity. *Exp Neurol*, 1:491–527, 1959.

Stefan Remy, Jozsef Csicsvari, and Heinz Beck. Activity-dependent control of neuronal output by local and global dendritic spike attenuation. *Neuron*, 61(6):906–916, 2009.

Claire Ribrault, Ken Sekimoto, and Antoine Triller. From the stochasticity of molecular processes to the variability of synaptic transmission. *Nature reviews Neuroscience*, 12(7):375–387, 2011.

Fred Rieke, David Warland, Rob de Ruyter van Steveninck, and William Bialek. *Spikes: Exploring the Neural Code*. The MIT Press, USA, 1999.

J Rubin, D D Lee, and H Sompolinsky. Equilibrium properties of temporally asymmetric Hebbian plasticity. *Physical review letters*, 86(2):364–367, 2001.

Jonathan E Rubin, Richard C Gerkin, Guo-Qiang Bi, and Carson C Chow. Calcium time course as a signal for spike-timing-dependent plasticity. *Journal of neurophysiology*, 93(5):2600–2613, 2005.

Jay T Rubinstein. Threshold fluctuations in an N sodium channel model of the node of Ranvier. *Biophysical journal*, 68(3):779–785, 1995.

Bernardo L Sabatini, Thomas G Oertner, and Karel Svoboda. The life cycle of Ca(2+) ions in dendritic spines. *Neuron*, 33(3):439–452, 2002.

Ignacio Sáez and Michael J Friedlander. Plasticity between neuronal pairs in layer 4 of visual cortex varies with synapse state. *The Journal of neuroscience : the official journal of the Society for Neuroscience*, 29(48):15286–15298, 2009.

John W Scadding and Martin Koltzeburg. Painful peripheral neuropathies. In Stephen B McMahon and Martin Koltzenburg, editors, *Wall and Melzack's Textbook of Pain*, pages 973–1000. Elsevier, London, 2006.

E Schneidman, B Freedman, and I Segev. Ion channel stochasticity may be critical in determining the reliability and precision of spike timing. *Neural computation*, 10 (7):1679–1703, 1998.

Ruggero Scorcioni, Maciej T Lazarewicz, and Giorgio A Ascoli. Quantitative morphometry of hippocampal pyramidal cells: differences between anatomical classes and reconstructing laboratories. *The Journal of comparative neurology*, 473(2):177–193, 2004.

I Segev and C Koch, editors. *Methods in Neuronal Modeling*. MIT Press, 1998.

T J Sejnowski. Statistical constraints on synaptic plasticity. *Journal of theoretical biology*, 69(2):385–389, 1977.

B Sengupta, S B Laughlin, and J E Niven. Comparison of Langevin and Markov channel noise models for neuronal signal generation. *Physical review E, Statistical, nonlinear, and soft matter physics*, 81(1 Pt 1):011918, 2010.

C.E. Shannon and W. Weaver. *The mathematical theory of communication*. Illini books. University of Illinois Press, 1964.

Patrick L Sheets, James O Jackson, Stephen G Waxman, Sulayman D Dib-Hajj, and Theodore R Cummins. A Nav1.7 channel mutation associated with hereditary erythromelalgia contributes to neuronal hyperexcitability and displays reduced lidocaine sensitivity. *The Journal of physiology*, 581(Pt 3):1019–1031, 2007.

Harel Z Shouval. Clusters of interacting receptors can stabilize synaptic efficacies. *Proceedings of the National Academy of Sciences of the United States of America*, 102(40):14440–14445, 2005.

Harel Z Shouval, Mark F Bear, and Leon N Cooper. A unified model of NMDA receptor-dependent bidirectional synaptic plasticity. *Proceedings of the National Academy of Sciences of the United States of America*, 99(16):10831–10836, 2002.

F J Sigworth. The variance of sodium current fluctuations at the node of Ranvier. *The Journal of physiology*, 307:97–129, 1980.

Stephen B Simons, Yasmin Escobedo, Ryohei Yasuda, and Serena M Dudek. Regional differences in hippocampal calcium handling provide a cellular mechanism for limiting plasticity. *Proceedings of the National Academy of Sciences of the United States of America*, 106(33):14080–14084, August 2009.

P J Sjöström, G G Turrigiano, and S B Nelson. Rate, timing, and cooperativity jointly determine cortical synaptic plasticity. *Neuron*, 32(6):1149–1164, 2001.

Per Jesper Sjöström and Michael Häusser. A cooperative switch determines the sign of synaptic plasticity in distal dendrites of neocortical pyramidal neurons. *Neuron*, 51(2):227–238, 2006.

E Skaugen and L Walløe. Firing behaviour in a stochastic nerve membrane model based upon the Hodgkin-Huxley equations. *Acta physiologica Scandinavica*, 107 (4):343–363, 1979.

Aleksander Sobczyk, Volker Scheuss, and Karel Svoboda. NMDA receptor subunit-dependent [Ca2+] signaling in individual hippocampal dendritic spines. *The Journal of neuroscience : the official journal of the Society for Neuroscience*, 25(26):6037–6046, 2005.

S Song, K D Miller, and L F Abbott. Competitive Hebbian learning through spike-timing-dependent synaptic plasticity. *Nature neuroscience*, 3(9):919–926, 2000.

Sen Song, Per Jesper Sjöström, Markus Reigl, Sacha Nelson, and Dmitri B Chklovskii. Highly nonrandom features of synaptic connectivity in local cortical circuits. *PLoS biology*, 3(3):e68, 2005.

Nelson Spruston, Greg Stuart, and Michael Häusser. Dendritic integration. In Greg Stuart, Nelson Spruston, and Michael Häusser, editors, *Dendrites*, pages 351–400. Oxford University Press, Oxford, 2008.

W C Stacey and D M Durand. Stochastic resonance improves signal detection in hippocampal CA1 neurons. *Journal of neurophysiology*, 83(3):1394–1402, 2000.

W C Stacey and D M Durand. Synaptic noise improves detection of subthreshold signals in hippocampal CA1 neurons. *Journal of neurophysiology*, 86(3):1104–1112, 2001.

P N Steinmetz, A Manwani, C Koch, M London, and I Segev. Subthreshold voltage noise due to channel fluctuations in active neuronal membranes. *Journal of computational neuroscience*, 9(2):133–148, 2000.

J R Stiles and T M Bartol. Monte Carlo methods for simulating realistic synaptic microphysiology using MCell. In *Computational Neuroscience: Realistic Modeling for experimentalists*, pages 87–128. CRC Press, Boca Raton, FL, 2000.

J R Stiles, D Van Helden, T M Bartol, E E Salpeter, and M M Salpeter. Miniature endplate current rise times less than 100 microseconds from improved dual recordings can be modeled with passive acetylcholine diffusion from a synaptic vesicle. *Proceedings of the National Academy of Sciences of the United States of America*, 93(12):5747–5752, 1996.

J F Storm. Temporal integration by a slowly inactivating K+ current in hippocampal neurons. *Nature*, 336(6197):379–381, 1988.

Adam F Strassberg and Louis J DeFelice. Limitations of the Hodgkin-Huxley Formalism: Effects of Single Channel Kinetics on Transmembrane Voltage Dynamics. *Neural computation*, 1993.

G Stuart and N Spruston. Determinants of voltage attenuation in neocortical pyramidal neuron dendrites. *Journal of Neuroscience*, 18(10):3501–3510, May 1998.

G J Stuart and B Sakmann. Active propagation of somatic action potentials into neocortical pyramidal cell dendrites. *Nature*, 367(6458):69–72, 1994.

O Sugawara, Y Atsuta, T Iwahara, T Muramoto, M Watakabe, and Y Takemitsu. The effects of mechanical compression and hypoxia on nerve root and dorsal root ganglia. An analysis of ectopic firing using an in vitro model. *Spine*, 21(18):2089–2094, 1996.

Tibor Szilágyi and Erik De Schutter. Effects of variability in anatomical reconstruction techniques on models of synaptic integration by dendrites: a comparison of three Internet archives. *The European journal of neuroscience*, 19(5):1257–1266, 2004.

Shigeo Takamori, Matthew Holt, Katinka Stenius, Edward A Lemke, Mads Grønborg, Dietmar Riedel, Henning Urlaub, Stephan Schenck, Britta Brügger, Philippe Ringler, Shirley A Müller, Burkhard Rammner, Frauke Gräter, Jochen S Hub, Bert L De Groot, Gottfried Mieskes, Yoshinori Moriyama, Jürgen Klingauf, Helmut Grubmüller, John Heuser, Felix Wieland, and Reinhard Jahn. Molecular anatomy of a trafficking organelle. *Cell*, 127(4):831–846, 2006.

Y Takumi, V Ramírez-León, P Laake, E Rinvik, and O P Ottersen. Different modes of expression of AMPA and NMDA receptors in hippocampal synapses. *Nature neuroscience*, 2(7):618–624, 1999.

Taro Toyoizumi, Jean-Pascal Pfister, Kazuyuki Aihara, and Wulfram Gerstner. Optimality model of unsupervised spike-timing-dependent plasticity: synaptic memory and weight distribution. *Neural computation*, 19(3):639–671, 2007.

Joshua T Trachtenberg, Brian E Chen, Graham W Knott, Guoping Feng, Joshua R Sanes, Egbert Welker, and Karel Svoboda. Long-term in vivo imaging of experience-dependent synaptic plasticity in adult cortex. *Nature*, 420(6917):788–794, 2002.

Antoine Triller and Daniel Choquet. Surface trafficking of receptors between synaptic and extrasynaptic membranes: and yet they do move! *Trends in neurosciences*, 28 (3):133–139, March 2005.

G G Turrigiano, K R Leslie, N S Desai, L C Rutherford, and S B Nelson. Activity-dependent scaling of quantal amplitude in neocortical neurons. *Nature*, 391(6670): 892–896, 1998.

Ronald A J van Elburg and Arjen van Ooyen. Impact of dendritic size and dendritic topology on burst firing in pyramidal cells. *PLoS computational biology*, 6 (5):e1000781, 2010.

N G van Kampen. *Stochastic processes in physics and chemistry*. North-Holland, Amsterdam, 2nd edition, 1992.

M C van Rossum, G Q Bi, and G G Turrigiano. Stable Hebbian learning from spike timing-dependent plasticity. *The Journal of neuroscience : the official journal of the Society for Neuroscience*, 20(23):8812–8821, 2000.

Mark van Rossum, B J O'Brien, and R G Smith. Effects of noise on the spike timing precision of retinal ganglion cells. *Journal of neurophysiology*, 89(5):2406–2419, 2003.

Mark C W van Rossum, Gina G Turrigiano, and Sacha B Nelson. Fast propagation of firing rates through layered networks of noisy neurons. *The Journal of neuroscience : the official journal of the Society for Neuroscience*, 22(5):1956–1966, 2002.

A A Verveen. On the Fluctuation of Threshold of the Nerve Fibre. In D P Tower and J P Schade, editors, *Structure and Function of the Cerebral Cortex*, pages 282–288. Elsevier, Amsterdam, 1960.

A A Verveen and H E Derksen. Fluctuation phenomena in nerve membrane. In *Proceedings of the IEEE*, pages 906–916, 1968.

AA Verveen, HE Derksen, and K L Schik. Voltage fluctuations of neural membrane. *Nature*, 216:588–589, 1967.

P Vetter, Arnd Roth, and Michael Häusser. Propagation of action potentials in dendrites depends on dendritic morphology. *Journal of neurophysiology*, 85(2):926–937, 2001.

M Volgushev, L L Voronin, M Chistiakova, and W Singer. Relations between long-term synaptic modifications and paired-pulse interactions in the rat neocortex. *The European journal of neuroscience*, 9(8):1656–1665, 1997.

Huai-Xing Wang, Richard C Gerkin, David W Nauen, and Guo-Qiang Bi. Coactivation and timing-dependent integration of synaptic potentiation and depression. *Nature neuroscience*, 8(2):187–193, 2005.

Xiao-bin Wang, Yunlei Yang, and Qiang Zhou. Independent expression of synaptic and morphological plasticity associated with long-term depression. *The Journal of neuroscience : the official journal of the Society for Neuroscience*, 27(45):12419–12429, 2007b.

John A White, R Klink, Angel A Alonso, and A R Kay. Noise from voltage-gated ion channels may influence neuronal dynamics in the entorhinal cortex. *Journal of neurophysiology*, 80(1):262–269, 1998.

T N Wiesel and D H Hubel. Comparison of the effects of unilateral and bilateral eye closure on cortical unit responses in kittens. *Journal of neurophysiology*, 28(6): 1029–1040, 1965.

Stephen R Williams and S Mitchell. Direct measurement of somatic voltage clamp errors in central neurons. *Nature neuroscience*, 2008.

Gayle M Wittenberg and Samuel S-H Wang. Malleability of spike-timing-dependent plasticity at the CA3-CA1 synapse. *The Journal of neuroscience : the official journal of the Society for Neuroscience*, 26(24):6610–6617, 2006.

G Wu, M Ringkamp, T V Hartke, B B Murinson, J N Campbell, J W Griffin, and R A Meyer. Early onset of spontaneous activity in uninjured C-fiber nociceptors after injury to neighboring nerve fibers. *The Journal of neuroscience : the official journal of the Society for Neuroscience*, 21(8):RC140, 2001.

Xundong E Wu and Bartlett W Mel. Capacity-enhancing synaptic learning rules in a medial temporal lobe online learning model. *Neuron*, 62(1):31–41, 2009.

Wen-Hua Xiao and Gary J Bennett. Persistent low-frequency spontaneous discharge in A-fiber and C-fiber primary afferent neurons during an inflammatory pain condition. *Anesthesiology*, 107(5):813–821, 2007.

S N Yang, Y G Tang, and R S Zucker. Selective induction of LTP and LTD by postsynaptic [Ca2+]i elevation. *Journal of neurophysiology*, 81(2):781–787, 1999.

Yunlei Yang, Xiao-bin Wang, Matthew Frerking, and Qiang Zhou. Spine expansion and stabilization associated with long-term potentiation. *The Journal of neuroscience : the official journal of the Society for Neuroscience*, 28(22):5740–5751, 2008.

Anat Yaron-Jakoubovitch, G Jacobson, Christof Koch, Idan Segev, and Y Yarom. A paradoxical isopotentiality: a spatially uniform noise spectrum in neocortical pyramidal cells. *Frontiers in Cellular Neuroscience*, 2008.

Ryohei Yasuda, Bernardo L Sabatini, and Karel Svoboda. Plasticity of calcium channels in dendritic spines. *Nature neuroscience*, 6(9):948–955, 2003.

Nobuaki Yasumatsu, Masanori Matsuzaki, Takashi Miyazaki, Jun Noguchi, and Haruo Kasai. Principles of long-term dynamics of dendritic spines. *The Journal of neuroscience : the official journal of the Society for Neuroscience*, 28(50):13592–13608, 2008.

Luk Chong Yeung, Harel Z Shouval, Brian S Blais, and Leon N Cooper. Synaptic homeostasis and input selectivity follow from a calcium-dependent plasticity model. *Proceedings of the National Academy of Sciences of the United States of America*, 101(41):14943–14948, 2004.

Alex Yuan, Celia M Santi, Aguan Wei, Zhao Wen Wang, Kelly Pollak, Michael Nonet, Leonard Kaczmarek, C Michael Crowder, and Lawrence Salkoff. The sodium-activated potassium channel is encoded by a member of the Slo gene family. *Neuron*, 37(5):765–773, 2003.

Rafael Yuste and W Denk. Dendritic spines as basic functional units of neuronal integration. *Nature*, 375(6533):682–684, 1995.

A Zador. Impact of synaptic unreliability on the information transmitted by spiking neurons. *Journal of neurophysiology*, 79(3):1219–1229, 1998.

Qiang Zhou, Koichi J Homma, and Mu-Ming Poo. Shrinkage of dendritic spines associated with long-term depression of hippocampal synapses. *Neuron*, 44(5):749–757, 2004.

Quan Zou and Alain Destexhe. Kinetic models of spike-timing dependent plasticity and their functional consequences in detecting correlations. *Biological cybernetics*, 97(1):81–97, 2007.

R S Zucker. Calcium- and activity-dependent synaptic plasticity. *Current opinion in neurobiology*, 9(3):305–313, 1999.

Yi Zuo, Aerie Lin, Paul Chang, and Wen-Biao Gan. Development of long-term dendritic spine stability in diverse regions of cerebral cortex. *Neuron*, 46(2):181–189, 2005.